**MARMARA UNIVERSITY**

**INSTITUTE FOR GRADUATE STUDIES IN PURE AND APPLIED SCIENCES**

# AN ANALYSIS OF THE EFFECTS OF BATTERY LOCATION IN ELECTRIC AUTOMOBILES ON RIDE COMFORT CONSIDERING SPRING AND DAMPER NONLINEARITIES OF SUSPENSION SYSTEM

ERALP OSMAN ERDOĞAN

**MASTER THESIS**

Department of Mechanical Engineering

**Thesis Supervisor**

Assoc. Prof. Dr. Mustafa ÖZDEMİR

ISTANBUL, 2022

MARMARA UNIVERSITY
INSTITUTE FOR GRADUATE STUDIES
IN PURE AND APPLIED SCIENCES

# AN ANALYSIS OF THE EFFECTS OF BATTERY LOCATION IN ELECTRIC AUTOMOBILES ON RIDE COMFORT CONSIDERING SPRING AND DAMPER NONLINEARITIES OF SUSPENSION SYSTEM

ERALP OSMAN ERDOĞAN

(524619015)

**MASTER THESIS**

Department of Mechanical Engineering

**Thesis Supervisor**
Assoc. Prof. Dr. Mustafa ÖZDEMİR

ISTANBUL, 2022

# TABLE OF CONTENTS

# ÖZET

SÜSPANSİYON SİSTEMİNİN YAY VE AMORTİSÖR DOĞRUSALSIZLIKLARI DİKKATE ALINARAK ELEKTRİKLİ OTOMOBİLLERDE BATARYA KONUMUNUN SÜRÜŞ KONFORU ÜZERİNE ETKİLERİNİN ANALİZİ

Elektrikli otomobiller, içten yanmalı motorlu emsallerine göre hava ve gürültü kirliliğini azaltmak ve fosil yakıtlara olan ihtiyacı azaltmak gibi kayda değer avantajlara sahiptir. Bu nedenle otomotiv sektörünün geleceği olarak görülmektedirler. Tasarımlarındaki güncel konulardan biri de batarya yerleşimi için uygun yerlerin tespit edilmesidir. Bunun nedeni, bataryanın aracın toplam ağırlığına katkıda bulunan en büyük kalemlerden biri olması ve konumunun sürüş konforunu doğrudan etkilemesidir. Bu konu üzerine literatürde son zamanlarda birtakım çalışmalar yapılmıştır. Önceki bu çalışmalar, yayların ve amortisörlerin doğrusal olduğunun varsayıldığı süspansiyon modellerine dayanmaktadır. Bununla birlikte, gerçek yay ve amortisörler, ihmal edildikleri takdirde sürüş kalitesini olumsuz etkileyebilecek doğrusal olmayan karakteristiklere sahiptir. Bildiğimiz kadarıyla, bugüne kadar literatürde süspansiyonun yay ve amortisör doğrusalsızlıkları varlığında elektrikli otomobillerin batarya yerleşimi problemine odaklanmış herhangi bir çalışma mevcut değildir. Bu tez, literatürdeki bu önemli eksikliği gidermeyi amaçlamaktadır: Elektrikli otomobillerde batarya konumunun süspansiyon performansı üzerindeki etkileri literatürde ilk kez dinamik modelde doğrusal olmayan yaylar ve amortisörler kullanılarak analiz edilmiştir. Analizlerde tekerlek içi motorların ve bunların titreşim izolatörlerinin eklendiği ve tüm yay ve amortisörlerin kübik doğrusalsızlığa sahip olduğu modifiye bir yarım araba modeli kullanılmıştır. Tarif edilen bu matematiksel model kullanılarak bataryanın boylamasına eksen boyunca konumunun sürüş kalitesi üzerindeki etkileri incelenmiştir. İyi bir sürüş konforu için uygun batarya konumlarını oldukça gerçekçi bir şekilde belirlemek suretiyle, bu tezin elektrikli otomobillerin yaygınlaşmasını sağlayacağına inanılmaktadır.

# ABSTRACT

AN ANALYSIS OF THE EFFECTS OF BATTERY LOCATION IN ELECTRIC AUTOMOBILES ON RIDE COMFORT CONSIDERING SPRING AND DAMPER NONLINEARITIES OF SUSPENSION SYSTEM

Electric vehicles have remarkable advantages over internal combustion engine vehicles such as reducing air and noise pollution and decreasing the need for fossil fuels. These advantages make electric vehicles the future of automobile industry. One recent problem in the design of electric vehicles is determination of suitable battery locations. This is because battery pack is one of the heaviest parts of electric vehicles and its location directly affects ride comfort. There is a growing number of studies on this topic. These previous studies are based on a model which assumes that springs and dampers are linear. In fact, real springs and dampers have nonlinearities which may affect ride comfort if neglected. To our best knowledge, there is not any research that investigates the effects of nonlinearities of the springs and dampers on suitable battery locations for electric vehicles. This thesis aims to fulfil this important gap in the literature. Effects of the battery location on the performance of suspension system of electric vehicles are analysed using a dynamic model with nonlinear springs and dampers for the first time in literature. A modified half-car model is used for the analyses, in which the in-wheel motors and their vibration isolators are included, and all the springs and dampers have cubic nonlinearities. Effects of the longitudinal battery location on ride comfort are analysed using the described model. This thesis is believed to contribute for increasing the usage of electric automobiles by realistically determining the appropriate battery locations for high quality ride comfort.

# SYMBOLS

## Lagrangian Method

| | |
|---|---|
| $L$ | : Lagrangian of the system |
| $K$ | : Total kinetic energy of the system |
| $U$ | : Total potential energy of the system |
| $D$ | : Dissipation function |

## Rear Axle

| | |
|---|---|
| $k_{Susp,R}$ | : Linear spring coefficient of rear suspension spring |
| $y_{UnMass,R}$ | : Vertical displacement of rear unsprung mass |
| $k_{Susp,R,NonLi}$ | : Nonlinear spring coefficient of rear suspension spring |
| $c_{Susp,R}$ | : Linear damping coefficient of rear suspension damper |
| $\dot{y}_{UnMass,R}$ | : Vertical velocity of rear unsprung mass |
| $c_{Susp,R,NonLi}$ | : Nonlinear damping coefficient of rear suspension damper |
| $k_{Tire,R}$ | : Linear spring coefficient of rear tire |
| $y_{UnMass,R}$ | : Vertical displacement of rear unsprung mass |
| $k_{Tire,R,NonLi}$ | : Nonlinear spring coefficient of rear tire |
| $c_{Tire,R}$ | : Linear damping coefficient of rear tire |
| $\dot{y}_{UnMass,R}$ | : Vertical velocity of rear unsprung mass |
| $c_{Tire,R,NonLi}$ | : Nonlinear damping coefficient of rear tire |
| $m_{UnMass,R}$ | : Rear unsprung mass |
| $\ddot{y}_{UnMass,R}$ | : Acceleration of rear unsprung mass |

**Front Axle**

$k_{Susp,F}$ : Linear spring coefficient of front suspension spring

$y_{UnMass,F}$ : Vertical displacement of front unsprung mass

$k_{Susp,F,NonLi}$ : Nonlinear spring coefficient of front suspension spring

$c_{Susp,F}$ : Linear damping coefficient of front suspension damper

$\dot{y}_{UnMass,F}$ : Vertical velocity of front unsprung mass

$c_{Susp,F,NonLi}$ : Nonlinear damping coefficient of front suspension damper

$k_{Tire,F}$ : Linear spring coefficient of front tire

$y_{UnMass,F}$ : Vertical displacement of front unsprung mass

$k_{Tire,F,NonLi}$ : Nonlinear spring coefficient of front tire

$c_{Tire,F}$ : Linear damping coefficient of front tire

$\dot{y}_{UnMass,F}$ : Vertical velocity of front unsprung mass

$c_{Tire,F,NonLi}$ : Nonlinear damping coefficient of front tire

$m_{UnMass,F}$ : Front unsprung mass

$\ddot{y}_{UnMass,F}$ : Acceleration of the front unsprung mass

**Vehicle Body**

$m_{Body}$ : Mass of the vehicle body

$m_{Ch}$ : Mass of the chassis

$m_{Bat}$ : Mass of the battery

$y_{Body}$ : Vertical displacement of the vehicle body

$\dot{y}_{Body}$ : Vertical velocity of the vehicle body

$\ddot{y}_{Body}$ : Acceleration of the vehicle body

$l_{CG}$ : Distance of centre of gravity of the vehicle body from rear axle

$l$ : Wheelbase of the vehicle

$l_{Ch}$ : Distance of centre of gravity of the chassis from rear axle

$l_{Bat}$ : Directed distance of centre of gravity of the battery from rear axle

$I_{Body}$ : Mass moment of inertia of the vehicle body

$I_{Ch}$ : Mass moment of inertia of the chassis

$I_{Bat}$ : Mass moment of inertia of the battery

$\theta$ : Pitch angle of the vehicle body

$\dot{\theta}$ : Pitch velocity of the vehicle body

$\ddot{\theta}$ : Pitch acceleration of the vehicle body

**Rear Motor**

$e_R$ : Eccentricity of rear in-wheel motor's unbalanced mass

$\omega_R$ : Angular velocity of rear in-wheel motor

$RPM_R$ : Revolutions per minute of rear in-wheel motor

$V$ : Velocity of the vehicle

$D_{Tire,R}$ : Diameter of the rear tire

$m_{MotorUnb,R}$ : Rear in-wheel motor's unbalanced mass

$k_{MVI,R}$ : Linear spring coefficient of rear in-wheel motor isolator spring

$y_{M,R}$ : Vertical displacement of rear in-wheel motor

$y_{UnMass,R}$ : Vertical displacement of rear unsprung mass

$k_{MVI,R,NonLi}$ : Nonlinear spring coefficient of rear in-wheel motor isolator spring

$c_{MVI,R}$ : Linear damping coefficient of rear in-wheel motor isolator damper

$\dot{y}_{M,R}$ : Vertical velocity of rear in-wheel motor

$\dot{y}_{UnMass,R}$ : Vertical velocity of rear unsprung mass

$c_{MVI,R,NonLi}$ : Nonlinear damping coefficient of rear in-wheel motor isolator damper

$m_{Motor,R}$ : Mass of rear in-wheel motor

$\ddot{y}_{M,R}$ : Vertical acceleration of rear in-wheel motor

**Front Motor**

$e_F$ : Eccentricity of front in-wheel motor’s unbalanced mass

$\omega_F$ : Angular velocity of front in-wheel motor

$RPM_F$ : Revolutions per minute of front in-wheel motor

$D_{Tire,F}$ : Diameter of the front tire

$m_{MotorUnb,F}$ : Front in-wheel motor’s unbalanced mass

$k_{MVI,F}$ : Linear spring coefficient of front in-wheel motor isolator spring

$y_{M,F}$ : Vertical displacement of front in-wheel motor

$y_{UnMass,F}$ : Vertical displacement of front unsprung mass

$k_{MVI,F,NonLi}$ : Nonlinear spring coefficient of front in-wheel motor isolator spring

$c_{MVI,F}$ : Linear damping coefficient of front in-wheel motor isolator damper

$\dot{y}_{M,F}$ : Vertical velocity of front in-wheel motor

$\dot{y}_{UnMass,F}$ : Vertical velocity of front unsprung mass

$c_{MVI,F,NonLi}$ : Nonlinear damping coefficient of front in-wheel motor isolator damper

$m_{Motor,F}$ : Mass of front in-wheel motor

$\ddot{y}_{M,F}$ : Vertical acceleration of front in-wheel motor

**Driver and Seat**

$k_{Seat}$ : Linear spring coefficient of driver's seat suspension spring

$y_{Seat}$ : Vertical displacement of driver and seat

$l_{Seat,CG}$ : Distance of driver's seat from vehicle's centre of gravity

$k_{Seat,NonLi}$ : Nonlinear spring coefficient of driver's seat suspension spring

$c_{Seat}$ : Linear damping coefficient of driver's seat suspension damper

$\dot{y}_{Seat}$ : Vertical velocity of driver and seat

$c_{Seat,NonLi}$ : Nonlinear damping coefficient of driver's seat suspension damper

$m_{Seat}$ : Mass of driver and seat

$\ddot{y}_{Seat}$ : Vertical acceleration of driver and seat

**Road Input**

$h$ : Height of the speed hump or bump

$\tau$ : Time difference between front and rear axle for passing the same obstacle

$u_F$ : Road displacement input to the front tire

$\dot{u}_F$ : Road velocity input to the front tire

$u_R$ : Road displacement input to the rear tire

$\dot{u}_R$ : Road velocity input to the rear tire

$x$ : Coordinate variable along the road

$\lambda$ : Wavelength of the sinusoidal road profile

$A$ : Amplitude of the sinusoidal road profile

# ABBREVIATIONS

MVI : Motor vibration isolator

RMS : Root-mean-square

# LIST OF FIGURES

# LIST OF TABLES

# 1 INTRODUCTION

Air pollution caused by motorway traffic is one of the most important problems for today's cities (Andre et al., 2020; Harrison et al., 2021). For example, according to U.S. Environmental Protection Agency (EPA), 29% of total greenhouse gas emission 2019 in USA is caused by transportation sector. 25% of total greenhouse gas emissions in European Union is caused by transportation sector (European Commission, 2020). This situation is the result of the fact that the transportation sector heavily depends on fossil fuels (Vatsa et al., 2021) and it is the second largest energy consumer after the industry sector (Alimujiang and Jiang, 2020). According to World Health Organization (WHO), more than 80% of the world population lives in cities that have air pollution above the standard emission limits (Sofia et al., 2020). This statistical figure suggests that automotive industry should focus its efforts on increasing air quality in cities and decreasing the global climate change effects (Shafique et al., 2021). Electric vehicles are considered to provide an effective solution to these problems (Choma et al., 2020; Guo et al., 2020) and are expected to be the future of automotive industry (Verma et al., 2021). In addition to the advantages described above, electric vehicles operate quieter (Hua et al., 2021) and this advantage plays a key role to solve noise pollution (Pardo-Ferreira et al., 2020; Campello-Vicente et al., 2017). At this point it should be mentioned that electric vehicle technology product range is not just limited only to passenger cars but covers a wide variety from bicycles (e.g Tuncel, 2019; Uyar, 2019) to public transportation vehicles (e.g Avcı, 2019; Sazak, 2019; Tanyeri, 2019). This master thesis concentrates on battery electric passenger cars which have the biggest share in the market. There are three reasons for this: First, the number of electric vehicles that use other power sources including fuel cells is at relatively low levels (Parajuly et al., 2020). Second, the ultimate goal of the automotive industry is the full electric vehicle that uses battery as power source and hybrid vehicles are just an intermediate step in this market transition (Li et al., 2019a). Third, statistical analyses showed that in the European Union (UN) countries, 72% of greenhouse gas emissions are caused by highway transportation vehicles and the passenger cars are the first among the vehicles in this category (European Commission, 2020).

Increasing consumer awareness has begun to affect vehicle sales data. Market share of full electric vehicles and plug-in hybrid vehicles increased in 2020 to 74.8% in Norway, 52.4% in Iceland and 32.3% in Sweden (International Energy Agency (IEA), 2021). In order to increase these sales to desired levels globally, universities and industrial establishments are performing more and more research and development (R&D) studies on electric vehicles. Some of these studies can be reviewed under the following categories:

a) Charging solutions (Arif et al., 2021; Bagchi et al., 2021; Mohammed and Jung, 2021; Triviño et al., 2021; Machura and Li, 2019; Zhao et al., 2019; Ahmad et al., 2018; Sun et al., 2018)
b) Charging stations (Mishra et al., 2021; Chen et al., 2020; Funke et al., 2019; Deb et al., 2018; Khan et al., 2018)
c) Battery cooling systems (Tete et al., 2021; Akinlabi and Solyali, 2020; Aswin Karthik et al., 2020; Choudhari et al., 2020; Kalaf et al., 2020; Kumar et al., 2020; Kim et al., 2019a; Xia et al., 2017)
d) Battery safety (Aalund et al., 2021; Xu et al., 2020; Feng et al., 2018)
e) Estimation of battery state-of-charge (Zhang et al., 2021; How et al., 2020; Ali et al., 2019; Kim et al., 2019b; Wang and Mu, 2019; Zhou et al., 2019)
f) Estimation of remaining useful life of battery (Li et al., 2020; Lipu et al., 2018; Li et al., 2017b)
g) Battery degradation (Nimesh et al., 2021; Iwafune and Ogimoto, 2020; Han et al., 2019; Redondo-Iglesias et al., 2019; Pelletier et al., 2017)
h) Reuse of used batteries (Braco et al., 2021; Gu et al., 2021; Živčák et al., 2021; Wu et al., 2020; Yang et al., 2020; Ioakimidis et al., 2019; Reinhardt et al., 2019; Casals et al., 2017a, 2017b; Li et al., 2017a)
i) Waste battery management (Li et al., 2021; Preeti and Sayali, 2021; Skeete et al., 2020; Hu et al., 2017; Xu et al., 2017)
j) Crashworthiness and collision safety of electric vehicles (Albarella et al., 2021; Navale et al., 2021; Ijeh, 2020; Li et al., 2019b; Wu et al., 2019; Lian et al., 2018)

However, perhaps the most important criterion influencing consumers' automobile preferences is the satisfaction of the driving comfort needs at the highest level. For that reason, suspension system becomes a key component of automobiles. Ride comfort analysis of traditional internal combustion engine vehicles is a classical subject of vehicle dynamics (Jazar, 2014). In electric vehicles, depending on the vehicle's manufacturer and model, batteries can be located under the front or rear seats, or at the middle, underneath the floor (Ganesh and Venkatesan, 2021; Arora et al., 2016; Mazumder et al., 2012; Besselink et al., 2010). This fact makes the battery location an additional parameter that must be considered in the ride comfort analysis. Wang (2020) focusing on passive suspension systems stated that battery location must be optimised to improve ride comfort quality. Wang et al. reached similar results on their study focused on active suspension systems published in 2014. However, in these studies, suspension system members are modelled as linear springs and dampers. This modelling approach is commonly used in ride comfort analysis to simplify calculations (Narayanan and Senthill, 1998). But in all real springs and dampers, there are always nonlinearities (Doebelin, 1998).

For the reasons and facts given above, this master thesis's main research question is determined as follows: "What are the effects of battery location on electric vehicle vibrations in cases where the nonlinear characteristics of springs and dampers within the suspension system are not negligible?"

## 1.1 Aim and Scope of the Thesis

In recent years, global warming due to the climate change has reached critical points (Jena, 2020). A recent compilation of the reports published by World Health Organization (WHO) and United Nations (UN) can be found in an article by Nguyen et al. (2020). With transition to electric vehicles, emission of greenhouse gasses, air and noise pollution and the need for fossil fuels will decrease (Di Felice et al., 2020; Pandey et al., 2020; Praticò et al., 2020; Varma et al., 2020) and important gains for human health are being expected (Choma et al., 2020; Gai et al., 2020). Different types of electric motors and batteries are used in electric vehicles (Kaya and Kıyak, 2020; Iclodean et al., 2017). For this reason, developments on battery and charging technologies have a key role in this transition (Yang et al., 2021; Ball et al., 2020; Daga et al., 2017; Bindra, 2017). Some of the other important factors that contribute to the growth of the electric automobile market are growth of charging infrastructure (Illmann and Kluge, 2020; Ou et al., 2020), financial incentives for electric vehicles (Münzel et al., 2019; Lévay et al., 2017), and development and improvement of product portfolios (Kieckhäfer et al., 2017). Another worthy factor regarding to this transition is consumers' habits and their willingness towards the adoption of new technologies (Huang et al., 2021; Jaiswal et al., 2021; Shetty et al., 2020; Rezvani et al., 2015). Ride comfort is one of the indispensable criteria for customers while selecting a car. For that reason, the analysis of vehicle vibrations is a main research subject in automotive engineering. As shown in a recent study by Wang (2020) where linear spring and damper models are used, battery location is a key parameter that must be taken into account while analysing ride comfort of electric vehicles. Linear spring and damper models are used to simplify the computations; however, it is well known that real springs and real dampers inherently have nonlinear characteristics (Sever et al., 2019). To our best knowledge, there is no previous study or research that analysed the effects of battery location on vibrations of electric vehicles in the presence of suspension nonlinearities. This master thesis aims to fulfil this important gap in literature.

The objectives of the thesis are as follows:

1. To analyse the effects of battery location on vehicle vibrations induced by road irregularities and rotating unbalance of the in-wheel motors by using a dynamic model that has nonlinear suspension springs and dampers
2. To model the wheels' structural elasticity and damping characteristics as nonlinear spring and damper model in the analyses described in the first objective
3. To model the seat suspension and the in-wheel motor vibration isolators by using nonlinear springs and dampers in order to ensure the completeness of the work
4. To determine the optimal battery location for electric vehicles based on the results of the analyses performed under conditions that are very close to those of the real-world situations as described in first, second and third objectives
5. To contribute to the design of electric vehicles with high ride comfort

The theories and models that the thesis is built on are explained below:

a) The vehicle is modelled based on the bicycle vibration model (Jazar, 2014). In-wheel motors and motor isolators are added to this model by using the studies of Quynh et al. (2019) and Wang (2020).

b) The equations of motion of the vehicle are derived using the Lagrange theory (Wachter and Hoeber, 2006).

c) Each spring is modelled as Duffing spring (Schmitz and Smith, 2012).

d) Each damper is modelled to have cubic nonlinearities (Shafiei, 2021; Zilletti et al., 2017; Ho et al., 2014, 2012; Peng et al., 2012; Meskell, 2006).

# 2 DYNAMIC MODEL OF THE VEHICLE

Vibration model of the electric vehicle relies on the bicycle vibration model (Jazar, 2014). This model is also known as the half-car model, and it has four degrees of freedom. These are the vehicle body's heave and pitch motions, and vertical translations of the rear and front axles (Rajamani, 2012). For ensuring acceptable cornering performance, the centre of gravity of the vehicle is placed at the midpoint of the lateral axis (Mazumder et al., 2012). But the battery, which has a significant contribution to the total weight of the vehicle, is placed at various locations along the longitudinal axis according to the manufacturer and model (Ganesh and Venkatesan, 2021; Arora et al., 2016; Mazumder et al., 2012; Besselink et al., 2010). This fact implies that the modified half-car model is suitable for realizing this thesis' aim and objectives. This model is modified in accordance with the studies done by Quynh et al. (2019) and Wang (2020) to include in-wheel motors and their vibration isolator. A model like this modified model was also used in an article published by Huang and Nguyen in 2021. The difference of the model in this thesis is in that all springs are modelled as Duffing spring (Schmitz and Smith, 2012) and all dampers modelled as they have cubic nonlinearities (Shafiei, 2021; Zilletti et al., 2017; Ho et al., 2014, 2012; Peng et al., 2012; Meskell, 2006). The seat suspension dynamics are also included in the model. The equations of motion of the vehicle are derived using the Lagrange method (Wachter and Hoeber, 2006). The obtained differential equations are numerically solved.

## 2.1 The Half-Car Model

The vehicle dynamic model used in this thesis is based on the classical half-car model shown in Figure 2.1. In this model, vehicle is considered as a two-wheeler which has four degrees of freedom. These are the vertical motion and pitch motion of the sprung mass, and the vertical motions of the unsprung masses. Tires and suspensions are modelled as spring-damper systems. Damping and spring characteristics are generally modelled using linear equations.

Battery is located within the sprung mass and does not have any suspension. In-wheel motors are attached to rear and front unsprung mass, as shown in Figure 2.2. Each motor vibration isolator is composed of one spring and one damper. Each motor has one translational degree of freedom in the vertical direction.

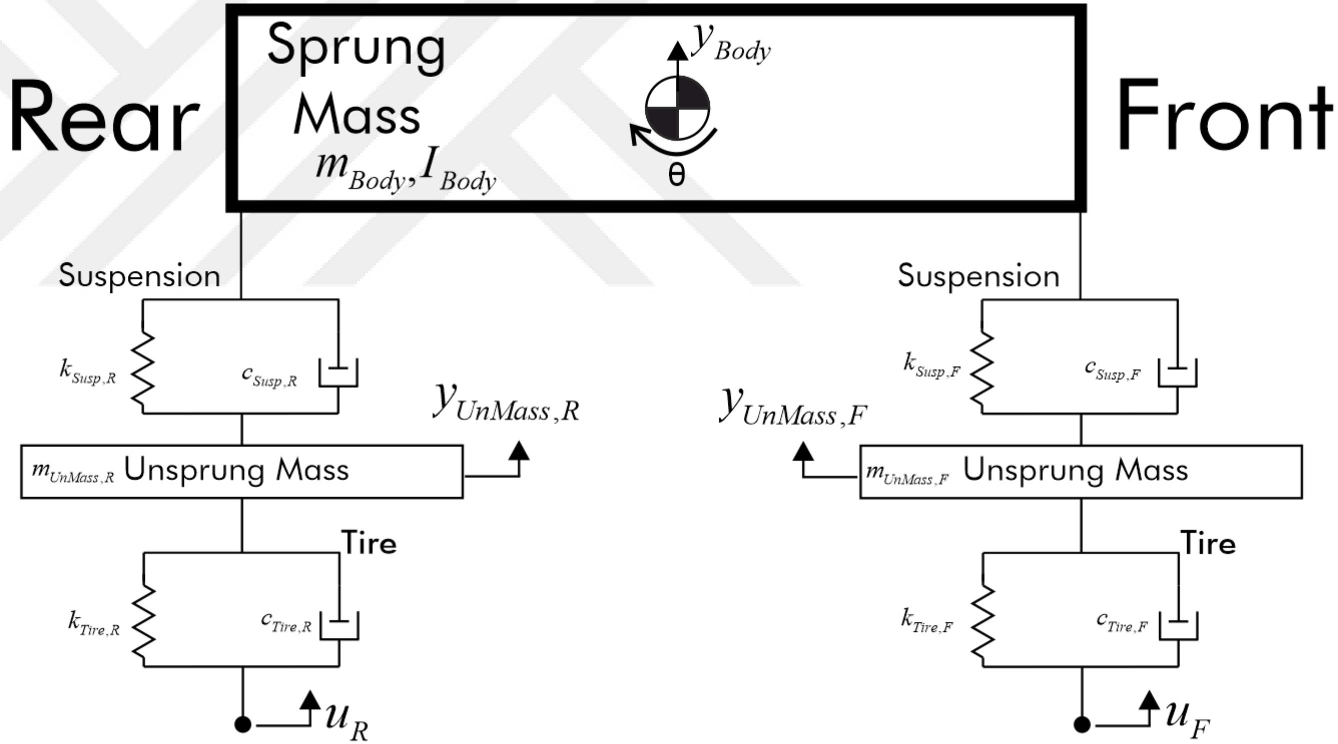


**Figure 2.1.** Schematics of the classical half-car model.

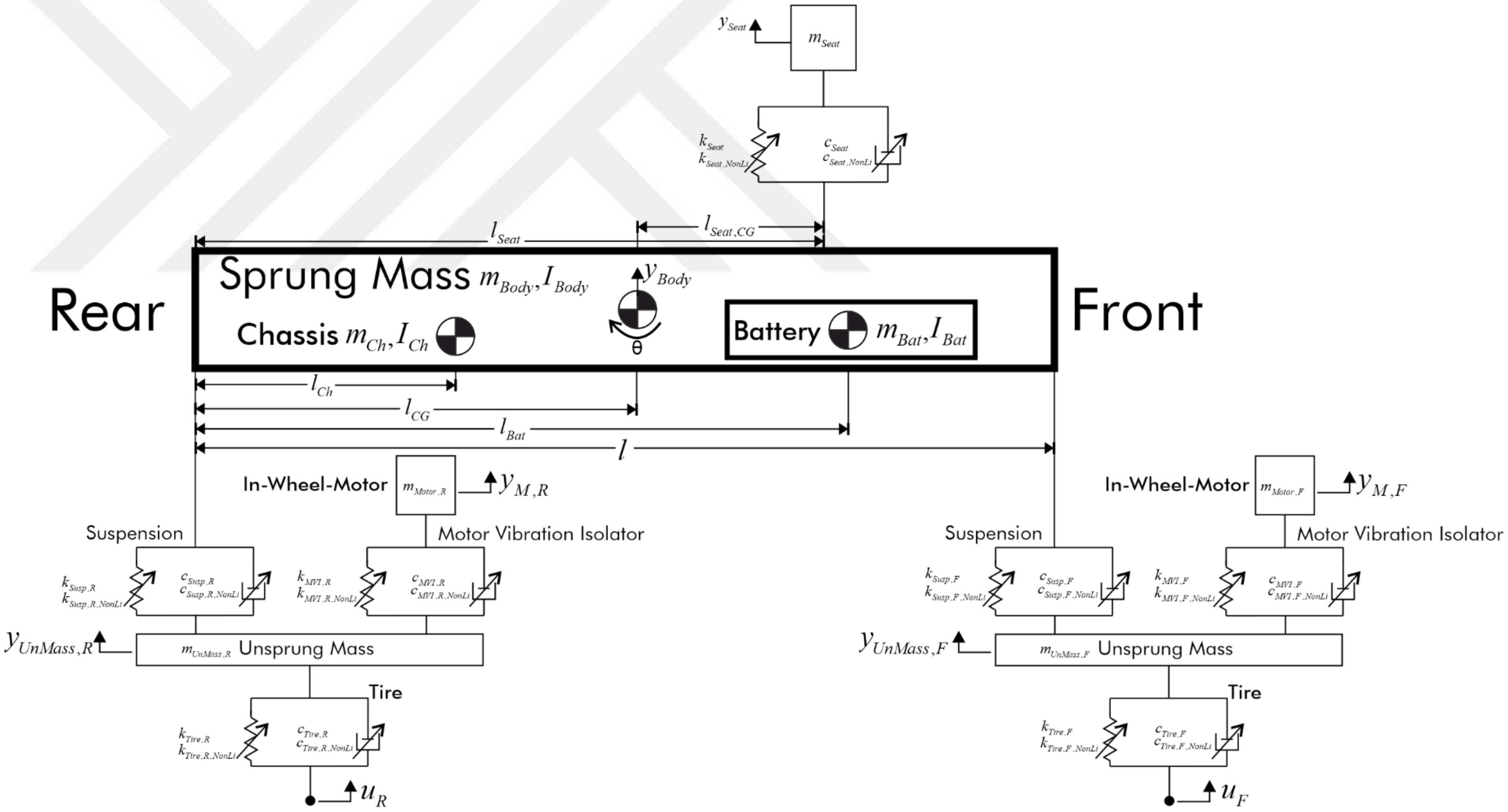


**Figure 2.2.** Considered half-car model.

For ride comfort analysis, driver and driver's seat with seat suspension is also included in the half-car model. Seat suspension has one spring and one damper. The combined mass of the driver and seat has one translational degree of freedom in the vertical direction. Model has totally seven degrees of freedom. All springs and dampers are modelled using nonlinear equations. Trigonometric nonlinearities are also considered.

### 2.2 Equations of Motion of the Vehicle

The equations of motion of the vehicle are derived by using the Lagrange's equation as follows:

$$\frac{d}{dt}\left(\frac{\partial L}{\partial \dot{q}_i}\right)-\frac{\partial L}{\partial q_i}+\frac{\partial D}{\partial \dot{q}_i}=Q_i, \qquad i = 1, 2\ldots, 7 \tag{1}$$

where $t$ denotes the time, $q_i$'s are the generalised coordinates of the system, $L$ is the Lagrangian, $D$ is the dissipation function, and $Q_i$'s are the nonconservative generalised forces other than the dissipation forces. The Lagrangian of the system is defined as

$$L = K - U \tag{2}$$

where $U$ is the total potential energy of the vehicle and $K$ is its total kinetic energy. For our modified half-car model, the kinetic energy expression is

$$\begin{aligned} K = \frac{1}{2}(m_{UnMass,R}\dot{y}_{UnMass,R}{}^2 + m_{Motor,R}\dot{y}_{M,R}{}^2 + m_{Body}\dot{y}_{Body}{}^2 \\ + m_{UnMass,F}\dot{y}_{UnMass,F}{}^2 + m_{Motor,F}\dot{y}_{M,F}{}^2 + m_{Seat}\dot{y}_{Seat}{}^2 + I_{Body}\dot{\theta}^2) \end{aligned} \tag{3}$$

where all the displacements are measured from the undeformed state. If the springs in the model were all linear, the total elastic potential energy of the vehicle would be written as

$$\begin{aligned} U_e = \frac{1}{2}(& k_{Tire,R}(y_{UnMass,R} - u_R)^2 + k_{Susp,R}((y_{Body} + l_{CG}\sin(\theta)) - y_{UnMass,R})^2 \\ & + k_{MVI,R}(y_{M,R} - y_{UnMass,R})^2 + k_{Tire,F}(y_{UnMass,F} - u_F)^2 \\ & + k_{Susp,F}((y_{Body} - (l - l_{CG})\sin(\theta)) - y_{UnMass,F})^2 \\ & + k_{MVI,F}(y_{M,F} - y_{UnMass,F})^2 + k_{Seat}(y_{Seat} - (y_{Body} - l_{Seat,CG}\sin(\theta)))^2) \end{aligned} \tag{4}$$

Similarly, if the viscous dampers in the model were all linear, the dissipation function would be expressed as

$$
\begin{aligned}
D = \frac{1}{2}(& c_{Tire,R}(\dot{y}_{UnMass,R} - \dot{u}_R)^2 + c_{Susp,R}((\dot{y}_{Body} + l_{CG}\dot{\theta}\cos(\theta)) - \dot{y}_{UnMass,R})^2 \\
& + c_{MVI,R}(\dot{y}_{M,R} - \dot{y}_{UnMass,R})^2 + c_{Tire,F}(\dot{y}_{UnMass,F} - \dot{u}_F)^2 \\
& + c_{Susp,F}((\dot{y}_{Body} - (l - l_{CG})\dot{\theta}\cos(\theta)) - \dot{y}_{UnMass,F})^2 \\
& + c_{MVI,F}(\dot{y}_{M,F} - \dot{y}_{UnMass,F})^2 + c_{Seat}(\dot{y}_{Seat} - (\dot{y}_{Body} - l_{Seat,CG}\dot{\theta}\cos(\theta)))^2)
\end{aligned} \tag{5}
$$

However, there are instances where a nonlinear model better describes the system behaviour. One way to incorporate nonlinear behaviour is the use of nonlinear springs. A common nonlinear spring model, referred to as a Duffing spring, includes a cubic nonlinearity and is given by (Schmitz and Smith, 2012)

$$
f = k_0\delta + k_1\delta^3 \tag{6}
$$

Here, $f$ denotes the spring force, $\delta$ denotes deflection of spring, and $k_0$ and $k_1$ are linear and cubic spring constants, respectively. When the nonlinearities of the springs are taken into account, the total elastic potential energy expression becomes

$$
\begin{aligned}
U_e = & \frac{1}{2}k_{Tire,R}(y_{UnMass,R} - u_R)^2 + \frac{1}{4}k_{Tire,R,NonLi}(y_{UnMass,R} - u_R)^4 \\
& + \frac{1}{2}k_{Susp,R}(y_{Body} + l_{CG}\sin(\theta) - y_{UnMass,R})^2 \\
& + \frac{1}{4}k_{Susp,R,NonLi}(y_{Body} + l_{CG}\sin(\theta) - y_{UnMass,R})^4 \\
& + \frac{1}{2}k_{MVI,R}(y_{M,R} - y_{UnMass,R})^2 + \frac{1}{4}k_{MVI,R,NonLi}(y_{M,R} - y_{UnMass,R})^4 \\
& + \frac{1}{2}k_{Tire,F}(y_{UnMass,F} - u_F)^2 + \frac{1}{4}k_{Tire,F,NonLi}(y_{UnMass,F} - u_F)^4 \\
& + \frac{1}{2}k_{Susp,F}(y_{Body} - (l - l_{CG})\sin(\theta) - y_{UnMass,F})^2 \\
& + \frac{1}{4}k_{Susp,F,NonLi}(y_{Body} - (l - l_{CG})\sin(\theta) - y_{UnMass,F})^4 \\
& + \frac{1}{2}k_{MVI,F}(y_{M,F} - y_{UnMass,F})^2 + \frac{1}{4}k_{MVI,F,NonLi}(y_{M,F} - y_{UnMass,F})^4 \\
& + \frac{1}{2}k_{Seat}(y_{Seat} - (y_{Body} - l_{Seat,CG}\sin(\theta)))^2 \\
& + \frac{1}{4}k_{Seat,NonLi}(y_{Seat} - (y_{Body} - l_{Seat,CG}\sin(\theta)))^4
\end{aligned} \tag{7}
$$

So, the total potential energy of the system is

$$U = U_e + m_{UnMass,R} g y_{UnMass,R} + m_{Motor,R} g y_{M,R} + m_{Body} g y_{Body} + m_{UnMass,F} g y_{UnMass,F} + m_{Motor,F} g y_{M,F} + m_{Seat} g y_{Seat} + U_0 \tag{8}$$

where $g$ denotes the gravitational acceleration, and $U_0$ is a constant that depends on the selected datum for gravitational potential energy.

In the presence of cubic damping nonlinearities, the dissipation function can be written as

$$\begin{aligned} D = &\frac{1}{2} c_{Tire,R} (\dot{y}_{UnMass,R} - \dot{u}_R)^2 + \frac{1}{4} c_{Tire,R,NonLi} (\dot{y}_{UnMass,R} - \dot{u}_R)^4 \\ &+ \frac{1}{2} c_{Susp,R} (\dot{y}_{Body} + l_{CG} \dot{\theta} \cos(\theta) - \dot{y}_{UnMass,R})^2 \\ &+ \frac{1}{4} c_{Susp,R,NonLi} (\dot{y}_{Body} + l_{CG} \dot{\theta} \cos(\theta) - \dot{y}_{UnMass,R})^4 \\ &+ \frac{1}{2} c_{MVI,R} (\dot{y}_{M,R} - \dot{y}_{UnMass,R})^2 + \frac{1}{4} c_{MVI,R,NonLi} (\dot{y}_{M,R} - \dot{y}_{UnMass,R})^4 \\ &+ \frac{1}{2} c_{Tire,F} (\dot{y}_{UnMass,F} - \dot{u}_F)^2 + \frac{1}{4} c_{Tire,F,NonLi} (\dot{y}_{UnMass,F} - \dot{u}_F)^4 \\ &+ \frac{1}{2} c_{Susp,F} (\dot{y}_{Body} - (l - l_{CG}) \dot{\theta} \cos(\theta) - \dot{y}_{UnMass,F})^2 \\ &+ \frac{1}{4} c_{Susp,F,NonLi} (\dot{y}_{Body} - (l - l_{CG}) \dot{\theta} \cos(\theta) - \dot{y}_{UnMass,F})^4 \\ &+ \frac{1}{2} c_{MVI,F} (\dot{y}_{M,F} - \dot{y}_{UnMass,F})^2 + \frac{1}{4} c_{MVI,F,NonLi} (\dot{y}_{M,F} - \dot{y}_{UnMass,F})^4 \\ &+ \frac{1}{2} c_{Seat} (\dot{y}_{Seat} - (\dot{y}_{Body} - l_{Seat,CG} \dot{\theta} \cos(\theta)))^2 \\ &+ \frac{1}{4} c_{Seat,NonLi} (\dot{y}_{Seat} - (\dot{y}_{Body} - l_{Seat,CG} \dot{\theta} \cos(\theta)))^4 \end{aligned} \tag{9}$$

Using the equations written above, we can derive equations of motion for rear axle, front axle, vehicle body, front motor, rear motor, and the driver and seat as explained below.

### 2.2.1 Rear motor

$$\frac{\partial L}{\partial \dot{y}_{M,R}} = m_{Motor,R} \dot{y}_{M,R} \tag{10}$$

$$\frac{d}{dt}\left( \frac{\partial L}{\partial \dot{y}_{M,R}} \right) = m_{Motor,R} \ddot{y}_{M,R} \tag{11}$$

$$\frac{\partial L}{\partial y_{M,R}} = -k_{MVI,R}(y_{M,R} - y_{UnMass,R}) - k_{MVI,R,NonLi}(y_{M,R} - y_{UnMass,R})^3 - m_{Motor,R}g \tag{12}$$

$$\frac{\partial D}{\partial \dot{y}_{M,R}} = c_{MVI,R}(\dot{y}_{M,R} - \dot{y}_{UnMass,R}) + c_{MVI,R,NonLi}(\dot{y}_{M,R} - \dot{y}_{UnMass,R})^3 \tag{13}$$

$$\begin{aligned} \frac{d}{dt}\left(\frac{\partial L}{\partial \dot{y}_{M,R}}\right) - \frac{\partial L}{\partial y_{M,R}} + \frac{\partial D}{\partial \dot{y}_{M,R}} = m_{Motor,R}\ddot{y}_{M,R} \\ +k_{MVI,R}(y_{M,R} - y_{UnMass,R}) \\ +k_{MVI,R,NonLi}(y_{M,R} - y_{UnMass,R})^3 \\ +c_{MVI,R}(\dot{y}_{M,R} - \dot{y}_{UnMass,R}) \\ +c_{MVI,R,NonLi}(\dot{y}_{M,R} - \dot{y}_{UnMass,R})^3 \\ +m_{Motor,R}g \end{aligned} \tag{14}$$

Therefore, the equation of motion that corresponds to the generalised coordinate $y_{M,R}$ can be written as

$$\begin{aligned} & m_{Motor,R}\ddot{y}_{M,R} + k_{MVI,R}(y_{M,R} - y_{UnMass,R}) + k_{MVI,R,NonLi}(y_{M,R} - y_{UnMass,R})^3 \\ & +c_{MVI,R}(\dot{y}_{M,R} - \dot{y}_{UnMass,R}) + c_{MVI,R,NonLi}(\dot{y}_{M,R} - \dot{y}_{UnMass,R})^3 \\ & +m_{Motor,R}g = F_{MotorUnb,R} \end{aligned} \tag{15}$$

where

$$F_{MotorUnb,R} = m_{MotorUnb,R}\omega_R{}^2 e_R \sin(\omega_R t) \tag{16}$$

with

$$\omega_R = 2\pi \frac{RPM_R}{60} \tag{17}$$

$$RPM_R = \frac{60V}{3.6\pi D_{Tire,R}} \tag{18}$$

Here, $\omega_R$ is in rad/s, the vehicle velocity $V$ is in km/h, and $D_{Tire,R}$ is in meters.

### 2.2.2 Front motor

$$\frac{\partial L}{\partial \dot{y}_{M,F}} = m_{Motor,F}\dot{y}_{M,F} \tag{19}$$

$$\frac{d}{dt}\left(\frac{\partial L}{\partial \dot{y}_{M,F}}\right) = m_{Motor,F}\ddot{y}_{M,F} \tag{20}$$

$$\frac{\partial L}{\partial y_{M,F}} = -k_{MVI,F}(y_{M,F} - y_{UnMass,F}) - k_{MVI,F,NonLi}(y_{M,F} - y_{UnMass,F})^3 - m_{Motor,F}\,g \tag{21}$$

$$\frac{\partial D}{\partial \dot{y}_{M,F}} = c_{MVI,F}(\dot{y}_{M,F} - \dot{y}_{UnMass,F}) + c_{MVI,F,NonLi}(\dot{y}_{M,F} - \dot{y}_{UnMass,F})^3 \tag{22}$$

$$\begin{aligned} \frac{d}{dt}\left(\frac{\partial L}{\partial \dot{y}_{M,F}}\right) - \frac{\partial L}{\partial y_{M,F}} + \frac{\partial D}{\partial \dot{y}_{M,F}} = m_{Motor,F}\,\ddot{y}_{M,F} \\ +k_{MVI,F}(y_{M,F} - y_{UnMass,F}) \\ +k_{MVI,F,NonLi}(y_{M,F} - y_{UnMass,F})^3 \\ +c_{MVI,F}(\dot{y}_{M,F} - \dot{y}_{UnMass,F}) \\ +c_{MVI,F,NonLi}(\dot{y}_{M,F} - \dot{y}_{UnMass,F})^3 \\ +m_{Motor,F}\,g \end{aligned} \tag{23}$$

Hence, the equation of motion that corresponds to the generalised coordinate $y_{M,F}$ can be written as

$$\begin{aligned} & m_{Motor,F}\,\ddot{y}_{M,F} + k_{MVI,F}(y_{M,F} - y_{UnMass,F}) + k_{MVI,F,NonLi}(y_{M,F} - y_{UnMass,F})^3 \\ & +c_{MVI,F}(\dot{y}_{M,F} - \dot{y}_{UnMass,F}) + c_{MVI,F,NonLi}(\dot{y}_{M,F} - \dot{y}_{UnMass,F})^3 \\ & +m_{Motor,F}\,g = F_{MotorUnb,F} \end{aligned} \tag{24}$$

where

$$F_{MotorUnb,F} = m_{MotorUnb,F}\,\omega_F{}^2 e_F \sin(\omega_F t) \tag{25}$$

with

$$\omega_F = 2\pi \frac{RPM_F}{60} \tag{26}$$

$$RPM_F = \frac{60V}{3.6\pi D_{Tire,F}} \tag{27}$$

Here, $\omega_F$ is in rad/s, the vehicle velocity $V$ is in km/h, and $D_{Tire,F}$ is in meters.

### 2.2.3 Rear axle

$$\frac{\partial L}{\partial \dot{y}_{UnMass,R}} = m_{UnMass,R}\,\dot{y}_{UnMass,R} \tag{28}$$

$$\frac{d}{dt}\left(\frac{\partial L}{\partial \dot{y}_{UnMass,R}}\right) = m_{UnMass,R}\,\ddot{y}_{UnMass,R} \tag{29}$$

$$\frac{\partial L}{\partial y_{UnMass,R}} = k_{Susp,R}(y_{Body} + l_{CG}\sin(\theta) - y_{UnMass,R})$$

$$+k_{Susp,R,NonLi}(y_{Body} + l_{CG}\sin(\theta) - y_{UnMass,R})^3$$

$$+k_{MVI,R}(y_{M,R} - y_{UnMass,R}) + k_{MVI,R,NonLi}(y_{M,R} - y_{UnMass,R})^3 \tag{30}$$

$$-k_{Tire,R}(y_{UnMass,R} - u_R) - k_{Tire,R,NonLi}(y_{UnMass,R} - u_R)^3$$

$$-m_{UnMass,R}\,g$$

$$\frac{\partial D}{\partial \dot{y}_{UnMass,R}} = -c_{Susp,R}(\dot{y}_{Body} + l_{CG}\dot{\theta}\cos(\theta) - \dot{y}_{UnMass,R})$$

$$-c_{Susp,R,NonLi}(\dot{y}_{Body} + l_{CG}\dot{\theta}\cos(\theta) - \dot{y}_{UnMass,R})^3 \tag{31}$$

$$-c_{MVI,R}(\dot{y}_{M,R} - \dot{y}_{UnMass,R}) - c_{MVI,R,NonLi}(\dot{y}_{M,R} - \dot{y}_{UnMass,R})^3$$

$$+c_{Tire,R}(\dot{y}_{UnMass,R} - \dot{u}_R) + c_{Tire,R,NonLi}(\dot{y}_{UnMass,R} - \dot{u}_R)^3$$

$$\begin{aligned}
\frac{d}{dt}\left(\frac{\partial L}{\partial \dot{y}_{UnMass,R}}\right) - \frac{\partial L}{\partial y_{UnMass,R}} + \frac{\partial D}{\partial \dot{y}_{UnMass,R}} = m_{UnMass,R}\ddot{y}_{UnMass,R} \\
-k_{Susp,R}(y_{Body} + l_{CG}\sin(\theta) - y_{UnMass,R}) \\
-k_{Susp,R,NonLi}(y_{Body} + l_{CG}\sin(\theta) - y_{UnMass,R})^3 \\
-k_{MVI,R}(y_{M,R} - y_{UnMass,R}) \\
-k_{MVI,R,NonLi}(y_{M,R} - y_{UnMass,R})^3 \\
+k_{Tire,R}(y_{UnMass,R} - u_R) \\
+k_{Tire,R,NonLi}(y_{UnMass,R} - u_R)^3 \\
+m_{UnMass,R}\,g \\
-c_{Susp,R}(\dot{y}_{Body} + l_{CG}\dot{\theta}\cos(\theta) - \dot{y}_{UnMass,R}) \\
-c_{Susp,R,NonLi}(\dot{y}_{Body} + l_{CG}\dot{\theta}\cos(\theta) - \dot{y}_{UnMass,R})^3 \\
-c_{MVI,R}(\dot{y}_{M,R} - \dot{y}_{UnMass,R}) \\
-c_{MVI,R,NonLi}(\dot{y}_{M,R} - \dot{y}_{UnMass,R})^3 \\
+c_{Tire,R}(\dot{y}_{UnMass,R} - \dot{u}_R) \\
+c_{Tire,R,NonLi}(\dot{y}_{UnMass,R} - \dot{u}_R)^3
\end{aligned} \tag{32}$$

Thus, the equation of motion that corresponds to the generalised coordinate $y_{UnMass,R}$ can be written as

$$
\begin{aligned}
& m_{UnMass,R}\ddot{y}_{UnMass,R} - k_{Susp,R}(y_{Body} + l_{CG}\sin(\theta) - y_{UnMass,R}) \\
& -k_{Susp,R,NonLi}(y_{Body} + l_{CG}\sin(\theta) - y_{UnMass,R})^3 \\
& -k_{MVI,R}(y_{M,R} - y_{UnMass,R}) - k_{MVI,R,NonLi}(y_{M,R} - y_{UnMass,R})^3 \\
& +k_{Tire,R}(y_{UnMass,R} - u_R) + k_{Tire,R,NonLi}(y_{UnMass,R} - u_R)^3 \\
& +m_{UnMass,R}g - c_{Susp,R}(\dot{y}_{Body} + l_{CG}\dot{\theta}\cos(\theta) - \dot{y}_{UnMass,R}) \\
& -c_{Susp,R,NonLi}(\dot{y}_{Body} + l_{CG}\dot{\theta}\cos(\theta) - \dot{y}_{UnMass,R})^3 \\
& -c_{MVI,R}(\dot{y}_{M,R} - \dot{y}_{UnMass,R}) - c_{MVI,R,NonLi}(\dot{y}_{M,R} - \dot{y}_{UnMass,R})^3 \\
& +c_{Tire,R}(\dot{y}_{UnMass,R} - \dot{u}_R) + c_{Tire,R,NonLi}(\dot{y}_{UnMass,R} - \dot{u}_R)^3 = 0
\end{aligned} \tag{33}
$$

### 2.2.4 Front axle

$$
\frac{\partial L}{\partial \dot{y}_{UnMass,F}} = m_{UnMass,F}\dot{y}_{UnMass,F} \tag{34}
$$

$$
\frac{d}{dt}\left(\frac{\partial L}{\partial \dot{y}_{UnMass,F}}\right) = m_{UnMass,F}\ddot{y}_{UnMass,F} \tag{35}
$$

$$
\begin{aligned}
\frac{\partial L}{\partial y_{UnMass,F}} = {} & k_{Susp,F}(y_{Body} - (l - l_{CG})\sin(\theta) - y_{UnMass,F}) \\
& +k_{Susp,F,NonLi}(y_{Body} - (l - l_{CG})\sin(\theta) - y_{UnMass,F})^3 \\
& +k_{MVI,F}(y_{M,F} - y_{UnMass,F}) + k_{MVI,F,NonLi}(y_{M,F} - y_{UnMass,F})^3 \\
& -k_{Tire,F}(y_{UnMass,F} - u_F) - k_{Tire,F,NonLi}(y_{UnMass,F} - u_F)^3 \\
& -m_{UnMass,F}g
\end{aligned} \tag{36}
$$

$$
\begin{aligned}
\frac{\partial D}{\partial \dot{y}_{UnMass,F}} = {} & -c_{Susp,F}(\dot{y}_{Body} - (l - l_{CG})\dot{\theta}\cos(\theta) - \dot{y}_{UnMass,F}) \\
& -c_{Susp,F,NonLi}(\dot{y}_{Body} - (l - l_{CG})\dot{\theta}\cos(\theta) - \dot{y}_{UnMass,F})^3 \\
& -c_{MVI,F}(\dot{y}_{M,F} - \dot{y}_{UnMass,F}) - c_{MVI,F,NonLi}(\dot{y}_{M,F} - \dot{y}_{UnMass,F})^3 \\
& +c_{Tire,F}(\dot{y}_{UnMass,F} - \dot{u}_F) + c_{Tire,F,NonLi}(\dot{y}_{UnMass,F} - \dot{u}_F)^3
\end{aligned} \tag{37}
$$

$$\frac{d}{dt}\left(\frac{\partial L}{\partial \dot{y}_{UnMass,F}}\right)-\frac{\partial L}{\partial y_{UnMass,F}}+\frac{\partial D}{\partial \dot{y}_{UnMass,F}}=m_{UnMass,F}\ddot{y}_{UnMass,F}$$
$$\begin{aligned}
&-k_{Susp,F}(y_{Body}-(l-l_{CG})\sin(\theta)\\
&-y_{UnMass,F})-k_{Susp,F,NonLi}(y_{Body}-\\
&(l-l_{CG})\sin(\theta)-y_{UnMass,F})^3\\
&-k_{MVI,F}(y_{M,F}-y_{UnMass,F})\\
&-k_{MVI,F,NonLi}(y_{M,F}-y_{UnMass,F})^3\\
&+k_{Tire,F}(y_{UnMass,F}-u_F)\\
&+k_{Tire,F,NonLi}(y_{UnMass,F}-u_F)^3\\
&+m_{UnMass,F}\,g\\
&-c_{Susp,F}(\dot{y}_{Body}-(l-l_{CG})\dot{\theta}\cos(\theta)\\
&-\dot{y}_{UnMass,F})\\
&-c_{Susp,F,NonLi}(\dot{y}_{Body}-(l-l_{CG})\dot{\theta}\cos(\theta)\\
&-\dot{y}_{UnMass,F})^3\\
&-c_{MVI,F}(\dot{y}_{M,F}-\dot{y}_{UnMass,F})\\
&-c_{MVI,F,NonLi}(\dot{y}_{M,F}-\dot{y}_{UnMass,F})^3\\
&+c_{Tire,F}(\dot{y}_{UnMass,F}-\dot{u}_F)\\
&+c_{Tire,F,NonLi}(\dot{y}_{UnMass,F}-\dot{u}_F)^3
\end{aligned} \tag{38}$$

Therefore, the equation of motion that corresponds to the generalised coordinate $y_{UnMass,F}$ can be written as

$$\begin{aligned}
&m_{UnMass,F}\ddot{y}_{UnMass,F}-k_{Susp,F}(y_{Body}-(l-l_{CG})\sin(\theta)-y_{UnMass,F})\\
&-k_{Susp,F,NonLi}(y_{Body}-(l-l_{CG})\sin(\theta)-y_{UnMass,F})^3\\
&-k_{MVI,F}(y_{M,F}-y_{UnMass,F})-k_{MVI,F,NonLi}(y_{M,F}-y_{UnMass,F})^3\\
&+k_{Tire,F}(y_{UnMass,F}-u_F)+k_{Tire,F,NonLi}(y_{UnMass,F}-u_F)^3\\
&+m_{UnMass,F}\,g-c_{Susp,F}(\dot{y}_{Body}-(l-l_{CG})\dot{\theta}\cos(\theta)-\dot{y}_{UnMass,F})\\
&-c_{Susp,F,NonLi}(\dot{y}_{Body}-(l-l_{CG})\dot{\theta}\cos(\theta)-\dot{y}_{UnMass,F})^3\\
&-c_{MVI,F}(\dot{y}_{M,F}-\dot{y}_{UnMass,F})-c_{MVI,F,NonLi}(\dot{y}_{M,F}-\dot{y}_{UnMass,F})^3\\
&+c_{Tire,F}(\dot{y}_{UnMass,F}-\dot{u}_F)+c_{Tire,F,NonLi}(\dot{y}_{UnMass,F}-\dot{u}_F)^3=0
\end{aligned} \tag{39}$$

### 2.2.5 Driver and seat

$$\frac{\partial L}{\partial \dot{y}_{Seat}}=m_{Seat}\dot{y}_{Seat} \tag{40}$$

$$\frac{d}{dt}\left(\frac{\partial L}{\partial \dot{y}_{Seat}}\right) = m_{Seat}\ddot{y}_{Seat} \tag{41}$$

$$\begin{aligned}\frac{\partial L}{\partial y_{Seat}} = &-k_{Seat}(y_{Seat} - (y_{Body} - l_{Seat,CG}\sin(\theta))) \\ &-k_{Seat,NonLi}(y_{Seat} - (y_{Body} - l_{Seat,CG}\sin(\theta)))^3 - m_{Seat}g\end{aligned} \tag{42}$$

$$\begin{aligned}\frac{\partial D}{\partial \dot{y}_{Seat}} = &c_{Seat}(\dot{y}_{Seat} - (\dot{y}_{Body} - l_{Seat,CG}\dot{\theta}\cos(\theta))) \\ &+c_{Seat,NonLi}(\dot{y}_{Seat} - (\dot{y}_{Body} - l_{Seat,CG}\dot{\theta}\cos(\theta)))^3\end{aligned} \tag{43}$$

$$\begin{aligned}\frac{d}{dt}\left(\frac{\partial L}{\partial \dot{y}_{Seat}}\right) - \frac{\partial L}{\partial y_{Seat}} + \frac{\partial D}{\partial \dot{y}_{Seat}} = &m_{Seat}\ddot{y}_{Seat} \\ &+k_{Seat}(y_{Seat} - (y_{Body} - l_{Seat,CG}\sin(\theta))) \\ &+k_{Seat,NonLi}(y_{Seat} - (y_{Body} - l_{Seat,CG}\sin(\theta)))^3 \\ &+m_{Seat}g \\ &+c_{Seat}(\dot{y}_{Seat} - (\dot{y}_{Body} - l_{Seat,CG}\dot{\theta}\cos(\theta))) \\ &+c_{Seat,NonLi}(\dot{y}_{Seat} - (\dot{y}_{Body} - l_{Seat,CG}\dot{\theta}\cos(\theta)))^3\end{aligned} \tag{44}$$

Hence, the equation of motion that corresponds to the generalised coordinate $y_{Seat}$ can be written as

$$\begin{aligned}&m_{Seat}\ddot{y}_{Seat} + k_{Seat}(y_{Seat} - (y_{Body} - l_{Seat,CG}\sin(\theta))) \\ &+k_{Seat,NonLi}(y_{Seat} - (y_{Body} - l_{Seat,CG}\sin(\theta)))^3 \\ &+m_{Seat}g + c_{Seat}(\dot{y}_{Seat} - (\dot{y}_{Body} - l_{Seat,CG}\dot{\theta}\cos(\theta))) \\ &+c_{Seat,NonLi}(\dot{y}_{Seat} - (\dot{y}_{Body} - l_{Seat,CG}\dot{\theta}\cos(\theta)))^3 = 0\end{aligned} \tag{45}$$

### 2.2.6 Vehicle body

The inertial parameters of the vehicle body can be computed as follows:

$$m_{Body} = m_{Ch} + m_{Bat} \tag{46}$$

$$l_{CG} = \frac{m_{Ch}l_{Ch} + m_{Bat}l_{Bat}}{m_{Ch} + m_{Bat}} \tag{47}$$

$$I_{Body} = I_{Ch} + m_{Ch}\left(l_{CG} - l_{Ch}\right)^2 + I_{Bat} + m_{Bat}\left(l_{Bat} - l_{CG}\right)^2 \tag{48}$$

Then,

$$\frac{\partial L}{\partial \dot{y}_{Body}} = m_{Body}\dot{y}_{Body} \tag{49}$$

$$\frac{d}{dt}\left(\frac{\partial L}{\partial \dot{y}_{Body}}\right) = m_{Body}\ddot{y}_{Body} \tag{50}$$

$$\begin{aligned}
\frac{\partial L}{\partial y_{Body}} = &-k_{Susp,R}(y_{Body} + l_{CG}\sin(\theta) - y_{UnMass,R}) \\
&-k_{Susp,R,NonLi}(y_{Body} + l_{CG}\sin(\theta) - y_{UnMass,R})^3 \\
&-k_{Susp,F}(y_{Body} - (l - l_{CG})\sin(\theta) - y_{UnMass,F}) \\
&-k_{Susp,F,NonLi}(y_{Body} - (l - l_{CG})\sin(\theta) - y_{UnMass,F})^3 \\
&+k_{Seat}(y_{Seat} - (y_{Body} - l_{Seat,CG}\sin(\theta))) \\
&+k_{Seat,NonLi}(y_{Seat} - (y_{Body} - l_{Seat,CG}\sin(\theta)))^3 - m_{Body}g
\end{aligned} \tag{51}$$

$$\begin{aligned}
\frac{\partial D}{\partial \dot{y}_{Body}} = &c_{Susp,R}(\dot{y}_{Body} + l_{CG}\dot{\theta}\cos(\theta) - \dot{y}_{UnMass,R}) \\
&+c_{Susp,R,NonLi}(\dot{y}_{Body} + l_{CG}\dot{\theta}\cos(\theta) - \dot{y}_{UnMass,R})^3 \\
&+c_{Susp,F}(\dot{y}_{Body} - (l - l_{CG})\dot{\theta}\cos(\theta) - \dot{y}_{UnMass,F}) \\
&+c_{Susp,F,NonLi}(\dot{y}_{Body} - (l - l_{CG})\dot{\theta}\cos(\theta) - \dot{y}_{UnMass,F})^3 \\
&-c_{Seat}(\dot{y}_{Seat} - (\dot{y}_{Body} - l_{Seat,CG}\dot{\theta}\cos(\theta))) \\
&-c_{Seat,NonLi}(\dot{y}_{Seat} - (\dot{y}_{Body} - l_{Seat,CG}\dot{\theta}\cos(\theta)))^3
\end{aligned} \tag{52}$$

$$\begin{aligned}
\frac{d}{dt}\left(\frac{\partial L}{\partial \dot{y}_{Body}}\right) - \frac{\partial L}{\partial y_{Body}} + \frac{\partial D}{\partial \dot{y}_{Body}} = &m_{Body}\ddot{y}_{Body} \\
&+k_{Susp,R}(y_{Body} + l_{CG}\sin(\theta) - y_{UnMass,R}) \\
&+k_{Susp,R,NonLi}(y_{Body} + l_{CG}\sin(\theta) - y_{UnMass,R})^3 \\
&+k_{Susp,F}(y_{Body} - (l - l_{CG})\sin(\theta) - y_{UnMass,F}) \\
&+k_{Susp,F,NonLi}(y_{Body} - (l - l_{CG})\sin(\theta) - y_{UnMass,F})^3 \\
&-k_{Seat}(y_{Seat} - (y_{Body} - l_{Seat,CG}\sin(\theta))) \\
&-k_{Seat,NonLi}(y_{Seat} - (y_{Body} - l_{Seat,CG}\sin(\theta)))^3 \\
&+m_{Body}g \\
&+c_{Susp,R}(\dot{y}_{Body} + l_{CG}\dot{\theta}\cos(\theta) - \dot{y}_{UnMass,R}) \\
&+c_{Susp,R,NonLi}(\dot{y}_{Body} + l_{CG}\dot{\theta}\cos(\theta) - \dot{y}_{UnMass,R})^3 \\
&+c_{Susp,F}(\dot{y}_{Body} - (l - l_{CG})\dot{\theta}\cos(\theta) - \dot{y}_{UnMass,F}) \\
&+c_{Susp,F,NonLi}(\dot{y}_{Body} - (l - l_{CG})\dot{\theta}\cos(\theta) - \dot{y}_{UnMass,F})^3 \\
&-c_{Seat}(\dot{y}_{Seat} - (\dot{y}_{Body} - l_{Seat,CG}\dot{\theta}\cos(\theta))) \\
&-c_{Seat,NonLi}(\dot{y}_{Seat} - (\dot{y}_{Body} - l_{Seat,CG}\dot{\theta}\cos(\theta)))^3
\end{aligned} \tag{53}$$

Thus, the equation of motion that corresponds to the generalised coordinate $y_{Body}$ can be written as

$$\begin{aligned}
& m_{Body}\ddot{y}_{Body} \\
& +k_{Susp,R}(y_{Body}+l_{CG}\sin(\theta)-y_{UnMass,R}) \\
& +k_{Susp,R,NonLi}(y_{Body}+l_{CG}\sin(\theta)-y_{UnMass,R})^3 \\
& +k_{Susp,F}(y_{Body}-(l-l_{CG})\sin(\theta)-y_{UnMass,F}) \\
& +k_{Susp,F,NonLi}(y_{Body}-(l-l_{CG})\sin(\theta)-y_{UnMass,F})^3 \\
& -k_{Seat}(y_{Seat}-(y_{Body}-l_{Seat,CG}\sin(\theta))) \\
& -k_{Seat,NonLi}(y_{Seat}-(y_{Body}-l_{Seat,CG}\sin(\theta)))^3 \\
& +m_{Body}g \\
& +c_{Susp,R}(\dot{y}_{Body}+l_{CG}\dot{\theta}\cos(\theta)-\dot{y}_{UnMass,R}) \\
& +c_{Susp,R,NonLi}(\dot{y}_{Body}+l_{CG}\dot{\theta}\cos(\theta)-\dot{y}_{UnMass,R})^3 \\
& +c_{Susp,F}(\dot{y}_{Body}-(l-l_{CG})\dot{\theta}\cos(\theta)-\dot{y}_{UnMass,F}) \\
& +c_{Susp,F,NonLi}(\dot{y}_{Body}-(l-l_{CG})\dot{\theta}\cos(\theta)-\dot{y}_{UnMass,F})^3 \\
& -c_{Seat}(\dot{y}_{Seat}-(\dot{y}_{Body}-l_{Seat,CG}\dot{\theta}\cos(\theta))) \\
& -c_{Seat,NonLi}(\dot{y}_{Seat}-(\dot{y}_{Body}-l_{Seat,CG}\dot{\theta}\cos(\theta)))^3=0
\end{aligned} \tag{54}$$

Similarly,

$$\frac{\partial L}{\partial \dot{\theta}} = I_{Body}\dot{\theta} \tag{55}$$

$$\frac{d}{dt}\left(\frac{\partial L}{\partial \dot{\theta}}\right) = I_{Body}\ddot{\theta} \tag{56}$$

$$\begin{aligned}
\frac{\partial L}{\partial \theta} = & -k_{Seat}l_{Seat,CG}\cos(\theta)(y_{Seat}-(y_{Body}-l_{Seat,CG}\sin(\theta))) \\
& -k_{Seat,NonLi}l_{Seat,CG}\cos(\theta)(y_{Seat}-(y_{Body}-l_{Seat,CG}\sin(\theta)))^3 \\
& +k_{Susp,F}(l-l_{CG})\cos(\theta)(y_{Body}-(l-l_{CG})\sin(\theta)-y_{UnMass,F}) \\
& +k_{Susp,F,NonLi}(l-l_{CG})\cos(\theta)(y_{Body}-(l-l_{CG})\sin(\theta)-y_{UnMass,F})^3 \\
& -k_{Susp,R}l_{CG}\cos(\theta)(y_{Body}+l_{CG}\sin(\theta)-y_{UnMass,R}) \\
& -k_{Susp,R,NonLi}l_{CG}\cos(\theta)(y_{Body}+l_{CG}\sin(\theta)-y_{UnMass,R})^3
\end{aligned} \tag{57}$$

$$
\begin{aligned}
\frac{\partial D}{\partial \dot{\theta}} = {} & c_{Seat} l_{Seat,CG} \cos(\theta)(\dot{y}_{Seat} - (\dot{y}_{Body} - l_{Seat,CG}\dot{\theta}\cos(\theta))) \\
& + c_{Seat,NonLi} l_{Seat,CG} \cos(\theta)(\dot{y}_{Seat} - (\dot{y}_{Body} - l_{Seat,CG}\dot{\theta}\cos(\theta)))^3 \\
& - c_{Susp,F}(l - l_{CG})\cos(\theta)(\dot{y}_{Body} - (l - l_{CG})\dot{\theta}\cos(\theta) - \dot{y}_{UnMass,F}) \\
& - c_{Susp,F,NonLi}(l - l_{CG})\cos(\theta)(\dot{y}_{Body} - (l - l_{CG})\dot{\theta}\cos(\theta) - \dot{y}_{UnMass,F})^3 \\
& + c_{Susp,R} l_{CG} \cos(\theta)(\dot{y}_{Body} + l_{CG}\dot{\theta}\cos(\theta) - \dot{y}_{UnMass,R}) \\
& + c_{Susp,R,NonLi} l_{CG} \cos(\theta)(\dot{y}_{Body} + l_{CG}\dot{\theta}\cos(\theta) - \dot{y}_{UnMass,R})^3
\end{aligned}
\tag{58}
$$

$$
\begin{aligned}
\frac{d}{dt}\left(\frac{\partial L}{\partial \dot{\theta}}\right) - \frac{\partial L}{\partial \theta} + \frac{\partial D}{\partial \dot{\theta}} = {} & I_{Body}\ddot{\theta} \\
& + k_{Seat} l_{Seat,CG} \cos(\theta)(y_{Seat} - (y_{Body} - l_{Seat,CG}\sin(\theta))) \\
& + k_{Seat,NonLi} l_{Seat,CG} \cos(\theta)(y_{Seat} - (y_{Body} \\
& - l_{Seat,CG}\sin(\theta)))^3 - k_{Susp,F}(l - l_{CG})\cos(\theta)(y_{Body} \\
& - (l - l_{CG})\sin(\theta) - y_{UnMass,F}) \\
& - k_{Susp,F,NonLi}(l - l_{CG})\cos(\theta)(y_{Body} - (l - l_{CG})\sin(\theta) \\
& - y_{UnMass,F})^3 + k_{Susp,R} l_{CG} \cos(\theta)(y_{Body} \\
& + l_{CG}\sin(\theta) - y_{UnMass,R}) \\
& + k_{Susp,R,NonLi} l_{CG} \cos(\theta)(y_{Body} + l_{CG}\sin(\theta) \\
& - y_{UnMass,R})^3 + c_{Seat} l_{Seat,CG} \cos(\theta)(\dot{y}_{Seat} - (\dot{y}_{Body} \\
& - l_{Seat,CG}\dot{\theta}\cos(\theta))) + c_{Seat,NonLi} l_{Seat,CG} \cos(\theta)(\dot{y}_{Seat} \\
& - (\dot{y}_{Body} - l_{Seat,CG}\dot{\theta}\cos(\theta)))^3 \\
& - c_{Susp,F}(l - l_{CG})\cos(\theta)(\dot{y}_{Body} - (l - l_{CG})\dot{\theta}\cos(\theta) \\
& - \dot{y}_{UnMass,F}) - c_{Susp,F,NonLi}(l - l_{CG})\cos(\theta)(\dot{y}_{Body} \\
& - (l - l_{CG})\dot{\theta}\cos(\theta) - \dot{y}_{UnMass,F})^3 \\
& + c_{Susp,R} l_{CG} \cos(\theta)(\dot{y}_{Body} + l_{CG}\dot{\theta}\cos(\theta) - \dot{y}_{UnMass,R}) \\
& + c_{Susp,R,NonLi} l_{CG} \cos(\theta)(\dot{y}_{Body} + l_{CG}\dot{\theta}\cos(\theta) \\
& - \dot{y}_{UnMass,R})^3
\end{aligned}
\tag{59}
$$

Finally, the equation of motion that corresponds to the generalised coordinate $\theta$ can be written as

$$
\begin{aligned}
& I_{Body}\ddot{\theta} \\
& +k_{Seat} l_{Seat,CG}\cos(\theta)(y_{Seat}-(y_{Body}-l_{Seat,CG}\sin(\theta))) \\
& +k_{Seat,NonLi} l_{Seat,CG}\cos(\theta)(y_{Seat}-(y_{Body}-l_{Seat,CG}\sin(\theta)))^3 \\
& -k_{Susp,F}(l-l_{CG})\cos(\theta)(y_{Body}-(l-l_{CG})\sin(\theta)-y_{UnMass,F}) \\
& -k_{Susp,F,NonLi}(l-l_{CG})\cos(\theta)(y_{Body}-(l-l_{CG})\sin(\theta)-y_{UnMass,F})^3 \\
& +k_{Susp,R} l_{CG}\cos(\theta)(y_{Body}+l_{CG}\sin(\theta)-y_{UnMass,R}) \\
& +k_{Susp,R,NonLi} l_{CG}\cos(\theta)(y_{Body}+l_{CG}\sin(\theta)-y_{UnMass,R})^3 \\
& +c_{Seat} l_{Seat,CG}\cos(\theta)(\dot{y}_{Seat}-(\dot{y}_{Body}-l_{Seat,CG}\dot{\theta}\cos(\theta))) \\
& +c_{Seat,NonLi} l_{Seat,CG}\cos(\theta)(\dot{y}_{Seat}-(\dot{y}_{Body}-l_{Seat,CG}\dot{\theta}\cos(\theta)))^3 \\
& -c_{Susp,F}(l-l_{CG})\cos(\theta)(\dot{y}_{Body}-(l-l_{CG})\dot{\theta}\cos(\theta)-\dot{y}_{UnMass,F}) \\
& -c_{Susp,F,NonLi}(l-l_{CG})\cos(\theta)(\dot{y}_{Body}-(l-l_{CG})\dot{\theta}\cos(\theta)-\dot{y}_{UnMass,F})^3 \\
& +c_{Susp,R} l_{CG}\cos(\theta)(\dot{y}_{Body}+l_{CG}\dot{\theta}\cos(\theta)-\dot{y}_{UnMass,R}) \\
& +c_{Susp,R,NonLi} l_{CG}\cos(\theta)(\dot{y}_{Body}+l_{CG}\dot{\theta}\cos(\theta)-\dot{y}_{UnMass,R})^3 = 0
\end{aligned} \tag{60}
$$

## 2.3 Initial Conditions for the Model

To solve the dynamic equations of the model, we need to find the initial values of the model's generalised coordinates. We can write the static equilibrium equations and solve them together to find the necessary initial conditions at position level. The initial generalised velocities of the model are zero.

### 2.3.1 Static equilibrium equation for rear axle

$$
\begin{aligned}
& k_{Susp,R}(y_{Body}+l_{CG}\sin(\theta)-y_{UnMass,R})+k_{Susp,R,NonLi}(y_{Body}+l_{CG}\sin(\theta)-y_{UnMass,R})^3 \\
& +k_{MVI,R}(y_{M,R}-y_{UnMass,R})+k_{MVI,R,NonLi}(y_{M,R}-y_{UnMass,R})^3 \\
& -k_{Tire,R}y_{UnMass,R}-k_{Tire,R,NonLi}y_{UnMass,R}^3-m_{UnMass,R}g=0
\end{aligned} \tag{61}
$$

### 2.3.2 Static equilibrium equation for front axle

$$
\begin{aligned}
& k_{Susp,F}(y_{Body}-(l-l_{CG})\sin(\theta)-y_{UnMass,F}) \\
& +k_{Susp,F,NonLi}(y_{Body}-(l-l_{CG})\sin(\theta)-y_{UnMass,F})^3 \\
& +k_{MVI,F}(y_{M,F}-y_{UnMass,F})+k_{MVI,F,NonLi}(y_{M,F}-y_{UnMass,F})^3 \\
& -k_{Tire,F}y_{UnMass,F}-k_{Tire,F,NonLi}y_{UnMass,F}^3-m_{UnMass,F}g=0
\end{aligned} \tag{62}
$$

### 2.3.3 Static equilibrium equation for front motor

$$
k_{MVI,F}(y_{M,F}-y_{UnMass,F})+k_{MVI,F,NonLi}(y_{M,F}-y_{UnMass,F})^3+m_{Motor,F}g=0 \tag{63}
$$

### 2.3.4 Static equilibrium equation for rear motor

$$k_{MVI,R}(y_{M,R}-y_{UnMass,R})+k_{MVI,R,NonLi}(y_{M,R}-y_{UnMass,R})^3+m_{Motor,R}g=0 \tag{64}$$

### 2.3.5 Static equilibrium equations for vehicle body

$$\begin{aligned}
&k_{Susp,R}(y_{Body}+l_{CG}\sin(\theta)-y_{UnMass,R})\\
&+k_{Susp,R,NonLi}(y_{Body}+l_{CG}\sin(\theta)-y_{UnMass,R})^3\\
&+k_{Susp,F}(y_{Body}-(l-l_{CG})\sin(\theta)-y_{UnMass,F})\\
&+k_{Susp,F,NonLi}(y_{Body}-(l-l_{CG})\sin(\theta)-y_{UnMass,F})^3\\
&-k_{Seat}(y_{Seat}-(y_{Body}-l_{Seat,CG}\sin(\theta)))\\
&-k_{Seat,NonLi}(y_{Seat}-(y_{Body}-l_{Seat,CG}\sin(\theta)))^3\\
&+m_{Body}g=0
\end{aligned} \tag{65}$$

$$\begin{aligned}
&k_{Seat}l_{Seat,CG}\cos(\theta)(y_{Seat}-(y_{Body}-l_{Seat,CG}\sin(\theta)))\\
&+k_{Seat,NonLi}l_{Seat,CG}\cos(\theta)(y_{Seat}-(y_{Body}-l_{Seat,CG}\sin(\theta)))^3\\
&-k_{Susp,F}(l-l_{CG})\cos(\theta)(y_{Body}-(l-l_{CG})\sin(\theta)-y_{UnMass,F})\\
&-k_{Susp,F,NonLi}(l-l_{CG})\cos(\theta)(y_{Body}-(l-l_{CG})\sin(\theta)-y_{UnMass,F})^3\\
&+k_{Susp,R}l_{CG}\cos(\theta)(y_{Body}+l_{CG}\sin(\theta)-y_{UnMass,R})\\
&+k_{Susp,R,NonLi}l_{CG}\cos(\theta)(y_{Body}+l_{CG}\sin(\theta)-y_{UnMass,R})^3=0
\end{aligned} \tag{66}$$

### 2.3.6 Static equilibrium equation for driver and seat

$$\begin{aligned}
&k_{Seat}(y_{Seat}-(y_{Body}-l_{Seat,CG}\sin(\theta)))\\
&+k_{Seat,NonLi}(y_{Seat}-(y_{Body}-l_{Seat,CG}\sin(\theta)))^3+m_{Seat}g=0
\end{aligned} \tag{67}$$

## 2.4 Selection of the Model Parameter Values

This section explains the procedure for the selection of the numerical values of the vehicle suspension model parameters.

### 2.4.1 Rear and front motor parameters

The numerical values found in the literature for rear and front in-wheel motor parameters are presented in Table 2.1.

### 2.4.2 Rear axle parameters

The numerical values found in the literature for rear axle parameters are presented in Table 2.2.

### 2.4.3 Front axle parameters

The numerical values found in the literature for front axle parameters are presented in Table 2.3.

**Table 2.1.** Parameter values for rear and front motors.

| Rear and front motors | | | | | | | |
|---|---|---|---|---|---|---|---|
| Reference | $k_{MVI}$ (N/m) | $k_{MVI,NonLi}$ (N/m$^3$) | $c_{MVI}$ (N·s/m) | $c_{MVI,NonLi}$ (N·s$^3$/m$^3$) | $m_{Motor}$ (kg) | $m_{MotorUnb}$ (kg) | $e$ (mm) |
| Tan et al., 2017 | - | - | - | - | 60 | - | - |
| Tan and Wang, 2016 | - | - | - | - | 50 | - | - |
| Liu et al., 2017 | 2615 | - | 3226 | - | 45 | - | - |
| Qin et al., 2018 | 53000 | - | 1900 | - | 45 | - | - |
| Toksoy, 2020 | 25000 | - | 1686 | - | 30 | - | - |
| Shao et al., 2017 | 41000 | - | 1000 | - | 30 | - | - |
| Yu et al., 2019 | - | - | - | - | 20 | - | 1.5 |
| Tong and Hou, 2013 | 13200 | - | 90 | - | 10 | - | - |
| Qin et al., 2021 | 53000 | - | 1900 | - | 45 | - | - |

### 2.4.4 Chassis and battery parameters

The numerical values found in the literature for chassis and battery parameters in the half-vehicle model are presented in Table 2.4.

### 2.4.5 Parameters for driver and seat

The numerical values found in the literature for driver and seat parameters are presented in Table 2.5.

### 2.4.6 Selected values for the vehicle dynamic model parameters

The numerical values provided in Tables 2.6 through 2.11 are used for the vehicle dynamic model parameters in our numerical analyses. These values are selected based on the averages of the corresponding values found in the literature. The values that are not found in the previous studies are reasonably estimated.

**Table 2.2.** Parameter values for rear axle.

| Rear axle | | | | | | | | | |
|---|---|---|---|---|---|---|---|---|---|
| Reference | $k_{Susp,R}$ (N/m) | $k_{Susp,R,NonLi}$ (N/m$^3$) | $c_{Susp,R}$ (N·s/m) | $c_{Susp,R,NonLi}$ (N·s$^3$/m$^3$) | $k_{Tire,R}$ (N/m) | $k_{Tire,R,NonLi}$ (N/m$^3$) | $c_{Tire,R}$ (N·s/m) | $c_{Tire,R,NonLi}$ (N·s$^3$/m$^3$) | $m_{UnMass,R}$ (kg) |
| Jiao, 2013 | 300000 | - | 20000 | - | 1000000 | - | 500 | - | 350 |
| Gao et al., 2007 | 66824.4 | - | 1190 | - | 101115 | - | - | - | 87.15 |
| Mahala et al., 2009 | 15000 | - | 1070 | - | 190000 | - | - | - | 59 |
| Shelke and Mitra, 2018 | 18000 | - | 500 | - | 102017.2 | - | 138 | - | 45 |
| Yildirim and Esen, 2020 | 20000 | - | 1000 | - | 120000 | - | 50 | - | 50 |
| Zou et al., 2018 | 46000 | - | - | - | 250000 | - | - | - | 42 |
| Patole and Sawant, 2015 | 14662 | - | 1635.2 | - | 181818.88 | - | 13.8 | - | 28 |
| Zhu and Ishitobi, 2006 | 38000 | 1.5 | 1000 | - | 190000 | 1.25 | 10 | - | 59 |
| Hassanzadeh et al., 2010 | 10000 | 10000 | 1000 | 500 | 100000 | - | - | - | 30 |
| El-Mezayen et al., 2020 | 15302 | 2728 | 3482 | 580 | 60063 | 22875 | - | - | 39 |
| Goga and Kľúčik, 2012 | 18615 | - | 1000 | - | 200000 | - | - | - | 140.04 |

**Table 2.3.** Parameter values for front axle.

| Front axle | | | | | | | | | |
|---|---|---|---|---|---|---|---|---|---|
| Reference | $k_{Susp,F}$ (N/m) | $k_{Susp,F,NonLi}$ (N/m$^3$) | $c_{Susp,F}$ (N·s/m) | $c_{Susp,F,NonLi}$ (N·s$^3$/m$^3$) | $k_{Tire,F}$ (N/m) | $k_{Tire,F,NonLi}$ (N/m$^3$) | $c_{Tire,F}$ (N·s/m) | $c_{Tire,F,NonLi}$ (N·s$^3$/m$^3$) | $m_{UnMass,F}$ (kg) |
| Jiao, 2013 | 400000 | - | 40000 | - | 1800000 | - | 1000 | - | 450 |
| Gao et al., 2007 | 18615 | - | 1000 | - | 101115 | - | - | - | 140.4 |
| Mahala et al., 2009 | 15000 | - | 1070 | - | 190000 | - | - | - | 59 |
| Shelke and Mitra, 2018 | 18000 | - | 500 | - | 102017.2 | - | 138 | - | 45 |
| Esen, 2020 | 30000 | - | 1200 | - | 150000 | - | 60 | - | 50 |
| Zou et al., 2018 | 42000 | - | - | - | 250000 | - | - | - | 40 |
| Patole and Sawant, 2015 | 12394 | - | 138.54 | - | 181818.88 | - | 13.8 | - | 23.61 |
| Zhu and Ishitobi, 2006 | 35000 | 1.5 | 720 | - | 190000 | 1.25 | 10 | - | 59 |
| Hassanzadeh et al., 2010 | 10000 | 10000 | 1000 | 500 | 100000 | - | - | - | 40 |
| El-Mezayen et al., 2020 | 15302 | 2728 | 3482 | 580 | 60063 | 22875 | - | - | 39 |
| Goga and Kľúčik, 2012 | 66824.2 | - | 1190 | - | 200000 | - | - | - | 87.15 |

**Table 2.4.** Parameter values for chassis and battery in the half-vehicle model.

| Chassis and battery | | | | | | |
|---|---|---|---|---|---|---|
| Reference | $m_{Ch}$ (kg) | $m_{Bat}$ (kg) | $l$ (mm) | $l_{Ch}$ (mm) | $I_{Ch}$ (kg·m$^2$) | Battery Location |
| Jiao, 2013 | 8800 | - | 3600 | 2540 | 50000 | - |
| Gao et al., 2007 | 1794.4 | - | 2987 | 1271 | 3443.05 | - |
| Mahala et al., 2009 | 677 | - | 3417 | 1633 | 1406.895 | - |
| Shelke and Mitra, 2018 | 600 | - | 2650 | 1150 | 730 | - |
| Esen, 2020 | 1500/2 | - | 2500 | 1100 | 1680/2 | - |
| Zou et al., 2018 | 900 | - | 2850 | 1480 | 1850 | - |
| Patole and Sawant, 2015 | 515.45 | - | 2500 | 1550 | 1238.369 | - |
| Zhu and Ishitobi, 2006 | 1500/2 | - | 3000 | 1700 | 2160/2 | - |
| Hassanzadeh et al., 2010 | 580 | - | 2700 | 1450 | 910 | - |
| El-Mezayen et al., 2020 | (4 × 295)/2 | - | - | - | - | - |
| Goga and Kľúčik, 2012 | 1794 | - | 2984 | 1713 | 3443.05 | - |
| Average of 28 recent EVs in the market (EVSpecifications, 2022) | 1360/2 | 382.73/2 | 2701 | - | - | Under the floor, middle |

**Table 2.5.** Parameter values for driver and seat.

| Driver and seat | | | | | |
|---|---|---|---|---|---|
| Reference | $k_{Seat}$ (N/m) | $k_{Seat,NonLi}$ (N/m$^3$) | $c_{Seat}$ (N·s/m) | $c_{Seat,NonLi}$ (N·s$^3$/m$^3$) | $m_{Seat}$ (kg) |
| Esen, 2020 | 8000 | - | 600 | - | 80 |
| Sever and Yazıcı, 2017 | 31000 | - | 830 | - | 67.2 |
| Toksoy, 2020 | 10000 | - | 800 | - | 100 |
| Rajkumar et al., 2015 | 31000 | - | 830 | - | 71.2 |
| Zhao et al., 2010 | 31000 | - | 830 | - | 71.2 |
| Devdutt, 2017 | 7550 | - | 850 | - | 75 |

**Table 2.6.** Selected parameter values for the rear motor.

| | |
|---|---|
| $k_{MVI,R}$ (N/m) | 27500 |
| $k_{MVI,R,NonLi}$ (N/m$^3$) | 5500 |
| $c_{MVI,R}$ (N•s/m) | 1520 |
| $c_{MVI,R,NonLi}$ (N•s$^3$/m$^3$) | 304 |
| $D_{Tire,R}$ (m) | 0.632 |
| $m_{Motor,R}$ (kg) | 36 |
| $m_{MotorUnb,R}$ (kg) | 30 |
| $e_R$ (m) | 0.015 |

**Table 2.7.** Selected parameter values for the front motor.

| | |
|---|---|
| $k_{MVI,F}$ (N/m) | 27500 |
| $k_{MVI,F,NonLi}$ (N/m$^3$) | 5500 |
| $c_{MVI,F}$ (N•s/m) | 1520 |
| $c_{MVI,F,NonLi}$ (N•s$^3$/m$^3$) | 304 |
| $D_{Tire,F}$ (m) | 0.632 |
| $m_{Motor,F}$ (kg) | 36 |
| $m_{MotorUnb,F}$ (kg) | 30 |
| $e_F$ (m) | 0.015 |

**Table 2.8.** Selected parameter values for the chassis and battery in the half-vehicle model.

| | |
|---|---|
| $m_{Ch}$ (kg) | 1450/2 |
| $m_{Bat}$ (kg) | 385/2 |
| $l$ (m) | 2.7 |
| $l_{Bat}$ (m) | From -0.4 to 3.1 |
| $l_{Ch}$ (m) | 1.5 |
| $I_{Ch}$ (kg·m$^2$) | 4400/2 |
| $I_{Bat}$ (kg·m$^2$) | 140/2 |

**Table 2.9.** Selected parameter values for the rear axle.

| | |
|---|---|
| $k_{Susp,R}$ (N/m) | 61000 |
| $k_{Susp,R,NonLi}$ (N/m$^3$) | 12000 |
| $c_{Susp,R}$ (N•s/m) | 3600 |
| $c_{Susp,R,NonLi}$ (N•s$^3$/m$^3$) | 720 |
| $k_{Tire,R}$ (N/m) | 280000 |
| $k_{Tire,R,NonLi}$ (N/m$^3$) | 56000 |
| $c_{Tire,R}$ (N•s/m) | 300 |
| $c_{Tire,R,NonLi}$ (N•s$^3$/m$^3$) | 60 |
| $m_{UnMass,R}$ (kg) | 45 |

**Table 2.10.** Selected parameter values for the front axle.

| | |
|---|---|
| $k_{Susp,F}$ (N/m) | 61000 |
| $k_{Susp,F,NonLi}$ (N/m$^3$) | 12000 |
| $c_{Susp,F}$ (N•s/m) | 3600 |
| $c_{Susp,F,NonLi}$ (N•s$^3$/m$^3$) | 720 |
| $k_{Tire,F}$ (N/m) | 280000 |
| $k_{Tire,F,NonLi}$ (N/m$^3$) | 56000 |
| $c_{Tire,F}$ (N•s/m) | 300 |
| $c_{Tire,F,NonLi}$ (N•s$^3$/m$^3$) | 60 |
| $m_{UnMass,F}$ (kg) | 45 |

**Table 2.11.** Selected parameter values for the driver and seat.

| | |
|---|---|
| $k_{Seat}$ (N/m) | 19000 |
| $k_{Seat,NonLi}$ (N/m$^3$) | 3800 |
| $c_{Seat}$ (N·s/m) | 600 |
| $c_{Seat,NonLi}$ (N·s$^3$/m$^3$) | 120 |
| $m_{Seat}$ (Including driver) (kg) | 85 |
| $l_{Seat}$ (m) | 1.45 |

## 2.5 Road Profiles for the Numerical Analyses

Equation (68) is used for generating the road profiles. Function parameters are modified to resemble speed bumps and speed humps used on city roads as shown in Figures 2.3 and 2.4.

$$u(x)=\begin{cases} h\sin^2\left(\dfrac{N\pi x}{70}\right), & 0\le x<70\text{ m} \\ 0, & 70\text{ m}\le x\le 140\text{ m} \end{cases} \tag{68}$$

where $N$ is the number of obstacles, $h$ is the height of the obstracle and $x$ is the coordinate variable along the road. Using the numerical values reported by Weber (1998), the road profiles with speed bumps and speed humps are generated as shown in Figures 2.3 and 2.4, respectively.

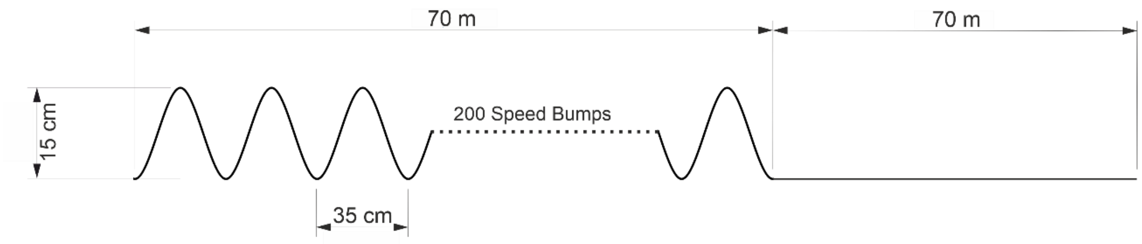


**Figure 2.3.** Road profile with speed bumps.

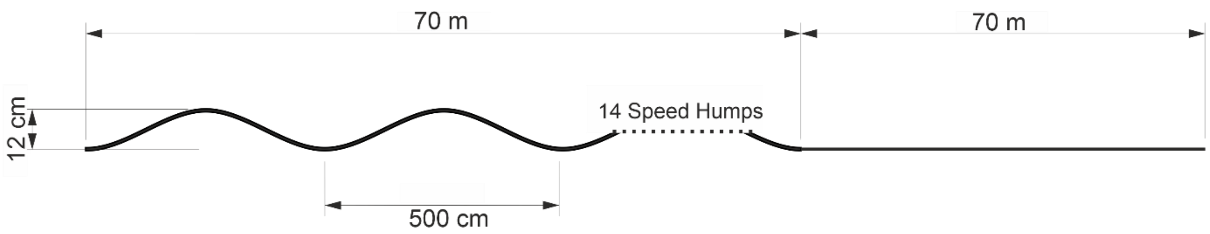


**Figure 2.4.** Road profile with speed humps.

### 2.5.1 Road input to the front tire

The road input functions acting on the front tire are given by

$$\dot{u}_F(t) = \begin{cases} (h\frac{\Omega}{2})\sin(\Omega t), & 0 \le t < \frac{70}{V} \text{ s} \\ 0, & \frac{70}{V} \text{ s} \le t \le \frac{140}{V} \text{ s} \end{cases} \tag{69}$$

$$u_F(t) = \begin{cases} h\sin^2(\frac{\Omega}{2}t), & 0 \le t < \frac{70}{V} \text{ s} \\ 0, & \frac{70}{V} \text{ s} \le t \le \frac{140}{V} \text{ s} \end{cases} \tag{70}$$

where $V$ is the vehicle speed in m/s and

$$\Omega = \frac{4\pi NV}{140} \tag{71}$$

### 2.5.2 Road input to the rear tire

The road input functions acting on the rear tire are given by

$$\dot{u}_R(t) = \begin{cases} 0, & 0 \le t < \tau \text{ s} \\ (h\frac{\Omega}{2})\sin(\Omega(t-\tau)), & \tau \le t < \left(\frac{70}{V}+\tau\right) \text{ s} \\ 0, & \left(\frac{70}{V}+\tau\right) \text{ s} \le t \le \frac{140}{V} \text{ s} \end{cases} \tag{72}$$

$$u_R(t) = \begin{cases} 0, & 0 \le t < \tau \text{ s} \\ h\sin^2(\frac{\Omega}{2}(t-\tau)), & \tau \le t < \left(\frac{70}{V}+\tau\right) \text{ s} \\ 0, & \left(\frac{70}{V}+\tau\right) \text{ s} \le t \le \frac{140}{V} \text{ s} \end{cases} \tag{73}$$

where $V$ is the vehicle speed in m/s and $\tau$ is the time delay in seconds for the rear tire to pass the same obstacle that the front tire passed. $\tau$ value is calculated by dividing the vehicle's wheelbase by the vehicle's velocity.

## 2.6 Root-Mean-Square

The root-mean-square (RMS) is used to analyse and compare the vertical accelerations of driver and seat obtained with different velocities, battery locations and road profiles.

The RMS value of an $n$-dimensional vector $\mathbf{p}$ is calculated as follows (MathWorks, 2022):

$$p_{RMS} = \sqrt{\frac{1}{n}\sum_{i=1}^{n}\left|p_i\right|^2} \tag{74}$$

## 2.7 Solving the Model and Obtaining the RMS Values

Dynamic model is numerically solved using a fixed-step solver, namely, the fourth order Runge-Kutta method (Burden and Faires, 2011). The step size is selected as 0.0001 s. An example of obtaining the RMS values with the vehicle speed 60 km/h and the battery located at $l_{Bat}$ = 0.5 m for the road with speed bumps is given below step by step.

First, we determine the initial conditions for the model. Equations (61)-(67) are solved together numerically to find the initial values of the generalised coordinates.

**Table 2.12.** Numerically found initial values of the generalised coordinates.

| Symbol | Value |
|---|---|
| $\theta_{st}$ | -0.0025 rad |
| $y_{Body,st}$ | -0.1011 m |
| $y_{M,F,st}$ | -0.0326 m |
| $y_{M,R,st}$ | -0.0338 m |
| $y_{Seat,st}$ | -0.1445 m |
| $y_{UnMass,F,st}$ | -0.0198 m |
| $y_{UnMass,R,st}$ | -0.0210 m |

Then, the road profile having speed bumps is generated according to Figure 2.3 and the road inputs are obtained for front and rear tires using equations (69), (70), (72) and (73). The resulting front and rear road displacement inputs are shown in Figures 2.5 and 2.6, respectively.

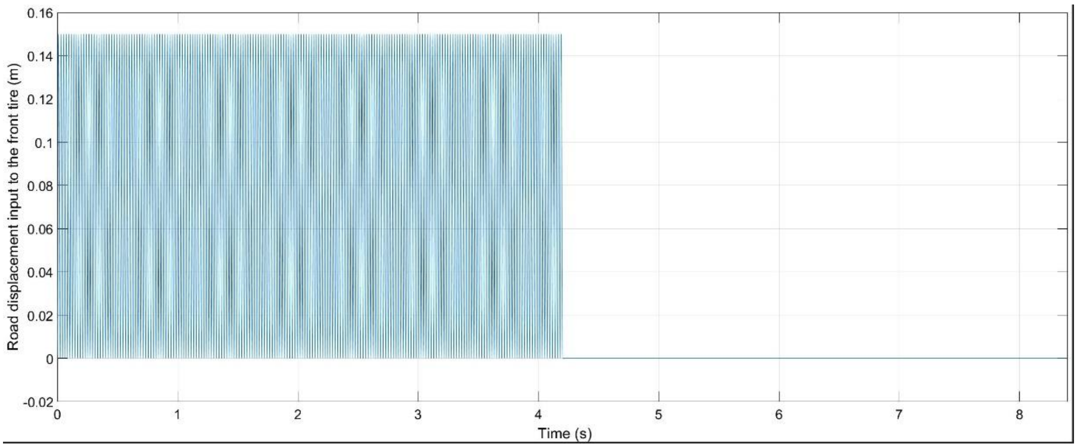


**Figure 2.5.** Bumpy road input to the front tire as a function of time.

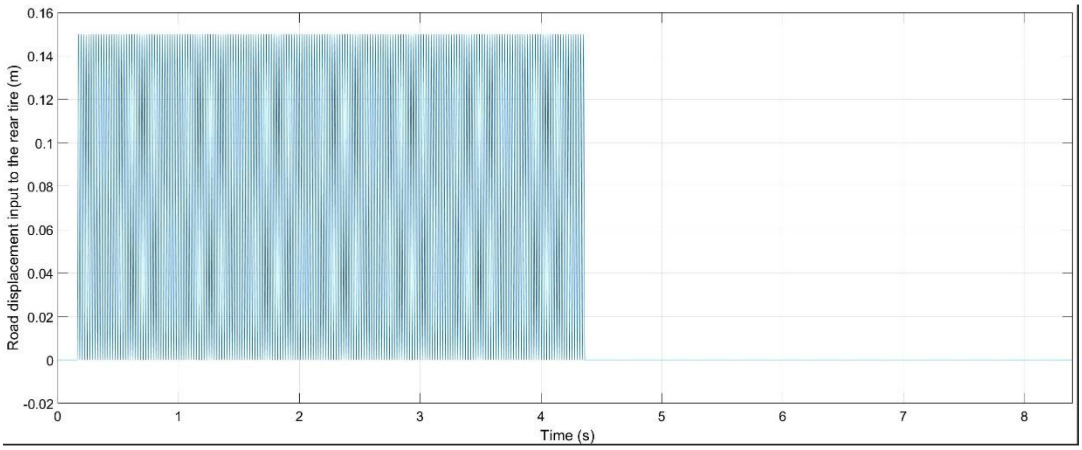


**Figure 2.6.** Bumpy road input to the rear tire as a function of time.

When we solve the equations of motions using the obtained initial conditions at position level and zero initial generalised velocities, we can find the time histories of the generalised coordinates, velocities, and accelerations for the given road profile with 60 km/h vehicle velocity and the battery located at $l_{Bat}$ = 0.5 m and these time histories are shown in Figures 2.7 through 2.27.

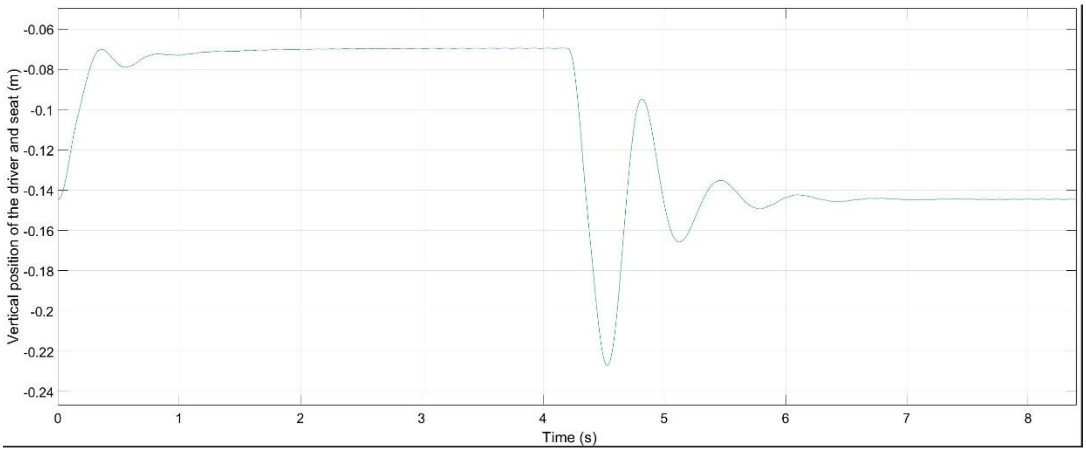


**Figure 2.7.** Vertical position of the driver and seat against time.

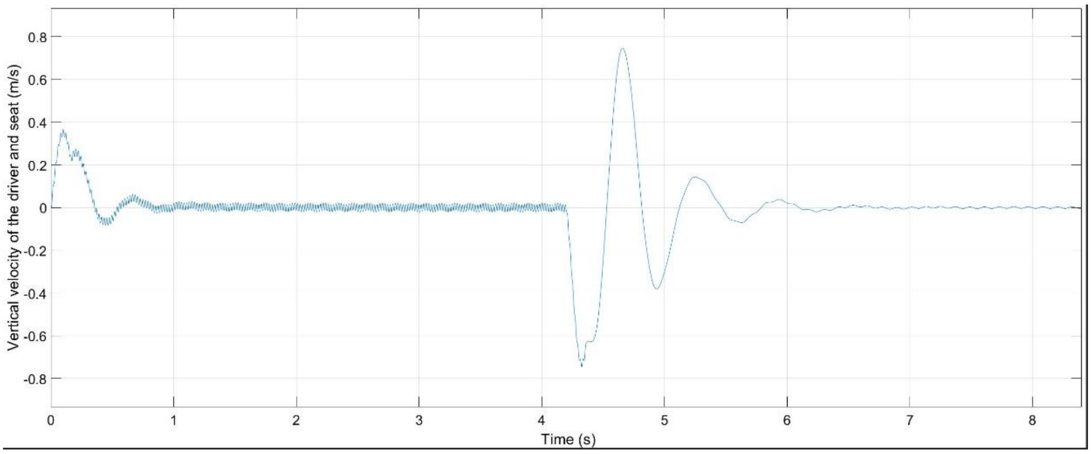


**Figure 2.8.** Vertical velocity of the driver and seat against time.

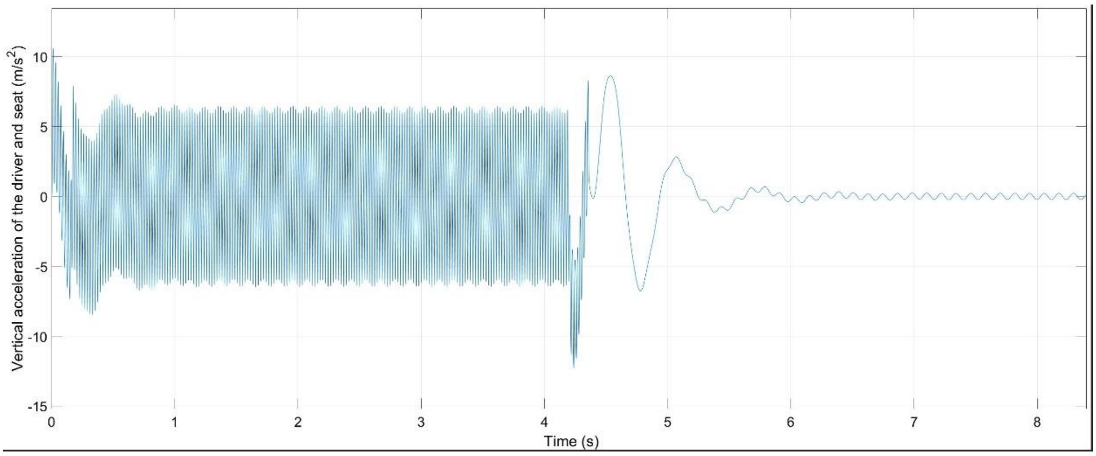


**Figure 2.9.** Vertical acceleration of the driver and seat against time.

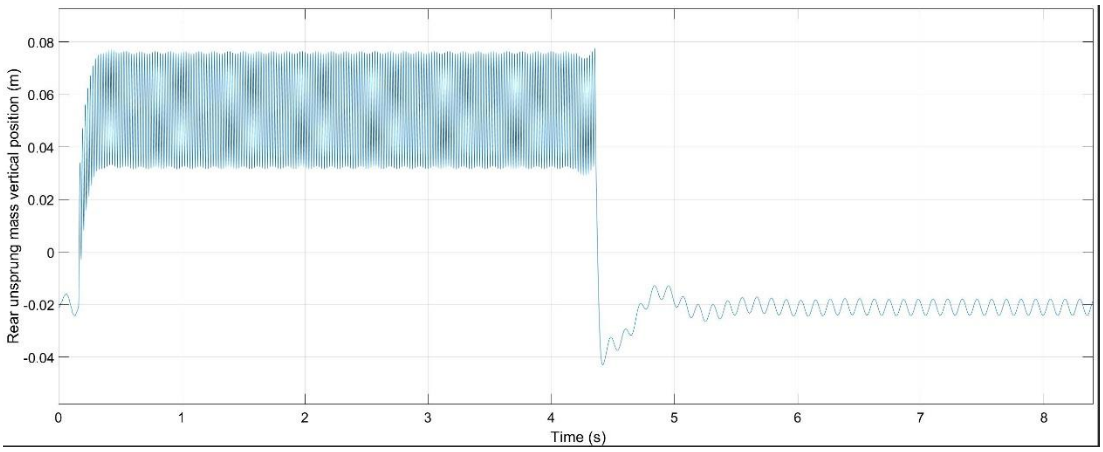


**Figure 2.10.** Rear unsprung mass vertical position against time.

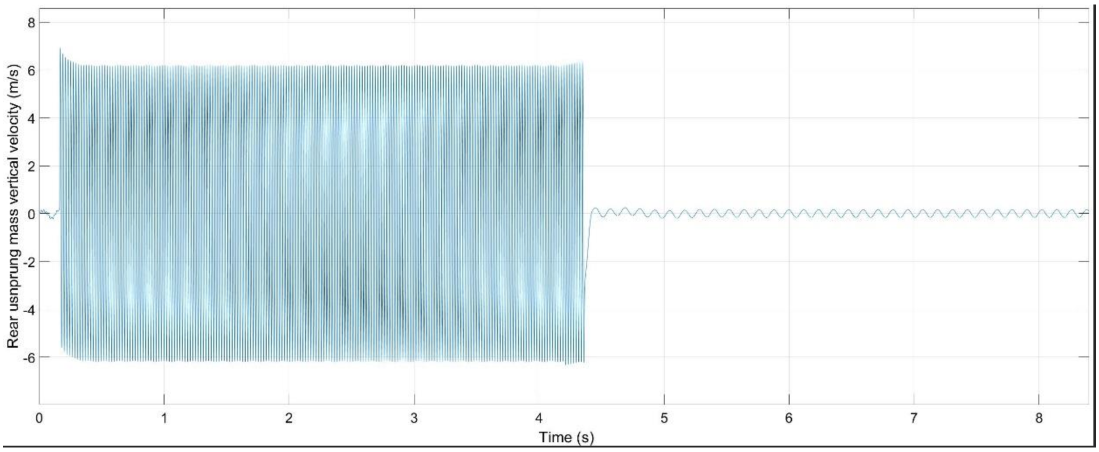


**Figure 2.11.** Rear unsprung mass vertical velocity against time.

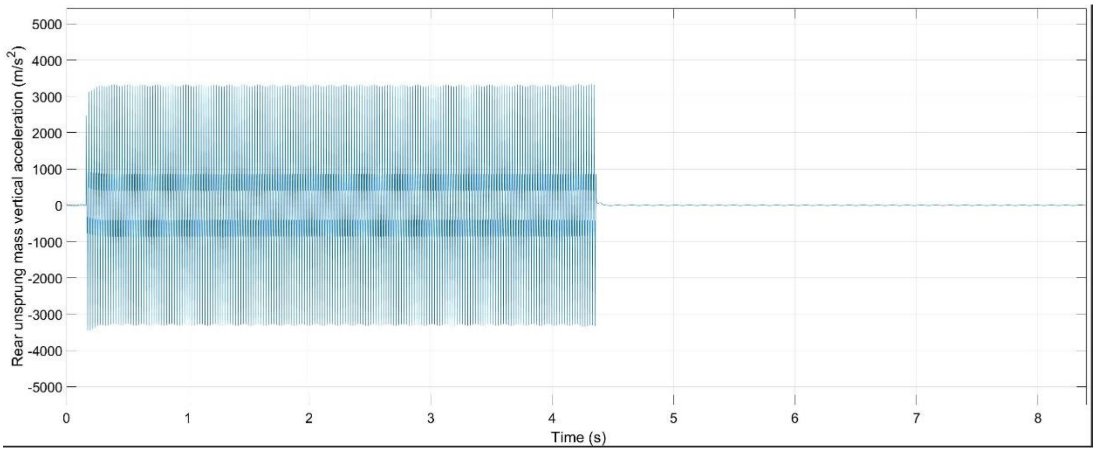


**Figure 2.12.** Rear unsprung mass vertical acceleration against time.

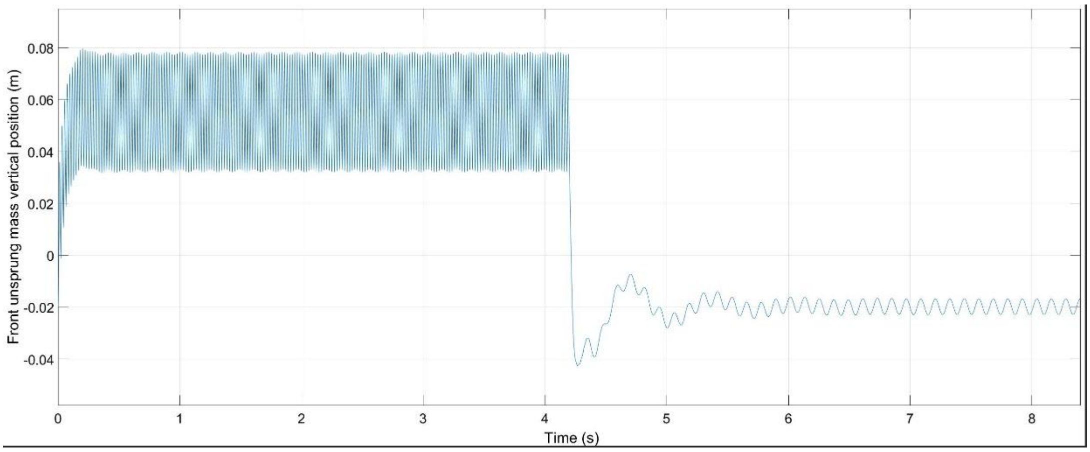


**Figure 2.13.** Front unsprung mass vertical position against time.

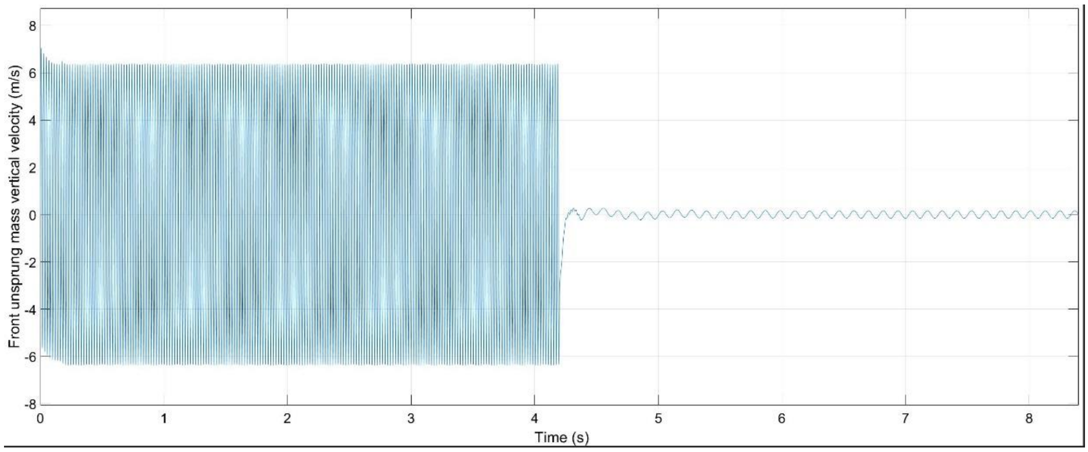


**Figure 2.14.** Front unsprung mass vertical velocity against time.

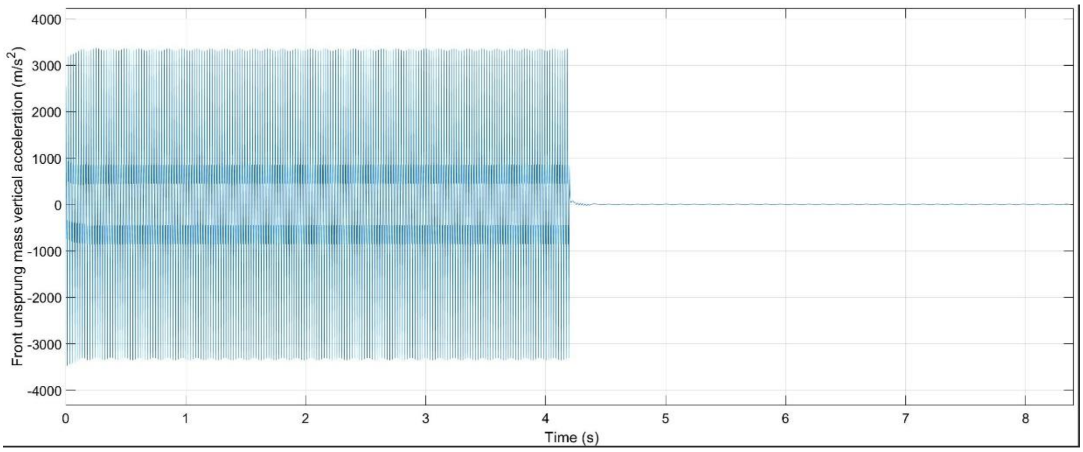


**Figure 2.15.** Front unsprung mass vertical acceleration against time.

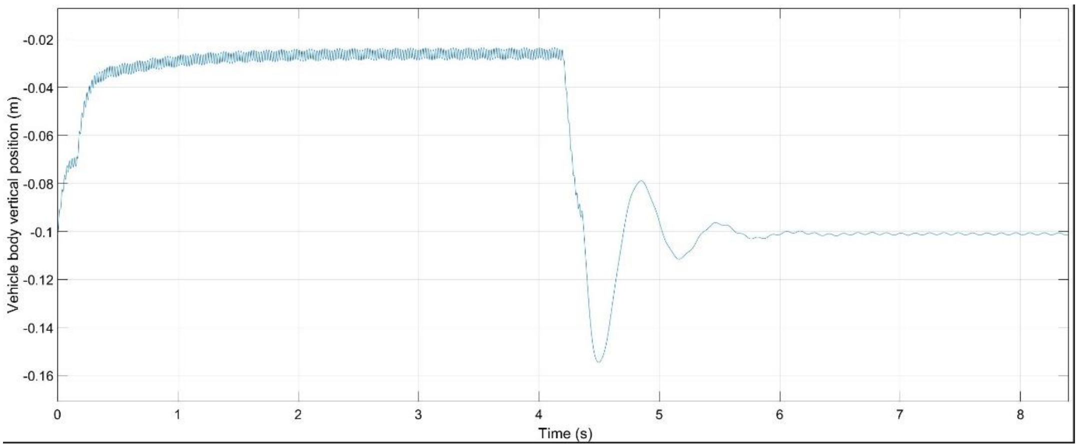


**Figure 2.16.** Vehicle body vertical position against time.

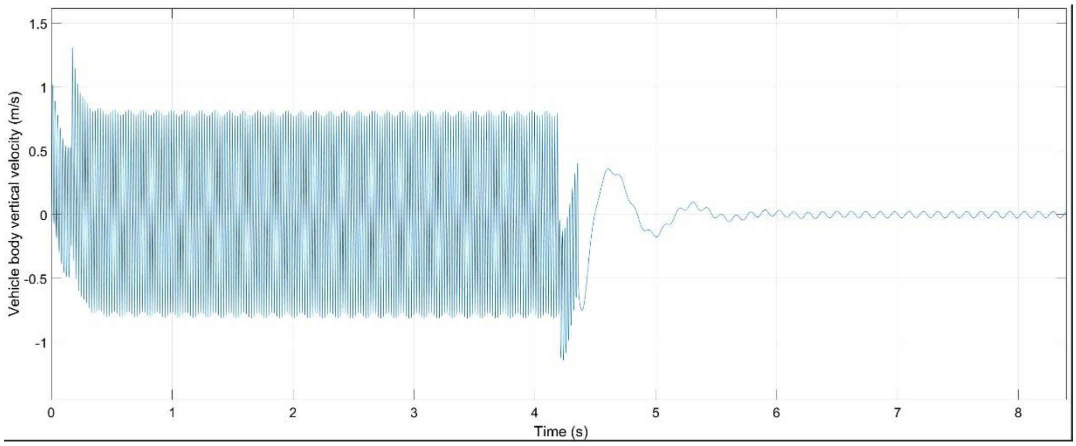


**Figure 2.17.** Vehicle body vertical velocity against time.

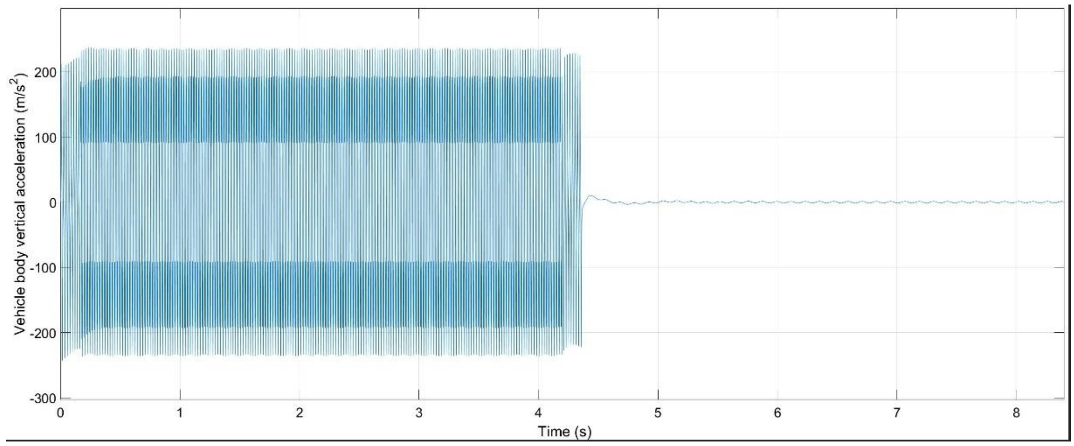


**Figure 2.18.** Vehicle body vertical acceleration against time.

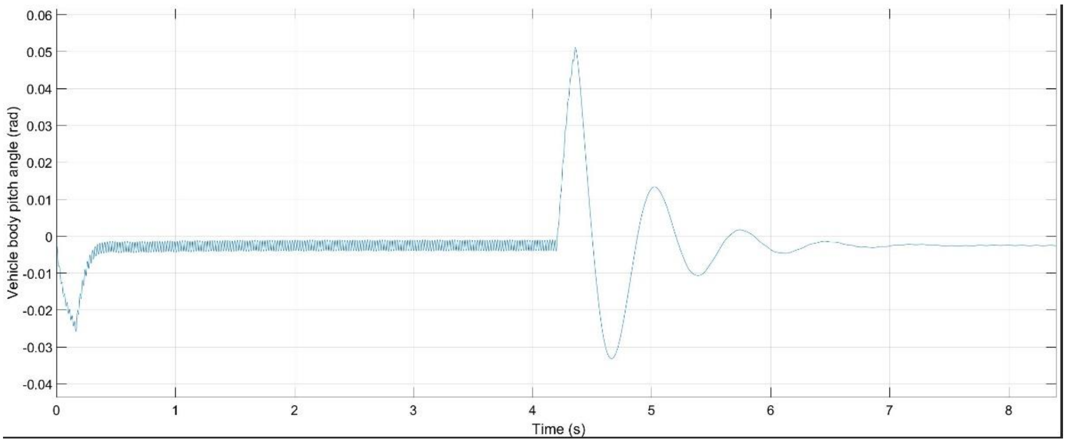


**Figure 2.19.** Vehicle body pitch angle against time.

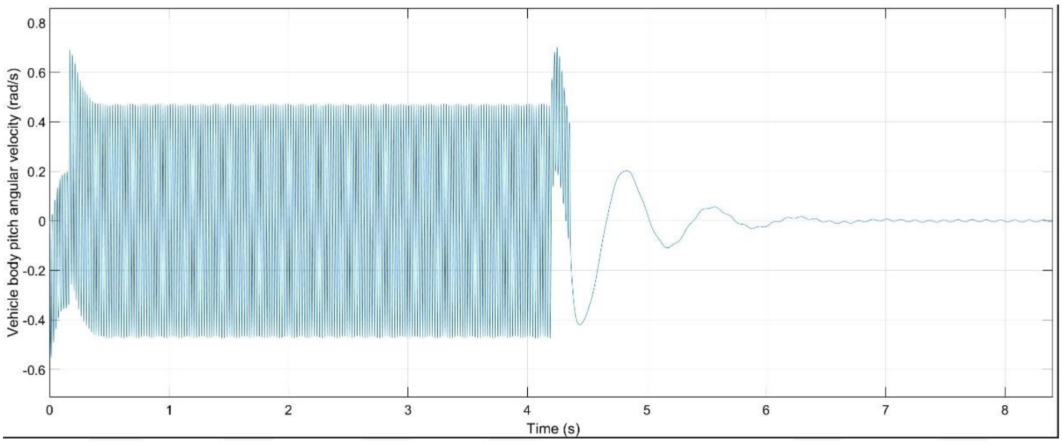


**Figure 2.20.** Vehicle body pitch angular velocity against time.

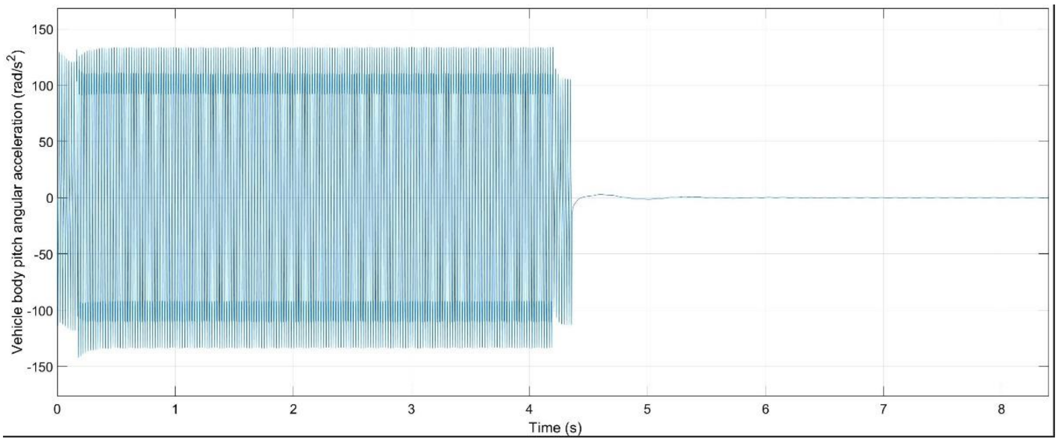


**Figure 2.21.** Vehicle body pitch angular acceleration against time.

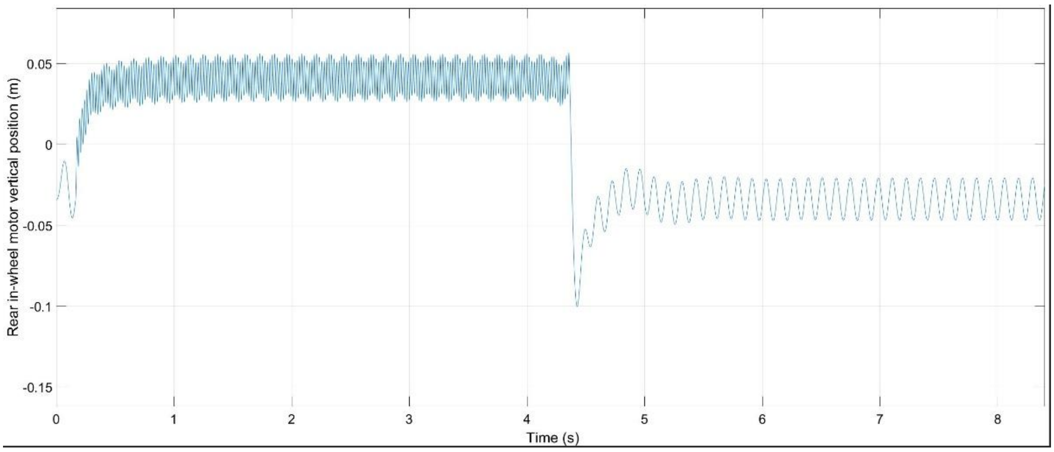


**Figure 2.22.** Rear in-wheel motor vertical position against time.

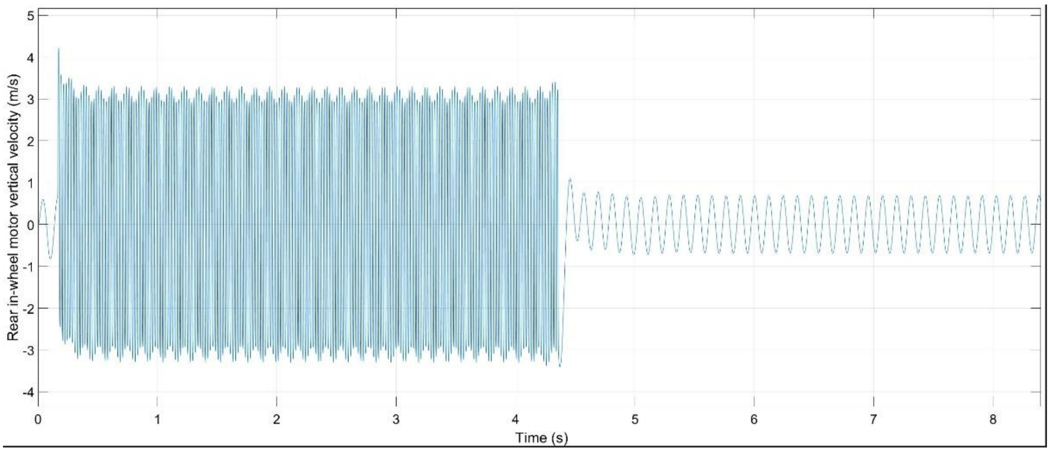


**Figure 2.23.** Rear in-wheel motor vertical velocity against time.

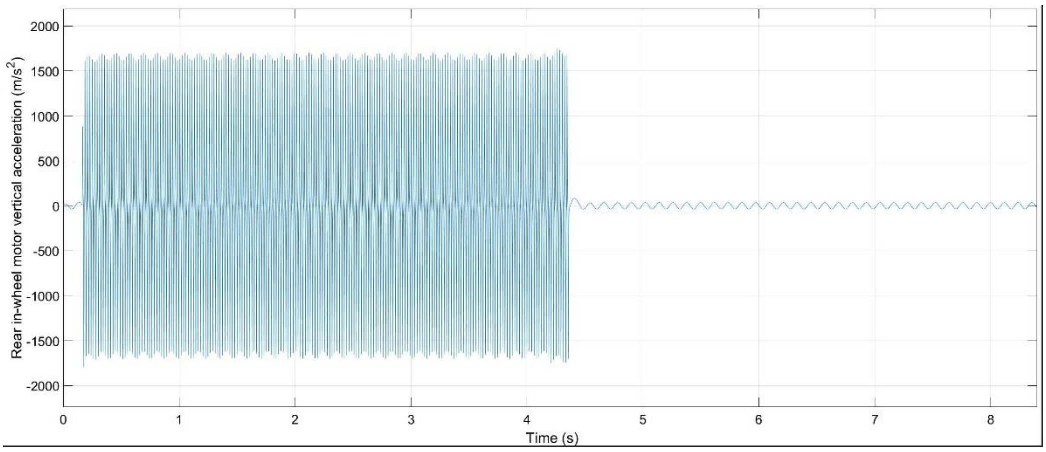


**Figure 2.24.** Rear in-wheel motor vertical acceleration against time.

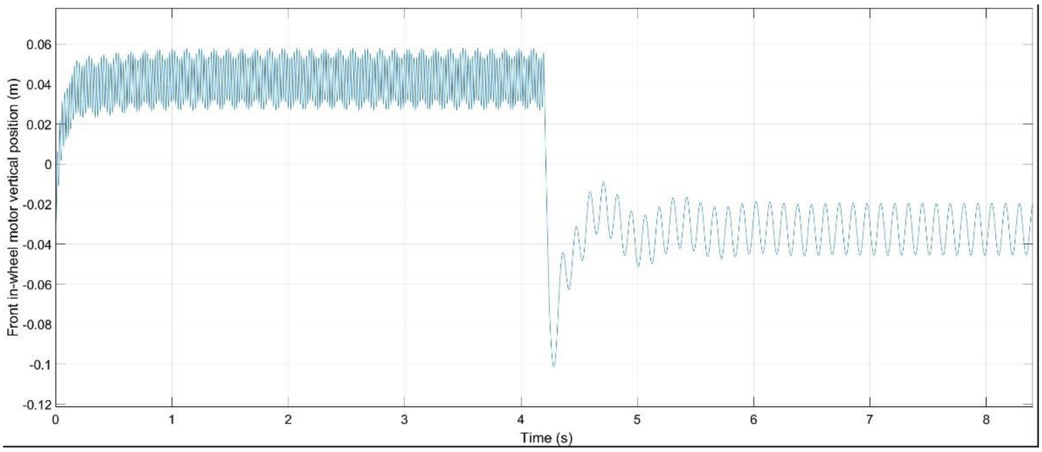


**Figure 2.25.** Front in-wheel motor vertical position against time.

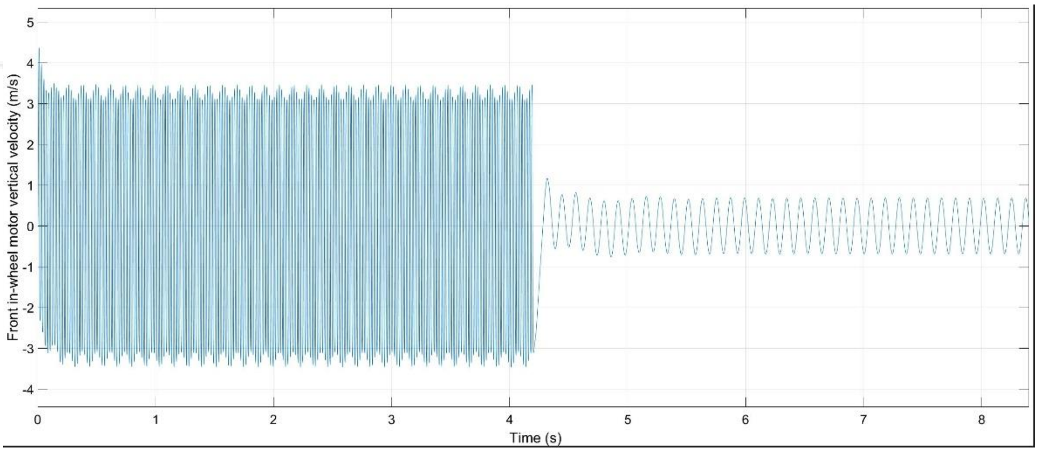


**Figure 2.26.** Front in-wheel motor vertical velocity against time.

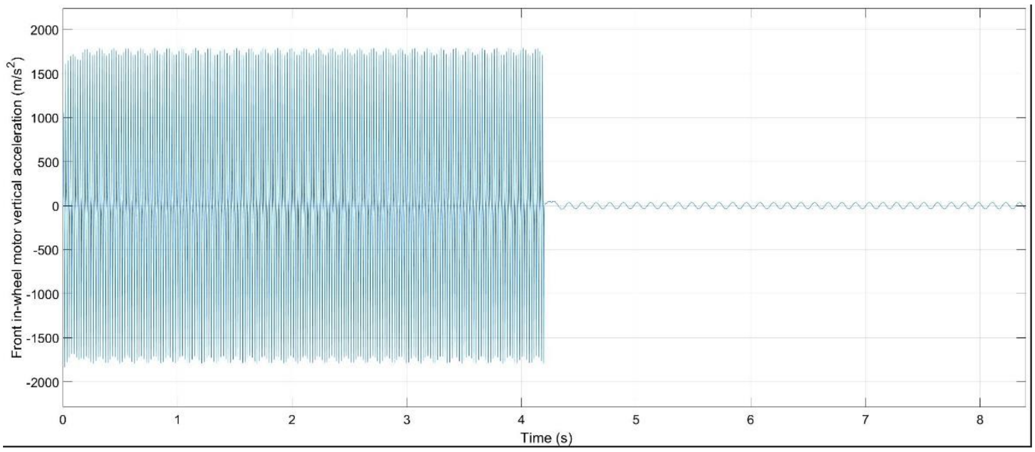


**Figure 2.27.** Front in-wheel motor vertical acceleration against time.

To compare ride comfort quality between different vehicle velocities and different battery locations, RMS accelerations of the driver and seat are computed using Equation (74) and are used for comparisons. The solution process exemplified above is repeated for each vehicle velocity, battery location and road profile.

# 3 RESULTS AND DISCUSSION

Dynamic model is numerically solved using vehicle speeds from 30 km/h to 120 km/h with 10 km/h increments and battery locations from -0.4 to 3.1 m when measured from the rear axle. All the model parameters are kept the same except the vehicle speed and battery location. The output response is considered as the vertical acceleration of the driver, and its RMS value is taken into account in the evaluations. The RMS acceleration values have been calculated for road profiles with speed bumps and speed humps that are given respectively in Figures 2.3. and 2.4.

## 3.1 Results for the Road Profile with Speed Bumps

The results of the RMS vertical acceleration of the driver and seat versus the battery location are given in Figure 3.1 and Table 3.1 for the road profile having speed bumps.

## 3.2 Results for the Road Profile with Speed Humps

The results of the RMS vertical acceleration of the driver and seat versus the battery location are given in Figure 3.2 and Table 3.2 for the road profile having speed humps.

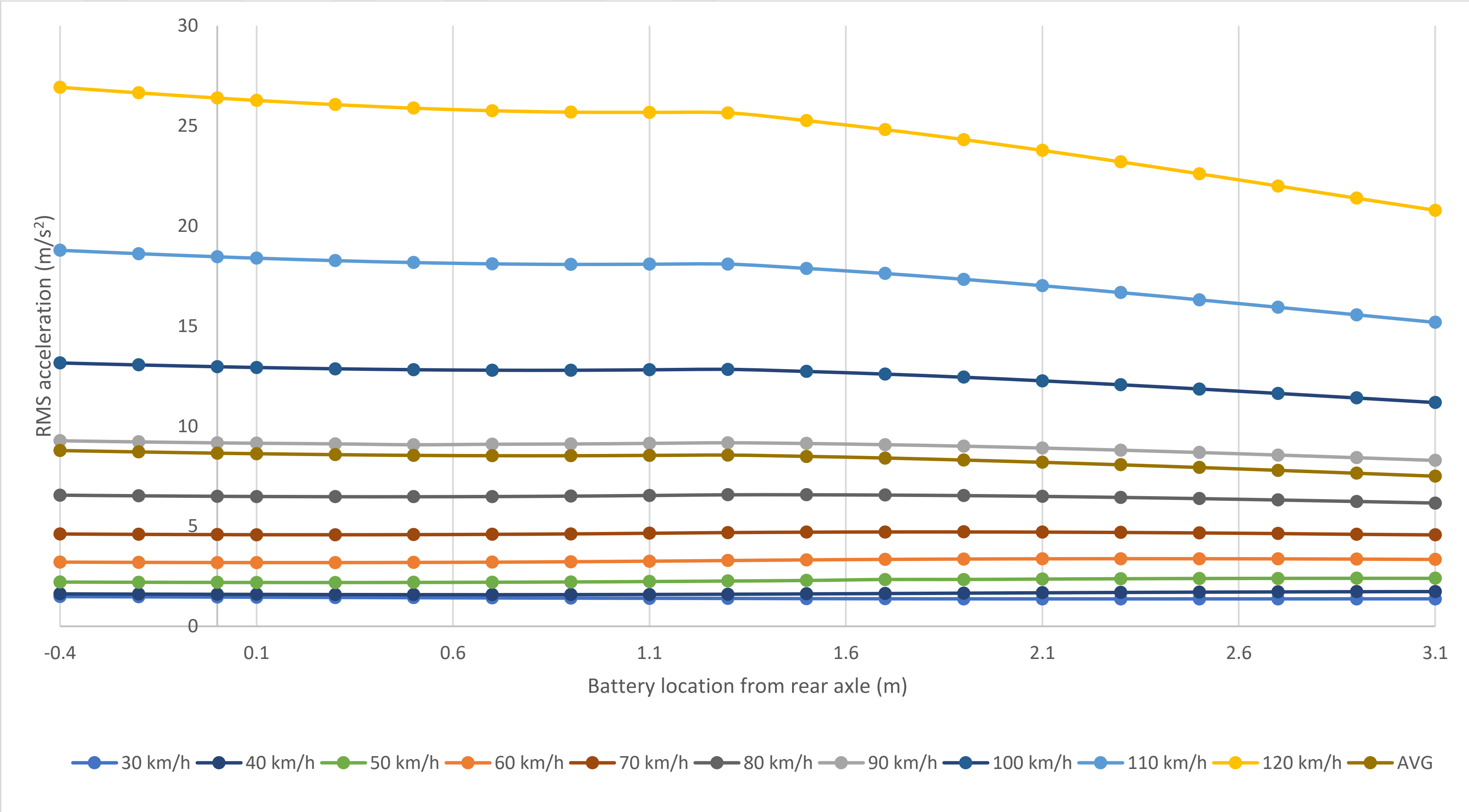


**Figure 3.1.** RMS acceleration versus battery location for bumpy road profile.

**Table 3.1.** RMS acceleration values (m/s$^2$) for different vehicle speeds and battery locations with bumpy road profile.

| $l_{Bat}$ (m) | $V$ Vehicle Speed (km/h) | | | | | | | | | | |
|---|---|---|---|---|---|---|---|---|---|---|---|
| | 30 | 40 | 50 | 60 | 70 | 80 | 90 | 100 | 110 | 120 | Average |
| 3.1 | 1.3728 | 1.7338 | 2.3956 | 3.3402 | 4.5673 | 6.1561 | 8.2848 | 11.1764 | 15.1831 | 20.7819 | 7.4992 |
| 2.9 | 1.3725 | 1.7278 | 2.397 | 3.3569 | 4.5941 | 6.2354 | 8.4219 | 11.4059 | 15.5593 | 21.385 | 7.64558 |
| 2.7 | 1.3715 | 1.7186 | 2.3942 | 3.369 | 4.6316 | 6.31 | 8.555 | 11.633 | 15.9362 | 21.996 | 7.79151 |
| 2.5 | 1.3703 | 1.7062 | 2.387 | 3.3757 | 4.6633 | 6.3782 | 8.6817 | 11.8542 | 16.3084 | 22.6036 | 7.93286 |
| 2.3 | 1.3695 | 1.6911 | 2.3754 | 3.3766 | 4.6881 | 6.4385 | 8.7994 | 12.0655 | 16.6698 | 23.1992 | 8.06731 |
| 2.1 | 1.3696 | 1.6739 | 2.3594 | 3.3713 | 4.705 | 6.4892 | 8.9055 | 12.2627 | 17.0138 | 23.7727 | 8.19231 |
| 1.9 | 1.3713 | 1.6553 | 2.3393 | 3.3596 | 4.7132 | 6.5286 | 8.9974 | 12.4418 | 17.3339 | 24.3136 | 8.3054 |
| 1.7 | 1.3753 | 1.6365 | 2.3384 | 3.3417 | 4.7121 | 6.5555 | 9.0729 | 12.5989 | 17.6237 | 24.812 | 8.4067 |
| 1.5 | 1.3821 | 1.6185 | 2.2894 | 3.3179 | 4.7017 | 6.5692 | 9.1301 | 12.7307 | 17.8777 | 25.2588 | 8.48761 |
| 1.3 | 1.392 | 1.6027 | 2.2615 | 3.2848 | 4.6821 | 6.5693 | 9.1679 | 12.8347 | 18.0916 | 25.6467 | 8.55333 |
| 1.1 | 1.3987 | 1.5905 | 2.2358 | 3.2525 | 4.6468 | 6.5341 | 9.1369 | 12.8133 | 18.0877 | 25.6725 | 8.53688 |
| 0.9 | 1.4067 | 1.5829 | 2.2155 | 3.2253 | 4.6158 | 6.5022 | 9.1072 | 12.7902 | 18.0769 | 25.6828 | 8.52055 |
| 0.7 | 1.4168 | 1.5798 | 2.2008 | 3.2046 | 4.5931 | 6.4814 | 9.0939 | 12.7922 | 18.1057 | 25.7551 | 8.52234 |
| 0.5 | 1.4283 | 1.5809 | 2.1917 | 3.1909 | 4.5789 | 6.4718 | 9.0692 | 12.8176 | 18.1703 | 25.8822 | 8.53818 |
| 0.3 | 1.4406 | 1.5854 | 2.188 | 3.184 | 4.5733 | 6.4731 | 9.1134 | 12.8642 | 18.2664 | 26.0595 | 8.57479 |
| 0.1 | 1.4531 | 1.5929 | 2.1893 | 3.1836 | 4.5757 | 6.4846 | 9.144 | 12.9294 | 18.3894 | 26.27 | 8.6212 |
| 0 | 1.4593 | 1.5974 | 2.1916 | 3.1857 | 4.5797 | 6.4938 | 9.1638 | 12.9681 | 18.4594 | 26.389 | 8.64878 |
| -0.2 | 1.4713 | 1.6078 | 2.1991 | 3.1936 | 4.5926 | 6.5185 | 9.2112 | 13.0559 | 18.6138 | 26.6469 | 8.71107 |
| -0.4 | 1.4827 | 1.6194 | 2.2096 | 3.2061 | 4.6112 | 6.5501 | 9.2674 | 13.1551 | 18.7833 | 26.9253 | 8.78102 |

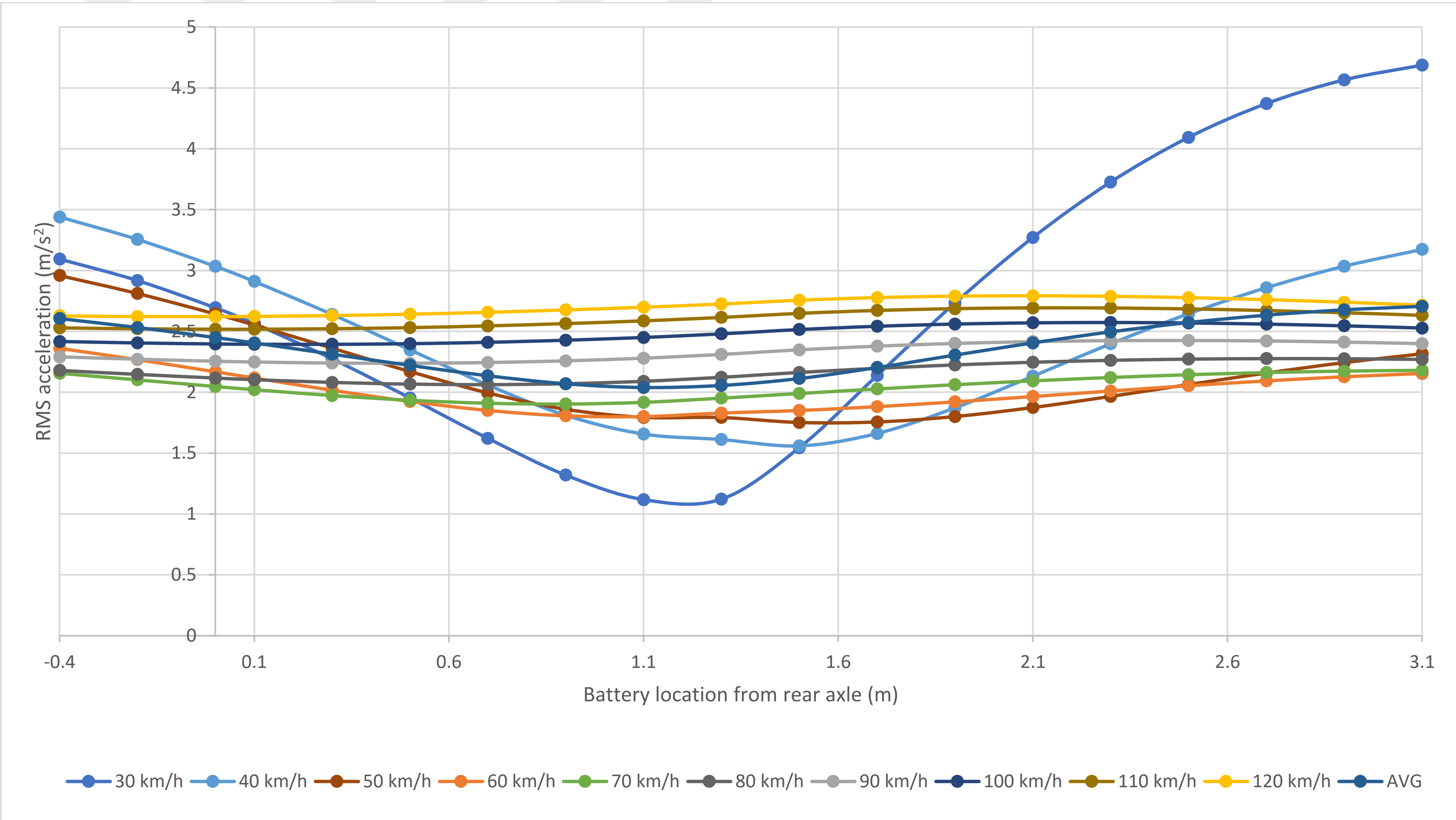


**Figure 3.2.** RMS acceleration versus battery location for the road profile with speed humps.

**Table 3.2.** RMS acceleration values (m/s$^2$) for different vehicle speeds and battery locations with the road profile having speed humps.

| $l_{Bat}$ (m) | $V$ Vehicle Speed (km/h) | | | | | | | | | | |
|---|---|---|---|---|---|---|---|---|---|---|---|
| | 30 | 40 | 50 | 60 | 70 | 80 | 90 | 100 | 110 | 120 | Average |
| 3.1 | 4.6872 | 3.1731 | 2.3161 | 2.1543 | 2.1804 | 2.2699 | 2.3992 | 2.5276 | 2.632 | 2.7154 | 2.70552 |
| 2.9 | 4.5659 | 3.0353 | 2.2435 | 2.1272 | 2.1737 | 2.2754 | 2.4123 | 2.5456 | 2.6533 | 2.7397 | 2.67719 |
| 2.7 | 4.3712 | 2.8589 | 2.158 | 2.0933 | 2.1616 | 2.2763 | 2.4213 | 2.5597 | 2.6711 | 2.7605 | 2.63319 |
| 2.5 | 4.0936 | 2.6446 | 2.0634 | 2.0537 | 2.144 | 2.272 | 2.4253 | 2.5692 | 2.6844 | 2.777 | 2.57272 |
| 2.3 | 3.727 | 2.3978 | 1.9659 | 2.0102 | 2.1212 | 2.2622 | 2.4238 | 2.573 | 2.6921 | 2.788 | 2.49612 |
| 2.1 | 3.2708 | 2.1317 | 1.8745 | 1.965 | 2.0936 | 2.2464 | 2.4159 | 2.5702 | 2.6933 | 2.7925 | 2.40539 |
| 1.9 | 2.7331 | 1.8718 | 1.8004 | 1.9212 | 2.062 | 2.2246 | 2.401 | 2.5601 | 2.6868 | 2.7893 | 2.30503 |
| 1.7 | 2.1377 | 1.6615 | 1.756 | 1.8819 | 2.027 | 2.1966 | 2.3787 | 2.5419 | 2.6719 | 2.7774 | 2.20306 |
| 1.5 | 1.5444 | 1.5595 | 1.7517 | 1.8503 | 1.9898 | 2.1626 | 2.3486 | 2.5151 | 2.6479 | 2.7561 | 2.1126 |
| 1.3 | 1.1219 | 1.6116 | 1.7925 | 1.8291 | 1.9517 | 2.123 | 2.3109 | 2.4795 | 2.6146 | 2.725 | 2.05598 |
| 1.1 | 1.1183 | 1.6568 | 1.7942 | 1.8002 | 1.9172 | 2.09 | 2.2799 | 2.4502 | 2.5867 | 2.6986 | 2.03921 |
| 0.9 | 1.3198 | 1.8107 | 1.8601 | 1.8064 | 1.9032 | 2.0702 | 2.2581 | 2.4276 | 2.5641 | 2.6764 | 2.06966 |
| 0.7 | 1.6217 | 2.0597 | 1.9946 | 1.8509 | 1.9099 | 2.0627 | 2.2442 | 2.4103 | 2.5452 | 2.6569 | 2.13561 |
| 0.5 | 1.9533 | 2.3486 | 2.1702 | 1.9244 | 1.9345 | 2.0669 | 2.2383 | 2.399 | 2.5309 | 2.6412 | 2.22073 |
| 0.3 | 2.2746 | 2.6394 | 2.362 | 2.0164 | 1.9731 | 2.0811 | 2.24 | 2.3937 | 2.5218 | 2.6298 | 2.31319 |
| 0.1 | 2.5643 | 2.91 | 2.5522 | 2.1171 | 2.0211 | 2.1034 | 2.2486 | 2.3944 | 2.5179 | 2.6232 | 2.40522 |
| 0 | 2.6936 | 3.034 | 2.643 | 2.1681 | 2.0473 | 2.1168 | 2.255 | 2.3967 | 2.5178 | 2.6218 | 2.44941 |
| -0.2 | 2.9175 | 3.2553 | 2.8113 | 2.2677 | 2.1016 | 2.1468 | 2.2714 | 2.4051 | 2.5213 | 2.6223 | 2.53203 |
| -0.4 | 3.0942 | 3.44 | 2.9586 | 2.3604 | 2.1557 | 2.1792 | 2.2912 | 2.4171 | 2.5291 | 2.6272 | 2.60527 |

### 3.3 Optimal Battery Location for Ride Comfort

Lower RMS acceleration values mean better ride comfort for vehicle driver and passengers. To find the optimal battery location for ride comfort, we need to find the battery location that gives the lowest RMS value.

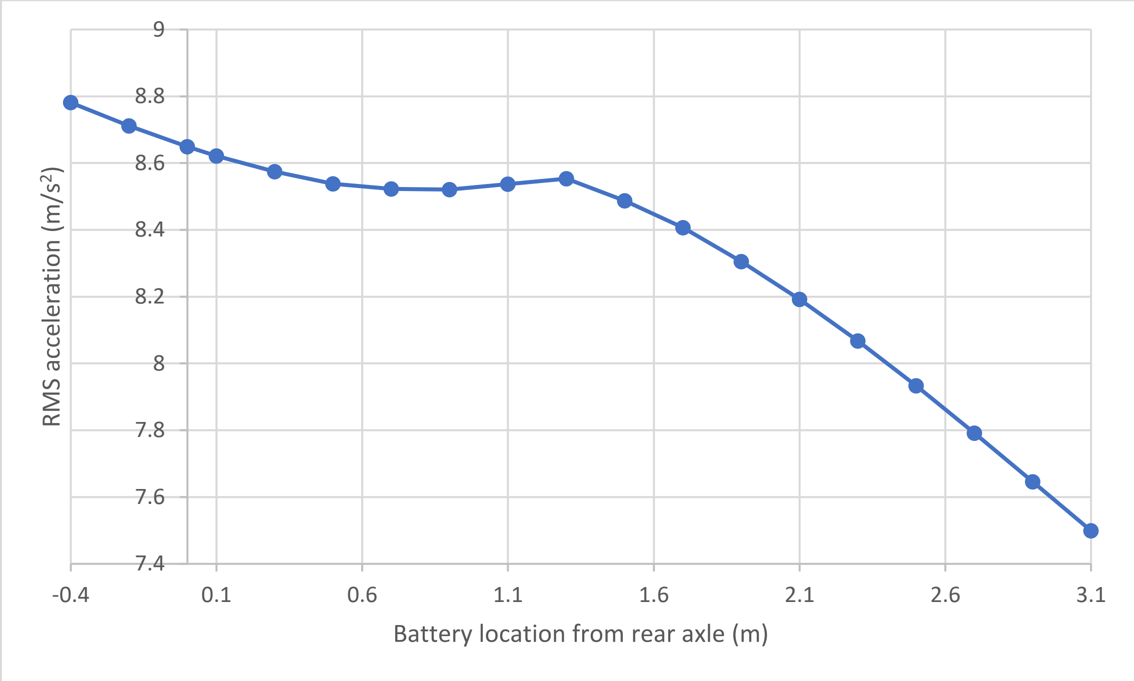


**Figure 3.3.** Average RMS values for different battery locations with bumpy road.

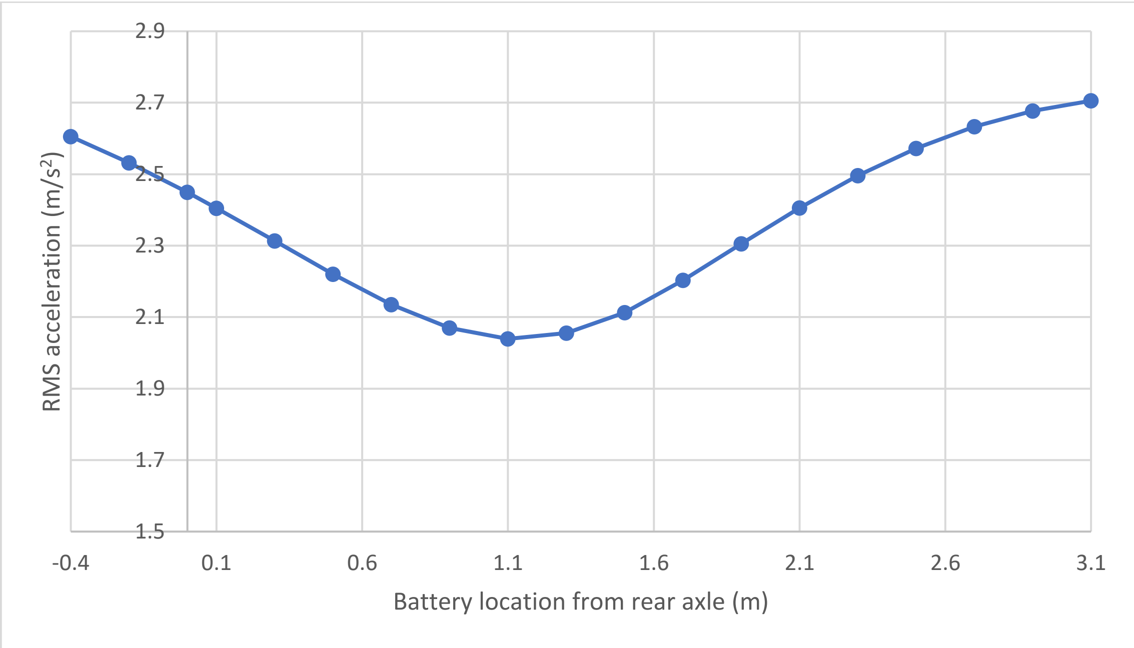


**Figure 3.4.** Average RMS values for different battery locations with the road having speed humps.

When vehicle is passing through speed bumps, the RMS acceleration of the driver and seat is the lowest with the battery located ahead of the front axle. RMS value increases as the battery location is shifted towards the rear of the vehicle. The RMS acceleration of the driver and seat increases with vehicle speed. However, when vehicle is passing through speed humps, the lowest RMS vertical acceleration of the driver and seat is attained with the battery located at the middle of the rear and front axles. At lower speeds, the effect of battery location for ride comfort is significant. As the speed increases, the effect of battery location for ride comfort decreases drastically.

For passenger cars, the road profile with speed humps represents daily usage and city driving scenarios better. The optimal battery location for ride comfort of passenger cars in daily driving is the middle of rear and front axles of the vehicle.

For off-road vehicles and passenger cars that are used in rural areas, dirt roads and cobblestone roads, bumpy road profile represents the corresponding driving scenarios better. The optimal battery location for ride comfort of such usages is the front of the vehicle.

If we want to design for highway usage with high speeds, the optimal battery location for ride comfort is between the rear axle and middle of the car.

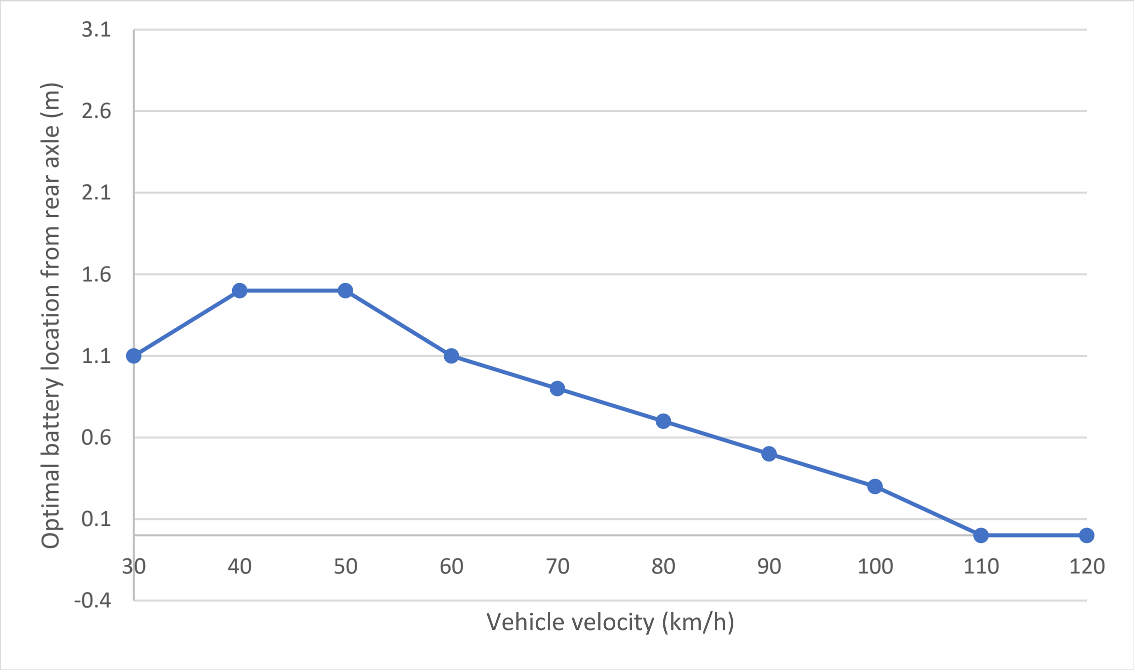


**Figure 3.5.** Optimal battery locations versus the corresponding velocity values for the road having speed humps.

If we want to design low speed off-road vehicles or construction and agricultural vehicles, the optimal battery location for ride comfort is between the middle of the vehicle and its rear axle and close to the rear axle.

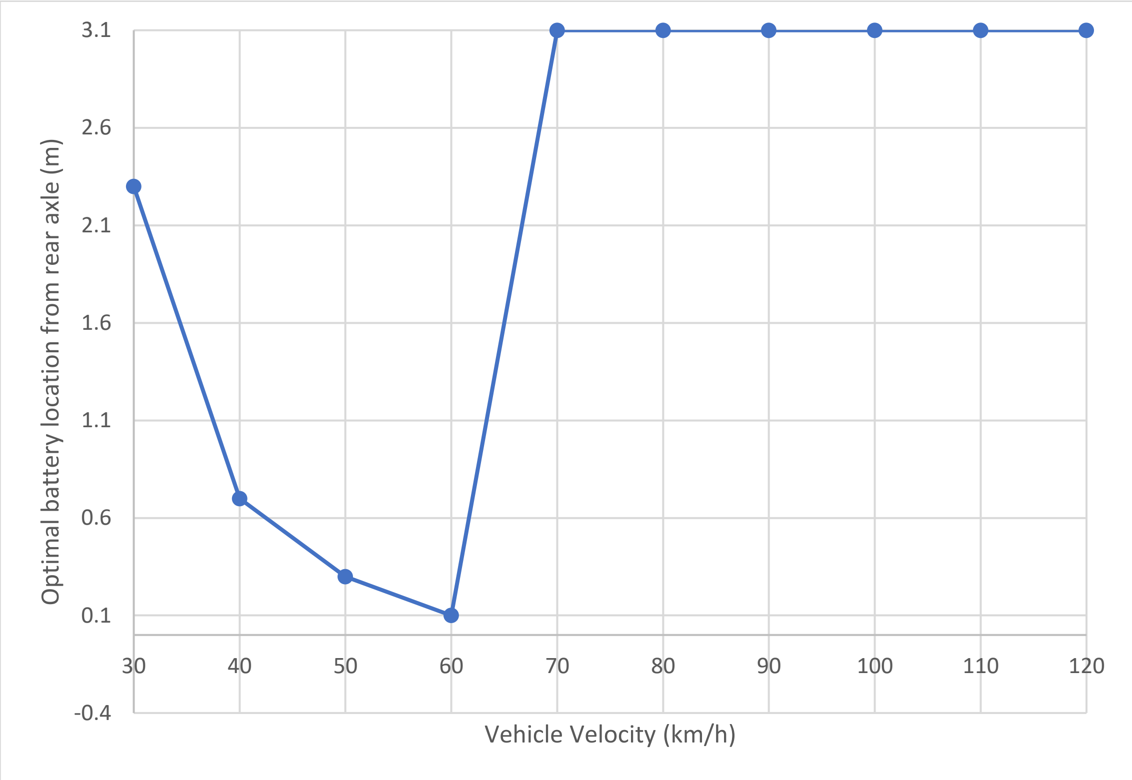


**Figure 3.6.** Optimal battery locations versus the corresponding velocity values for bumpy road.

### 3.4 Comparison Between Other Studies and Real-World Vehicles

In most of the recent electric passenger cars in the market, the battery is placed between rear and front axles of the vehicle (EVSpecifications, 2022; Ganesh, 2021). This is because there is a huge amount of spare space between rear and front axle, under the floor of the vehicle. Battery is the largest part of the vehicle in size and larger battery means higher driving range. Also, many vehicle manufacturers use the battery case as a part of chassis structure for rigidity and strength. For ride comfort, our study and the previous literature (Wang, 2020) found that placement of the battery in the middle of the rear and front axles is suitable for ride comfort. However, it is shown in this thesis that the optimal battery location for ride comfort in off-road usages is the front of the front axle of the vehicle.

## 3.5 Further Analyses to Understand the Effect of Battery Location on Ride Comfort with Different Road Roughness Profiles

In this section further driving scenarios are considered by using sinusoidal road profiles. Six different amplitude values, namely, $A$ = 0.01, 0.02, 0.03, 0.04, 0.05 and 0.1 m, and eight different wavelengths, namely, $\lambda$ = 0.2, 0.5, 1, 5, 10, 15, 20 and 30 m are used in the analyses. Road profile's total length is 60 m for all amplitudes and wavelengths without any straight section. The road input to the front tire is represented by $u_F = A\sin(\frac{2\pi V}{\lambda}t)$ and the road input to the rear tire is $u_R = A\sin(\frac{2\pi V}{\lambda}(t-\tau))$ where $\tau = l/V$, as previously explained. In this manner, 48 different road profiles are taken into account.

For each road profile, three different vehicle velocities, namely, $V$ = 30, 50 and 96 km/h, are used. Hence, 144 different riding scenarios are considered. For battery locations, 36 different $l_{Bat}$ values from -0.4 to 3.1 m with increments of 0.1 m are used. Therefore, 5184 different analyses are conducted. In-wheel motors' rotating unbalance forces are neglected in these analyses to concentrate on the effects of road roughness better. The analyses are performed using a variable-step solver. Results of the analyses are given in Tables 3.3 through 3.8, where $a_{RMS.min}$ is the minimum RMS value obtained for the vertical acceleration of the driver and seat, and $l_{Bat,opt}$ is the corresponding optimal value of battery location.

**Table 3.3.** Analysis results for *A* = 0.01 m.

| *A* = 0.01 m | | | | | | | | |
|---|---|---|---|---|---|---|---|---|
| $V$ = 30 km/h | | | $V$ = 50 km/h | | | $V$ = 96 km/h | | |
| $\lambda$ (m) | $l_{Bat,opt}$ (m) | $a_{RMS.min}$ (m/s$^2$) | $\lambda$ (m) | $l_{Bat,opt}$ (m) | $a_{RMS.min}$ (m/s$^2$) | $\lambda$ (m) | $l_{Bat,opt}$ (m) | $a_{RMS.min}$ (m/s$^2$) |
| 0.2 | 1.2 | 0.0010 | 0.2 | 1.2 | 0.0007 | 0.2 | 1.2 | 0.0006 |
| 0.5 | 1.3 | 0.0625 | 0.5 | 1.3 | 0.0437 | 0.5 | 1.7 | 0.0346 |
| 1 | 1.3 | 0.2770 | 1 | 1.2 | 0.2006 | 1 | 1.3 | 0.1740 |
| 5 | 1.2 | 0.1315 | 5 | 1.3 | 0.5631 | 5 | 1.4 | 0.6513 |
| 10 | -0.4 | 0.2281 | 10 | -0.4 | 0.7590 | 10 | 0.4 | 1.4281 |
| 15 | -0.4 | 0.1404 | 15 | -0.4 | 0.3337 | 15 | -0.4 | 1.3397 |
| 20 | -0.4 | 0.1001 | 20 | -0.4 | 0.1921 | 20 | -0.4 | 0.8117 |
| 30 | -0.4 | 0.0638 | 30 | -0.4 | 0.1021 | 30 | -0.4 | 0.2981 |

**Table 3.4.** Analysis results for $A$ = 0.02 m.

| $A$ = 0.02 m | | | | | | | | |
|---|---|---|---|---|---|---|---|---|
| $V$ = 30 km/h | | | $V$ = 50 km/h | | | $V$ = 96 km/h | | |
| $\lambda$ (m) | $l_{Bat,opt}$ (m) | $a_{RMS.min}$ (m/s$^2$) | $\lambda$ (m) | $l_{Bat,opt}$ (m) | $a_{RMS.min}$ (m/s$^2$) | $\lambda$ (m) | $l_{Bat,opt}$ (m) | $a_{RMS.min}$ (m/s$^2$) |
| 0.2 | 1.2 | 0.0018 | 0.2 | 1.3 | 0.0014 | 0.2 | 1.3 | 0.0031 |
| 0.5 | 1.4 | 0.1249 | 0.5 | 1.3 | 0.0797 | 0.5 | 1.2 | 0.0733 |
| 1 | 1.2 | 0.5749 | 1 | 1 | 0.3911 | 1 | 1.2 | 0.3318 |
| 5 | 1.2 | 0.2497 | 5 | 1.3 | 1.1148 | 5 | 1.5 | 1.2885 |
| 10 | -0.4 | 0.4557 | 10 | -0.4 | 1.5058 | 10 | 0.4 | 2.8392 |
| 15 | -0.4 | 0.2815 | 15 | -0.4 | 0.6651 | 15 | -0.4 | 2.6304 |
| 20 | -0.4 | 0.2008 | 20 | -0.4 | 0.3808 | 20 | -0.4 | 1.5956 |
| 30 | -0.4 | 0.1251 | 30 | -0.4 | 0.2037 | 30 | -0.4 | 0.5864 |

**Table 3.5.** Analysis results for $A$ = 0.03 m.

| $A$ = 0.03 m | | | | | | | | |
|---|---|---|---|---|---|---|---|---|
| $V$ = 30 km/h | | | $V$ = 50 km/h | | | $V$ = 96 km/h | | |
| $\lambda$ (m) | $l_{Bat,opt}$ (m) | $a_{RMS.min}$ (m/s$^2$) | $\lambda$ (m) | $l_{Bat,opt}$ (m) | $a_{RMS.min}$ (m/s$^2$) | $\lambda$ (m) | $l_{Bat,opt}$ (m) | $a_{RMS.min}$ (m/s$^2$) |
| 0.2 | 1.3 | 0.0027 | 0.2 | 1.3 | 0.0040 | 0.2 | 1.3 | 0.0256 |
| 0.5 | 1.4 | 0.1886 | 0.5 | 1.3 | 0.1297 | 0.5 | 1.2 | 0.1590 |
| 1 | 1.2 | 0.8987 | 1 | 1.3 | 0.5955 | 1 | 1.2 | 0.5087 |
| 5 | 1.2 | 0.3454 | 5 | 1.3 | 1.6293 | 5 | 1.4 | 1.9073 |
| 10 | -0.4 | 0.6858 | 10 | -0.4 | 2.2428 | 10 | 0.3 | 4.2422 |
| 15 | -0.4 | 0.4251 | 15 | -0.4 | 0.9982 | 15 | -0.4 | 3.8985 |
| 20 | -0.4 | 0.3034 | 20 | -0.4 | 0.5706 | 20 | -0.4 | 2.3791 |
| 30 | -0.4 | 0.1866 | 30 | -0.4 | 0.3056 | 30 | -0.4 | 0.8730 |

**Table 3.6.** Analysis results for $A$ = 0.04 m.

| $A$ = 0.04 m | | | | | | | | |
|---|---|---|---|---|---|---|---|---|
| $V$ = 30 km/h | | | $V$ = 50 km/h | | | $V$ = 96 km/h | | |
| $\lambda$ (m) | $l_{Bat,opt}$ (m) | $a_{RMS.min}$ (m/s$^2$) | $\lambda$ (m) | $l_{Bat,opt}$ (m) | $a_{RMS.min}$ (m/s$^2$) | $\lambda$ (m) | $l_{Bat,opt}$ (m) | $a_{RMS.min}$ (m/s$^2$) |
| 0.2 | 1.3 | 0.0050 | 0.2 | 1.3 | 0.0082 | 0.2 | 1.3 | 0.0873 |
| 0.5 | 1.3 | 0.2536 | 0.5 | 1.4 | 0.1822 | 0.5 | 1.4 | 0.3757 |
| 1 | 1.1 | 1.2436 | 1 | 1.2 | 0.8109 | 1 | 1.1 | 0.6919 |
| 5 | 1.2 | 0.4143 | 5 | 1.3 | 2.0909 | 5 | 1.3 | 2.4935 |
| 10 | -0.4 | 0.9188 | 10 | -0.4 | 2.9685 | 10 | 0.3 | 5.6417 |
| 15 | -0.4 | 0.5716 | 15 | -0.4 | 1.3335 | 15 | -0.4 | 5.1375 |
| 20 | -0.4 | 0.4080 | 20 | -0.4 | 0.7618 | 20 | -0.4 | 3.1598 |
| 30 | -0.4 | 0.2488 | 30 | -0.4 | 0.4082 | 30 | -0.4 | 1.1598 |

**Table 3.7.** Analysis results for $A$ = 0.05 m.

| $A$ = 0.05 m | | | | | | | | |
|---|---|---|---|---|---|---|---|---|
| $V$ = 30 km/h | | | $V$ = 50 km/h | | | $V$ = 96 km/h | | |
| $\lambda$ (m) | $l_{Bat,opt}$ (m) | $a_{RMS.min}$ (m/s$^2$) | $\lambda$ (m) | $l_{Bat,opt}$ (m) | $a_{RMS.min}$ (m/s$^2$) | $\lambda$ (m) | $l_{Bat,opt}$ (m) | $a_{RMS.min}$ (m/s$^2$) |
| 0.2 | 1.3 | 0.0087 | 0.2 | 1.3 | 0.0430 | 0.2 | 1.3 | 0.2451 |
| 0.5 | 1.3 | 0.3251 | 0.5 | 1.5 | 0.2793 | 0.5 | 1.5 | 0.7320 |
| 1 | 1.2 | 1.6014 | 1 | 1.3 | 1.0418 | 1 | 1 | 0.8589 |
| 5 | 1.2 | 0.4970 | 5 | 1.2 | 2.5081 | 5 | 1.3 | 2.9689 |
| 10 | -0.4 | 1.1548 | 10 | -0.4 | 3.6820 | 10 | 0.2 | 7.0486 |
| 15 | -0.4 | 0.7209 | 15 | -0.4 | 1.6713 | 15 | -0.4 | 6.3445 |
| 20 | -0.4 | 0.5147 | 20 | -0.4 | 0.9544 | 20 | -0.4 | 3.9381 |
| 30 | -0.4 | 0.3121 | 30 | -0.4 | 0.5117 | 30 | -0.4 | 1.4472 |

**Table 3.8.** Analysis results for $A$ = 0.1 m.

| $A$ = 0.1 m | | | | | | | | |
|---|---|---|---|---|---|---|---|---|
| $V$ = 30 km/h | | | $V$ = 50 km/h | | | $V$ = 96 km/h | | |
| $\lambda$ (m) | $l_{Bat,opt}$ (m) | $a_{RMS.min}$ (m/s$^2$) | $\lambda$ (m) | $l_{Bat,opt}$ (m) | $a_{RMS.min}$ (m/s$^2$) | $\lambda$ (m) | $l_{Bat,opt}$ (m) | $a_{RMS.min}$ (m/s$^2$) |
| 0.2 | 1.3 | 0.2122 | 0.2 | 1.3 | 0.5123 | 0.2 | 1.4 | 2.4692 |
| 0.5 | 1.4 | 0.9375 | 0.5 | 1.5 | 1.8071 | 0.5 | 1.3 | 7.8039 |
| 1 | 1.3 | 3.4033 | 1 | 1.4 | 1.8560 | 1 | 1 | 2.9883 |
| 5 | 1.4 | 1.0681 | 5 | 1.2 | 3.9596 | 5 | 1.5 | 4.3873 |
| 10 | -0.4 | 2.3731 | 10 | -0.4 | 7.1285 | 10 | -0.2 | 14.2349 |
| 15 | -0.4 | 1.5061 | 15 | -0.4 | 3.3816 | 15 | -0.4 | 11.9546 |
| 20 | -0.4 | 1.0754 | 20 | -0.4 | 1.9362 | 20 | -0.4 | 7.7847 |
| 30 | -0.4 | 0.6430 | 30 | -0.4 | 1.0417 | 30 | -0.4 | 2.8906 |

The variation of $a_{RMS.min}$ with respect to $\lambda$ and $A$ are shown for each vehicle velocity in Figures 3.7 through 3.9.

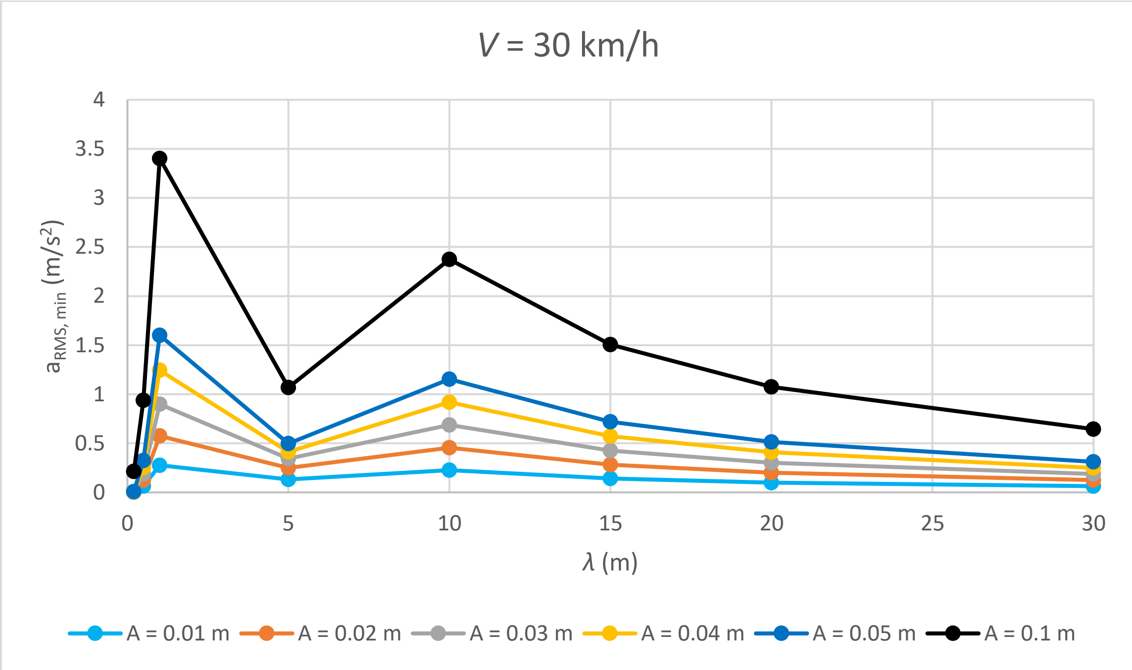


**Figure 3.7.** $a_{RMS.min}$ against $\lambda$ for different values of $A$ with $V$ = 30 km/h.

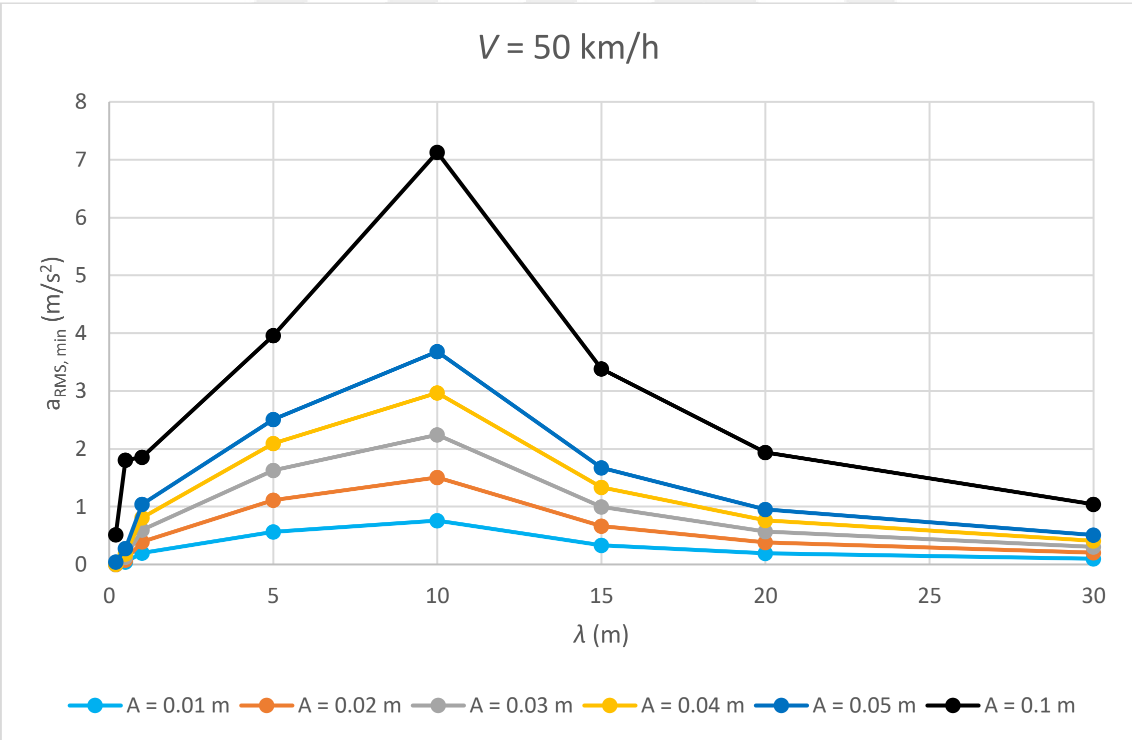


**Figure 3.8.** $a_{RMS.min}$ against $\lambda$ for different values of $A$ with $V$ = 50 km/h.

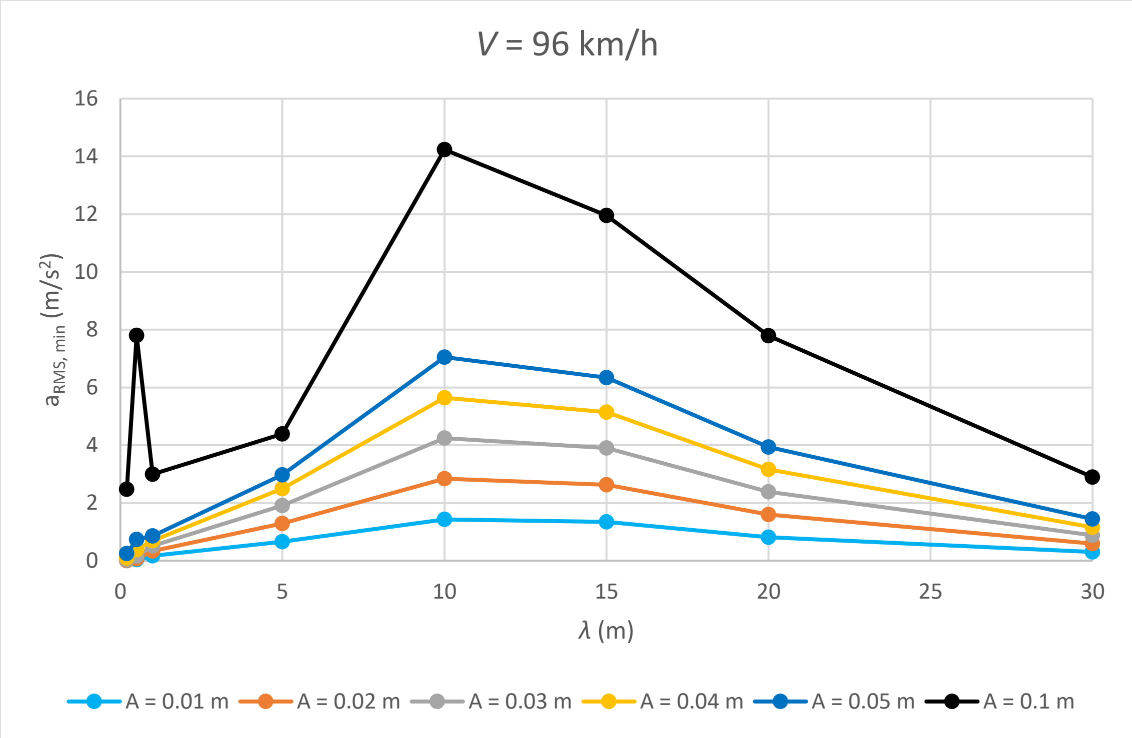


**Figure 3.9.** $a_{RMS.min}$ against $\lambda$ for different values of $A$ with $V$ = 96 km/h.

The variation of optimal battery location with respect to the road profile wavelength can be seen in Figures 3.10 through 3.15 for each wave amplitude and vehicle velocity.

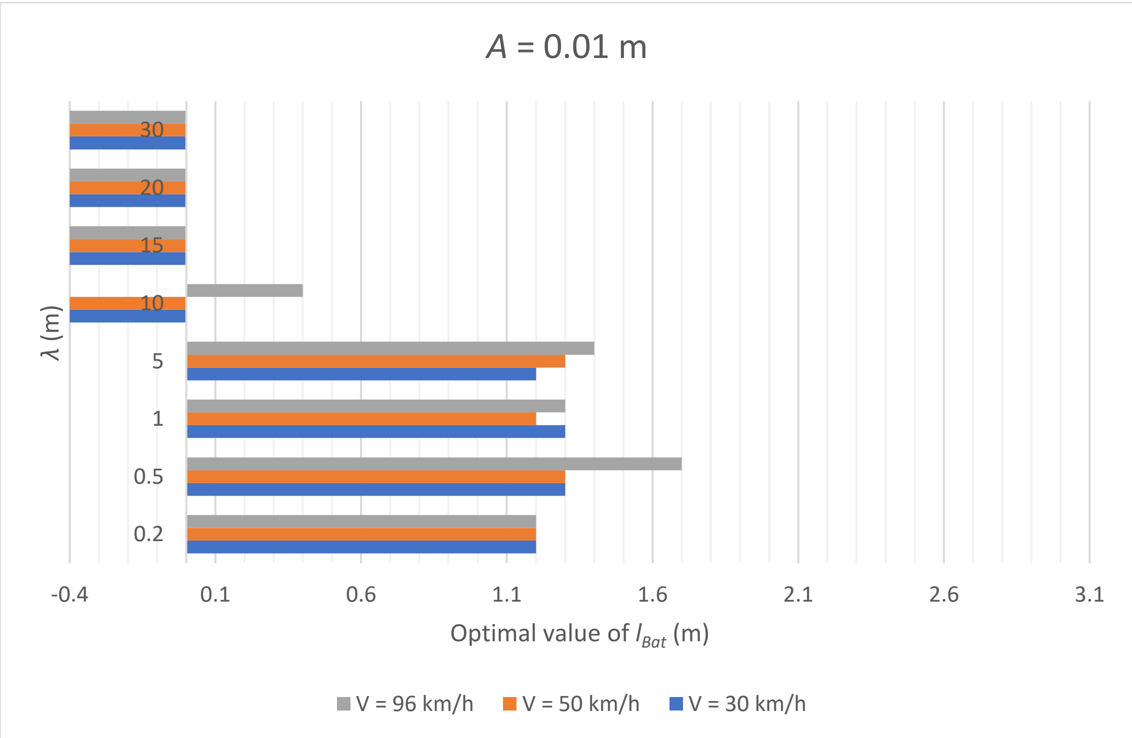


**Figure 3.10.** Optimal battery locations for $A$ = 0.01 m.

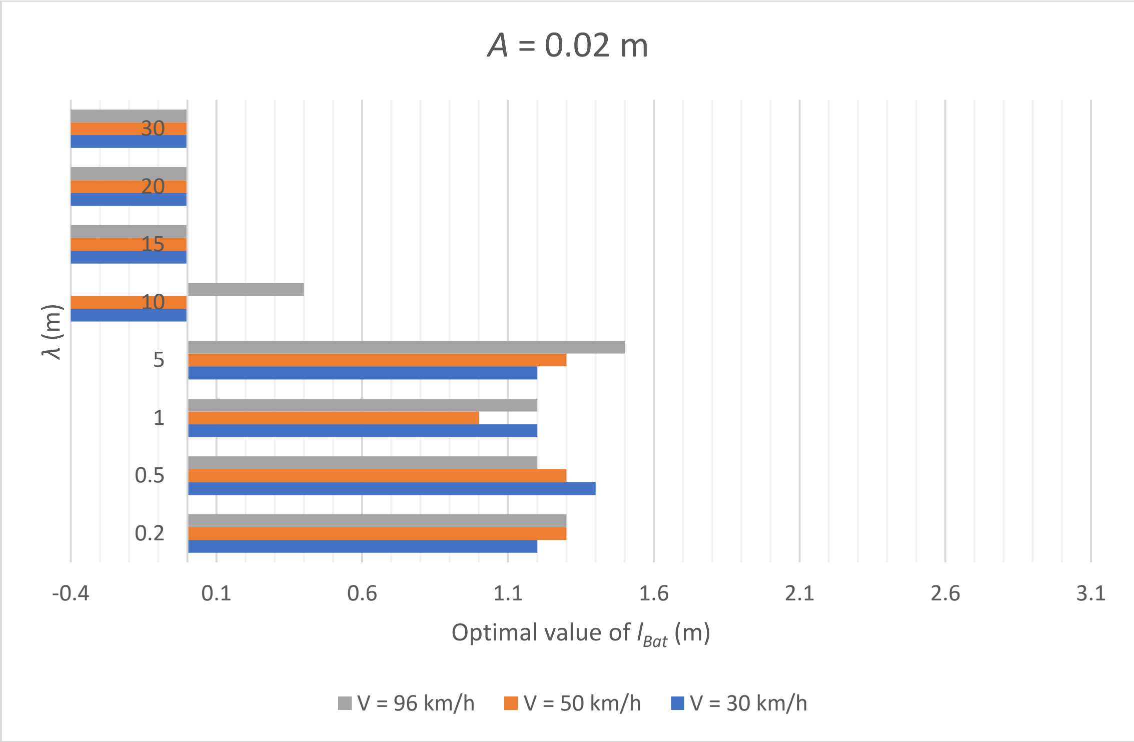


**Figure 3.11.** Optimal battery locations for $A$ = 0.02 m.

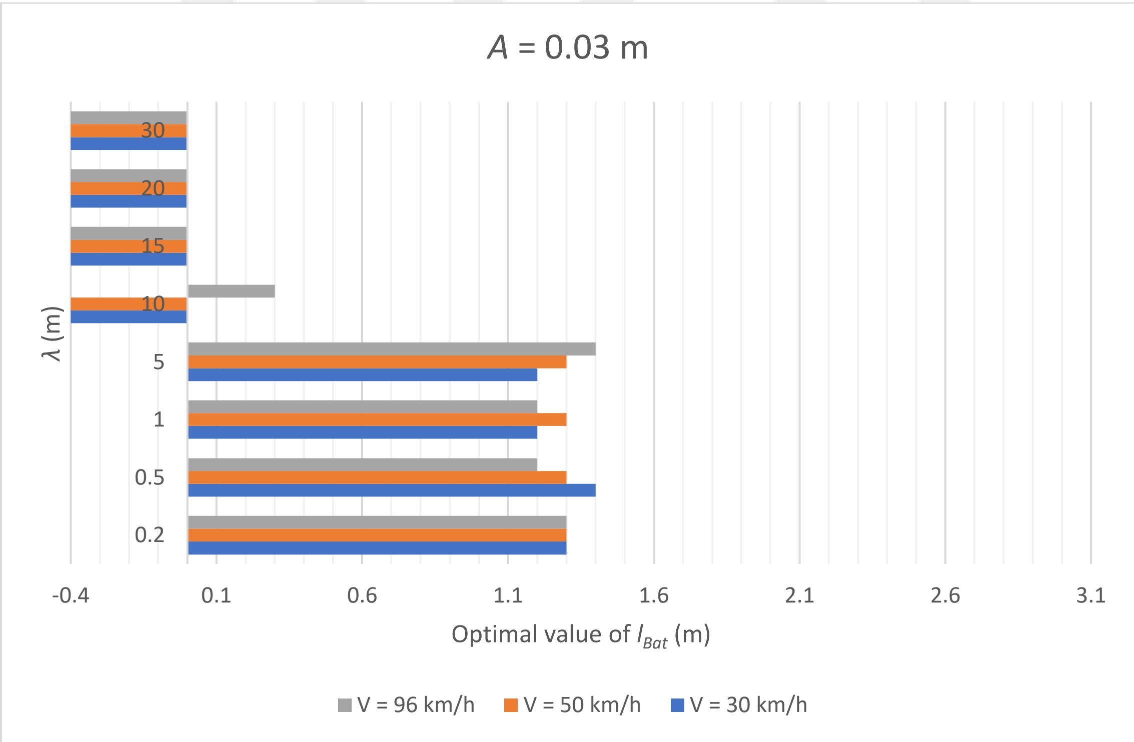


**Figure 3.12.** Optimal battery locations for $A$ = 0.03 m.

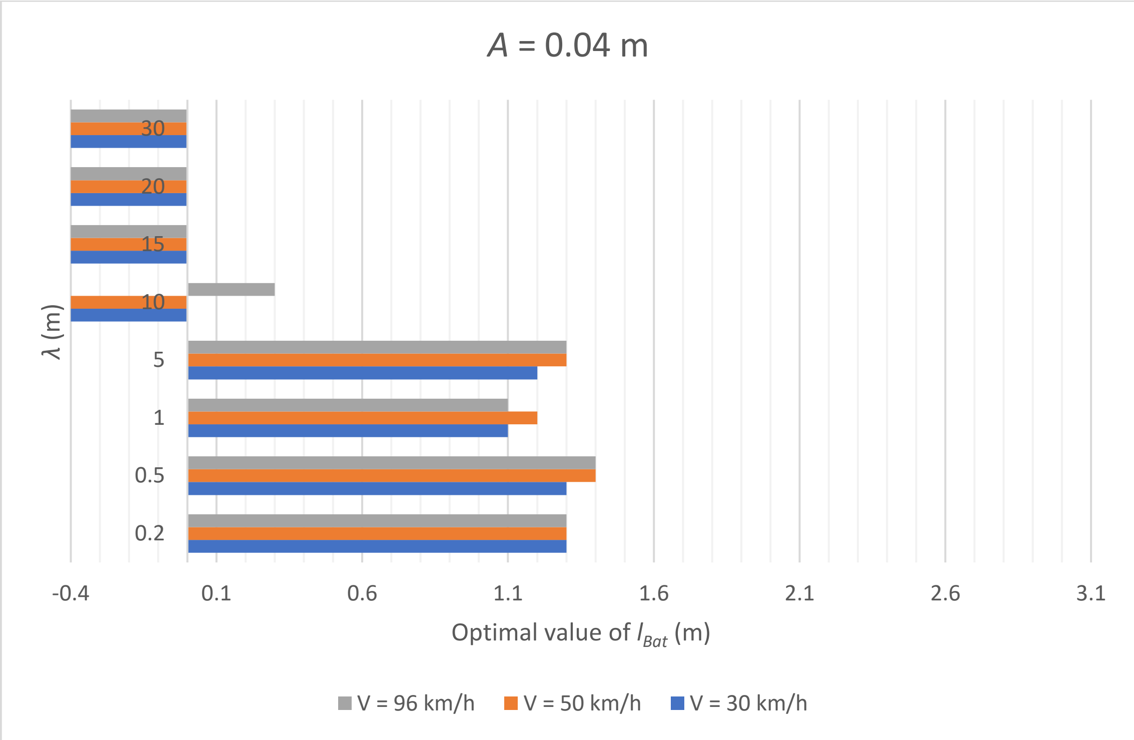


**Figure 3.13.** Optimal battery locations for $A$ = 0.04 m.

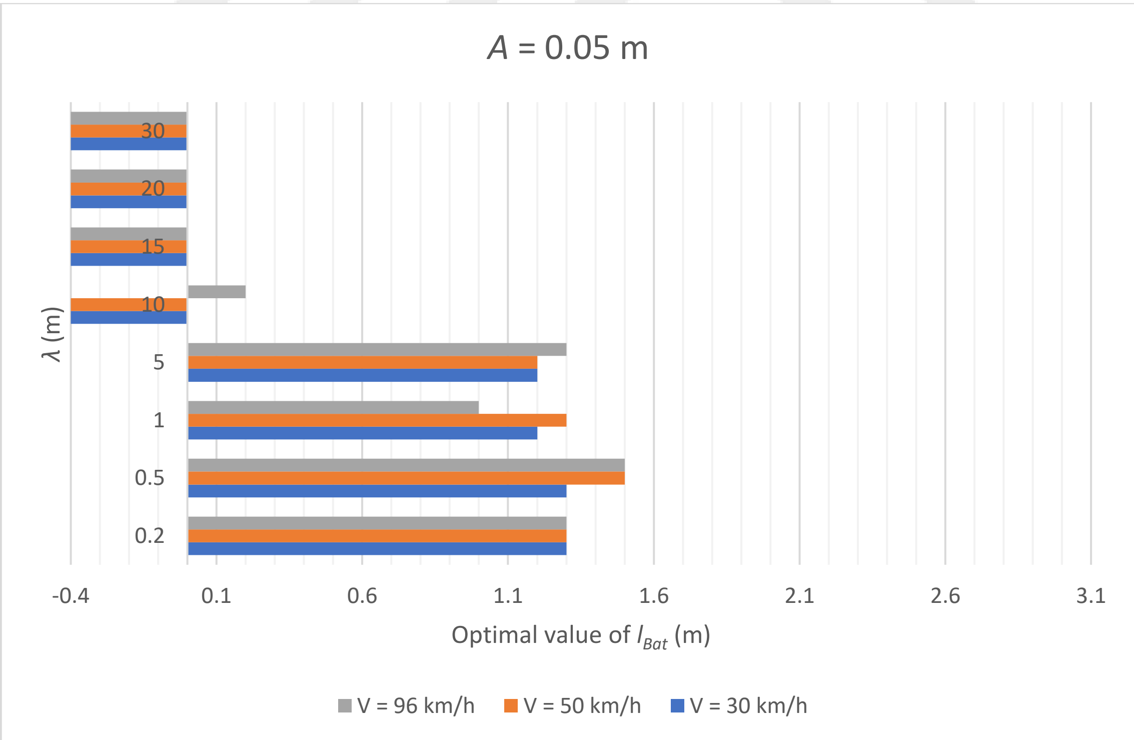


**Figure 3.14.** Optimal battery locations for $A$ = 0.05 m.

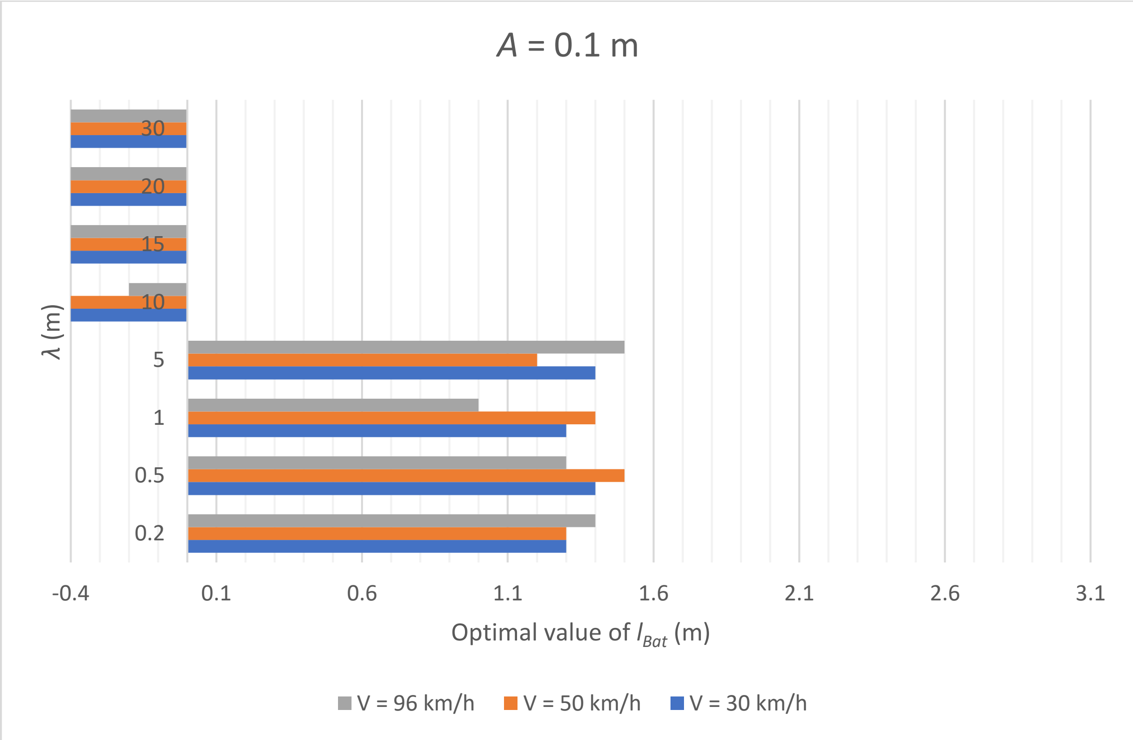


**Figure 3.15.** Optimal battery locations for $A = 0.1$ m.

Finally, Figure 3.16 gives a graphical abstract of the 5184 analyses performed.

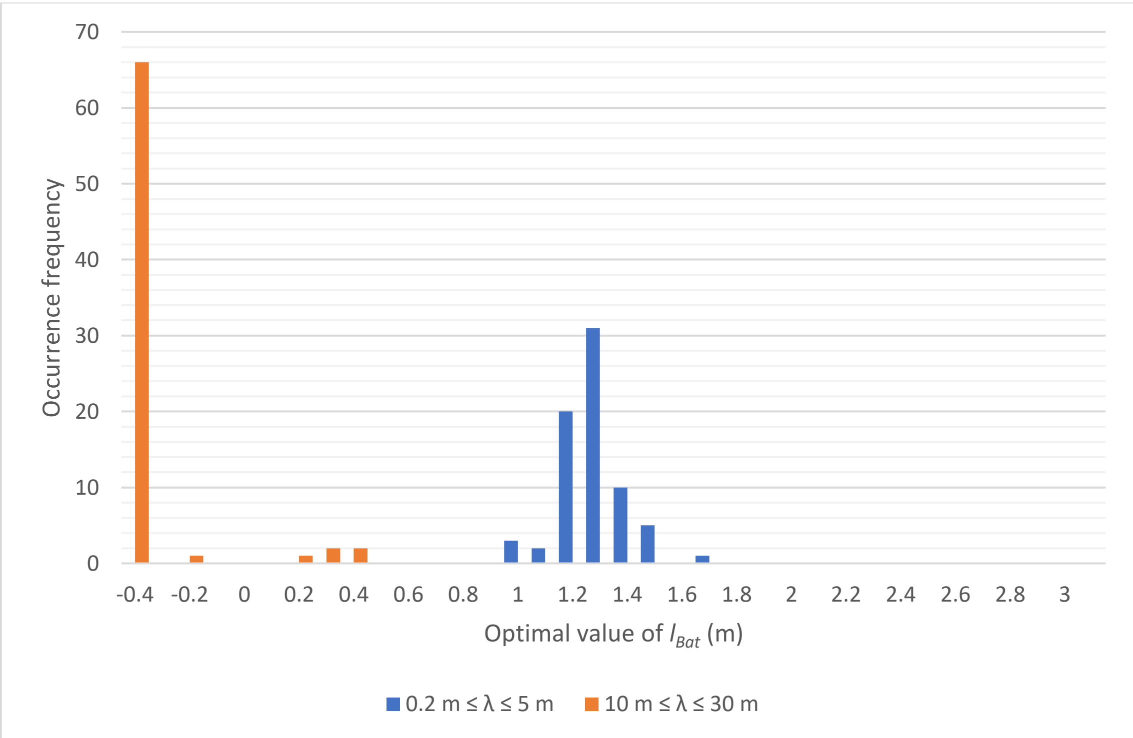


**Figure 3.16.** Occurrence frequency of optimal battery locations in 5184 analyses.

As the road wavelength increases, the road gets flatter. By reviewing the results of the 5184 analyses performed, we can conclude that the optimal battery location for wavelengths from 10 to 30 m is the rear end of the vehicle. For wavelengths from 0.2 to 5 m, on the other hand, the optimal battery location is found to be the middle portion of the vehicle. These conclusions hold for all amplitudes and vehicle velocities considered. Furthermore, when Figures 3.7 through 3.9 are examined, it is seen that 10 m wavelength seems a critical value for $a_{RMS.min}$, especially with 50 and 96 km/h vehicle velocities. However, this may be associated with the selected numerical values for the model parameters. For different values of the model parameters, different critical wavelengths can be observed.

# 4 CONCLUSIONS

In this thesis, ride comfort of electric vehicles is analysed using different road profiles and driving conditions.

Based on the analyses conducted, this thesis shows that the location of the battery in electric vehicles has a significant effect on ride comfort. The analyses performed in the study can be handled under two main groups. In the first group, two road profiles are considered, one with speed bumps and the other one with speed humps. The starting half of the road includes these obstacles, and the remaining half is straight. The rotating unbalance of in-wheel motors is taken into account. The following conclusions can be made based on the results of totally 380 analyses in this first group:

1. Battery location affects ride comfort of electric vehicles.
2. For electric vehicles in city driving conditions, the optimal battery location for ride comfort is the middle of rear and front axles of the vehicle.
3. For electric vehicles in off-road driving conditions, the optimal battery location for ride comfort is ahead of the front axle of the vehicle.

The previous literature (Wang, 2020) concluded that optimal battery location is the middle of the rear and front axles of the vehicle. This thesis gives similar result for passenger vehicles which are generally used in city roads and highways, while for electric vehicles which are used in off-road and rural areas, this thesis recommends that the optimal battery location for ride comfort is the front of the front axle of the vehicle. However, for low speeds the battery must be placed close to the rear axle.

In the second group of analyses performed, 36 different battery locations are tested in 144 different driving conditions. Sinusoidal road profiles are used and rotating unbalance of in-wheel motors is neglected to better focus on the effects of road roughness. Based on the results of totally 5184 analyses in this second group, the following conclusions are drawn:

1. For road profile wavelengths from 0.2 to 5 m, the optimal battery location is found to be the middle portion of the vehicle.
2. For road profile wavelengths from 10 to 30 m, the optimal battery location is at the rear section of the vehicle.

The results in the first and second groups also agree with each other.

With considering spring and damper nonlinearities, real world scenarios can be represented more accurately and optimisation of battery location with spring and damper nonlinearities taken into account is beneficial for designing different electric vehicles that can be used in city and rural areas.

## REFERENCES


[1] Aalund, R., Diao, W., Kong, L., & Pecht, M. (2021). Understanding the non-collision related battery safety risks in electric vehicles a case study in electric vehicle recalls and the LG chem battery. IEEE Access, 9, 89527–89532. doi:10.1109/access.2021.3090304

[2] Ahmad, A., Alam, M. S., & Chabaan, R. (2018). A comprehensive review of wireless charging technologies for electric vehicles. IEEE Transactions on Transportation Electrification, 4(1), 38–63. doi:10.1109/tte.2017.2771619

[3] Akinlabi, A. A. H., & Solyali, D. (2020). Configuration, design, and optimization of air-cooled battery thermal management system for electric vehicles: A review. Renewable and Sustainable Energy Reviews, 125, 109815. doi:10.1016/j.rser.2020.109815

[4] Albarella, N., Masuccio, F., Novella, L., Tufo, M., & Fiengo, G. (2021). A forward-collision warning system for electric vehicles: Experimental validation in virtual and real environment. Energies, 14(16), 4872. doi:10.3390/en14164872

[5] Ali, M. U., Zafar, A., Nengroo, S. H., Hussain, S., Alvi, M. J., & Kim, H.-J. (2019). Towards a smarter battery management system for electric vehicle applications: A critical review of lithium-ion battery state of charge estimation. Energies, 12(3), 446. doi:10.3390/en12030446

[6] Alimujiang, A., & Jiang, P. (2020). Synergy and co-benefits of reducing CO2 and air pollutant emissions by promoting electric vehicles—A case of Shanghai. Energy for Sustainable Development, 55, 181–189. doi:10.1016/j.esd.2020.02.005

[7] Andre, M., Sartelet, K., Moukhtar, S., Andre, J. M., & Redaelli, M. (2020). Diesel, petrol or electric vehicles: What choices to improve urban air quality in the Ile-de-France region? A simulation platform and case study. Atmospheric Environment, 241, 117752. doi:10.1016/j.atmosenv.2020.117752

[8] Arif, S. M., Lie, T. T., Seet, B. C., Ayyadi, S., & Jensen, K. (2021). Review of electric vehicle technologies, charging methods, standards and optimization techniques. Electronics, 10(16), 1910. doi:10.3390/electronics10161910

[9] Arora, S., Shen, W., & Kapoor, A. (2016). Review of mechanical design and strategic placement technique of a robust battery pack for electric vehicles. Renewable and Sustainable Energy Reviews, 60, 1319–1331. doi:10.1016/j.rser.2016.03.013

[10] Aswin Karthik, C., Kalita, P., Cui, X., & Peng, X. (2020). Thermal management for prevention of failures of lithium ion battery packs in electric vehicles: A review and critical future aspects. Energy Storage, 2(3). doi:10.1002/est2.137

[11] Avcı, G. Z. (2019) Elektrikli Toplu Taşıma Aracının Modellenmesi ve Optimizasyonu. Yüksek Lisans Tezi, Yıldız Teknik Üniversitesi Fen Bilimleri Enstitüsü, İstanbul, Türkiye.

[12] Bagchi, A. C., Kamineni, A., Zane, R. A., & Carlson, R. (2021). Review and comparative analysis of topologies and control methods in dynamic wireless charging of electric vehicles. IEEE Journal of Emerging and Selected Topics in Power Electronics, 9(4), 4947–4962. doi:10.1109/jestpe.2021.3058968

[13] Ball, S., Clark, J., & Cookson, J. (2020). Battery materials technology trends and market drivers for automotive applications. Johnson Matthey Technology Review, 64(3), 287–297. doi:10.1595/205651320x15783059820413

[14] Besselink, I. J. M., van Oorschot, P. F., Meinders, E., & Nijmeijer, H. (2010). Design of an efficient, low weight battery electric vehicle based on a VW Lupo 3L. The 25th World Battery, Hybrid and Fuel Cell Electric Vehicle Symposium & Exhibition (EVS-25) Proceedings, Vols 1 & 2, pp. 67-76, Shenzhen, China, Nov. 5-9, 2010.

[15] Bindra, A. (2017). Wireless power transfer is fueling the electric vehicles market [From the Editor]. IEEE Power Electronics Magazine, 4(2), 4–8. doi:10.1109/mpel.2017.2692382

[16] Braco, E., San Martin, I., Berrueta, A., Sanchis, P., & Ursua, A. (2021). Experimental assessment of first- and second-life electric vehicle batteries: Performance, capacity dispersion, and aging. IEEE Transactions on Industry Applications, 57(4), 4107–4117. doi:10.1109/tia.2021.3075180

[17] Burden, R. L., & Faires, J. D. (2011). Numerical Analysis, 9th Edition, Brooks/Cole, Cengage Learning, Boston, MA, USA.

[18] Campello-Vicente, H., Peral-Orts, R., Campillo-Davo, N., & Velasco-Sanchez, E. (2017). The effect of electric vehicles on urban noise maps. Applied Acoustics, 116, 59–64. doi:10.1016/j.apacoust.2016.09.018

[19] Casals, L. C., García, B. A., & Cremades, L. V. (2017a). Electric vehicle battery reuse: Preparing for a second life. Journal of Industrial Engineering and Management, 10(2), 266-285. doi:10.3926/jiem.2009

[20] Casals, L. C., García, B. A., Aguesse, F., & Iturrondobeitia, A. (2017b). Second life of electric vehicle batteries: Relation between materials degradation and environmental impact. The International Journal of Life Cycle Assessment, 22(1), 82–93. doi:10.1007/s11367-015-0918-3

[21] Chen, T., Zhang, X.-P., Wang, J., Li, J., Wu, C., Hu, M., & Bian, H. (2020). A review on electric vehicle charging infrastructure development in the UK. Journal of Modern Power Systems and Clean Energy, 8(2), 193–205. doi:10.35833/mpce.2018.000374

[22] Choma, E. F., Evans, J. S., Hammitt, J. K., Gómez-Ibáñez, J. A., & Spengler, J. D. (2020). Assessing the health impacts of electric vehicles through air pollution in the United States. Environment International, 144, 106015. doi:10.1016/j.envint.2020.106015

[23] Choudhari, V. G., Dhoble, A. S., & Sathe, T. M. (2020). A review on effect of heat generation and various thermal management systems for lithium ion battery used for electric vehicle. Journal of Energy Storage, 32, 101729. doi:10.1016/j.est.2020.101729

[24] Daga, A., Miller, J. M., Long, B. R., Kacergis, R., Schrafel, P., & Wolgemuth, J. (2017). Electric fuel pumps for wireless power transfer: Enabling rapid growth in the electric vehicle market. IEEE Power Electronics Magazine, 4(2), 24–35. doi:10.1109/mpel.2017.2692379

[25] Deb, S., Tammi, K., Kalita, K., & Mahanta, P. (2018). Review of recent trends in charging infrastructure planning for electric vehicles. WIREs Energy and Environment, 7(6). doi:10.1002/wene.306

[26] Devdutt. (2017). Passenger Seat Vibration Comparison Using ANFIS Control in Active Quarter Car Model. International Journal of Mechanical and Mechatronics Engineering, 11(7), 1358-1363.

[27] Di Felice, L. J., Renner, A., & Giampietro, M. (2021). Why should the EU implement electric vehicles? Viewing the relationship between evidence and dominant policy solutions through the lens of complexity. Environmental Science and Policy, 123, 1–10. doi:10.1016/j.envsci.2021.05.002

[28] Doebelin, E. O. (1998). System Dynamics: Modeling, Analysis, Simulation, Design, Marcel Dekker, New York, USA.

[29] El-Mezayen, O., Qasem, M., Ibrahim, H., Merabet, N., & Elnaggar, Z. (2020). Optimization of nonlinear quarter car suspension-driver seat model using GA based PID controller. Proceedings of the XI International Conference on Structural Dynamics, pp. 690–704. doi:10.47964/1120.9055.18892

[30] European Commission. (2020). EU Transport in Figures – Statistical Pocketbook 2020. Imprimerie Bietlot Frères, Belgium.

[31] EVSpecifications, https://www.evspecifications.com. Last accessed: 05 January 2022.

[32] Feng, X., Ouyang, M., Liu, X., Lu, L., Xia, Y., & He, X. (2018). Thermal runaway mechanism of lithium ion battery for electric vehicles: A review. Energy Storage Materials, 10, 246–267. doi:10.1016/j.ensm.2017.05.013

[33] Funke, S. Á., Sprei, F., Gnann, T., & Plötz, P. (2019). How much charging infrastructure do electric vehicles need? A review of the evidence and international comparison. Transportation Research Part D: Transport and Environment, 77, 224–242. doi:10.1016/j.trd.2019.10.024

[34] Gai, Y., Minet, L., Posen, I. D., Smargiassi, A., Tétreault, L.-F., & Hatzopoulou, M. (2020). Health and climate benefits of electric vehicle deployment in the Greater Toronto and Hamilton Area. Environmental Pollution, 265, Part A, 114983. doi:10.1016/j.envpol.2020.114983

[35] Ganesh, S., & Venkatesan, S. (2021). Evolution of flexible modular electric vehicle platforms among automotive industry and its influence on battery integration. International Journal of Vehicle Structures & Systems, 13(3), 361-366. doi:10.4273/ijvss.13.3.24

[36] Gao, W., Zhang, N., & Du, H. P. (2007). A half-car model for dynamic analysis of vehicles with random parameters. 5th Australasian Congress on Applied Mechanics, ACAM 2007, 10-12 December 2007, Brisbane, Australia.

[37] Goga, V., & Kľúčik, M. (2012). Optimization of vehicle suspension parameters with use of evolutionary computation. Procedia Engineering, 48, 174–179. doi:10.1016/j.proeng.2012.09.502

[38] Gu, X., Zhou, L., Huang, H., Shi, X., & Ieromonachou, P. (2021). Electric vehicle battery secondary use under government subsidy: A closed-loop supply chain perspective. International Journal of Production Economics, 234, 108035. doi:10.1016/j.ijpe.2021.108035

[39] Guo, J., Zhang, X., Gu, F., Zhang, H., & Fan, Y. (2020). Does air pollution stimulate electric vehicle sales? Empirical evidence from twenty major cities in China. Journal of Cleaner Production, 249, 119372. doi:10.1016/j.jclepro.2019.119372

[40] Han, X., Lu, L., Zheng, Y., Feng, X., Li, Z., Li, J., & Ouyang, M. (2019). A review on the key issues of the lithium ion battery degradation among the whole life cycle. eTransportation, 1, 100005. doi:10.1016/j.etran.2019.100005

[41] Harrison, R. M., Vu, T. V., Jafar, H., & Shi, Z. (2021). More mileage in reducing urban air pollution from road traffic. Environment International, 149, 106329. doi:10.1016/j.envint.2020.106329

[42] Hassanzadeh, I., Alizadeh, G., Pourqorban Shirjoposht, N., & Hashemzadeh, F. (2010). A new optimal nonlinear approach to half car active suspension control. International Journal of Engineering and Technology, 2(1), 78–84. doi:10.7763/ijet.2010.v2.104

[43] Ho, C., Lang, Z.-Q., & Billings, S. A. (2012). The benefits of nonlinear cubic viscous damping on the force transmissibility of a Duffing-type vibration isolator. Proceedings of the 2012 UKACC International Conference on Control, Cardiff, UK, 3-5 September 2012, IEEE, pp. 479–484. doi:10.1109/control.2012.6334677

[44] Ho, C., Lang, Z.-Q., & Billings, S. A. (2014). Design of vibration isolators by exploiting the beneficial effects of stiffness and damping nonlinearities. Journal of Sound and Vibration, 333(12), 2489–2504. doi:10.1016/j.jsv.2014.02.011

[45] How, D. N. T., Hannan, M. A., Lipu, M. S. H., Sahari, K. S. M., Ker, P. J., & Muttaqi, K. M. (2020). State-of-charge estimation of li-ion battery in electric vehicles: A deep neural network approach. IEEE Transactions on Industry Applications, 56(5), 5565–5574. doi:10.1109/tia.2020.3004294

[46] Hu, Y., Cheng, H., & Tao, S. (2017). Retired electric vehicle (EV) batteries: Integrated waste management and research needs. Environmental Science & Technology, 51(19), 10927–10929. doi:10.1021/acs.est.7b04207

[47] Hua, X., Thomas, A., & Shultis, K. (2021). Recent progress in battery electric vehicle noise, vibration, and harshness. Science Progress, 104(1), 003685042110052. doi:10.1177/00368504211005224

[48] Huang, S., & Nguyen, V. (2021). Influence of dynamic parameters of electric-vehicles on the ride comfort under different operation conditions. Journal of

Mechanical Engineering, Automation and Control Systems, 2(1), 1–8. doi:10.21595/jmeacs.2021.21862

[49] Huang, X., Lin, Y., Zhou, F., Lim, M. K., & Chen, S. (2021). Agent-based modelling for market acceptance of electric vehicles: Evidence from China. Sustainable Production and Consumption, 28, 206–217. doi:10.1016/j.spc.2021.04.007

[50] Iclodean, C., Varga, B., Burnete, N., Cimerdean, D., & Jurchiş, B. (2017). Comparison of different battery types for electric vehicles. IOP Conference Series: Materials Science and Engineering, 252, 012058, CAR-2017 International Congress of Automotive and Transport Engineering - Mobility Engineering and Environment 8–10 November 2017, Pitesti, Romania. doi:10.1088/1757-899x/252/1/012058

[51] Ijeh, I. C. (2020). A collision-avoidance system for an electric vehicle: A drive-by-wire technology initiative. SN Applied Sciences, 2(4), 744. doi:10.1007/s42452-020-2383-2

[52] Illmann, U., & Kluge, J. (2020). Public charging infrastructure and the market diffusion of electric vehicles. Transportation Research Part D: Transport and Environment, 86, 102413. doi:10.1016/j.trd.2020.102413

[53] International Energy Agency (IEA). (2021), Global EV Data Explorer, Paris, France, https://www.iea.org/articles/global-ev-data-explorer. Last Accessed: 10 September 2021.

[54] Ioakimidis, C. S., Murillo-Marrodán, A., Bagheri, A., Thomas, D., & Genikomsakis, K. N. (2019). Life cycle assessment of a lithium iron phosphate (LFP) electric vehicle battery in second life application scenarios. Sustainability, 11(9), 2527. doi:10.3390/su11092527

[55] Iwafune, Y., & Ogimoto, K. (2020). Economic impacts of the demand response of electric vehicles considering battery degradation. Energies, 13(21), 5771. doi:10.3390/en13215771

[56] Jaiswal, D., Kant, R., Singh, P. K., & Yadav, R. (2022). Investigating the role of electric vehicle knowledge in consumer adoption: evidence from an emerging market. Benchmarking: An International Journal, 29(3), 1027–1045. doi:10.1108/bij-11-2020-0579

[57] Jazar, R. N. (2014). Vehicle Dynamics: Theory and Application, 2nd Edition, Springer, New York, USA.

[58] Jena, R. (2020). An empirical case study on Indian consumers' sentiment towards electric vehicles: A big data analytics approach. Industrial Marketing Management, 90, 605-616. doi:10.1016/j.indmarman.2019.12.012

[59] Jiao, L. (2013). Vehicle model for tyre-ground contact force evaluation. Master Thesis in Vehicle Engineering, Department of Aeronautical and Vehicle Engineering, KTH Royal Institute of Technology, Stockholm, Sweden.

[60] Kalaf, O., Solyali, D., Asmael, M., Zeeshan, Q., Safaei, B., & Askir, A. (2020). Experimental and simulation study of liquid coolant battery thermal management system for electric vehicles: A review. International Journal of Energy Research, 45(5), 6495–6517. doi:10.1002/er.6268

[61] Kaya, K. Y., & Kıyak, İ. (2020). Elektrikli taşıtlarda kullanılan indüksiyon / sabit mıknatıslı motor sürücülerinin simülasyonu ve motor dinamiklerinin analizi. International Journal of Advances in Engineering and Pure Sciences, 32(2), 152-157. doi:10.7240/jeps.583114

[62] Khan, W., Ahmad, A., Ahmad, F., & Saad Alam, M. (2018). A comprehensive review of fast charging infrastructure for electric vehicles. Smart Science, 6(3), 256–270. doi:10.1080/23080477.2018.1437323

[63] Kieckhäfer, K., Wachter, K., & Spengler, T. S. (2017). Analyzing manufacturers' impact on green products' market diffusion – the case of electric vehicles. Journal of Cleaner Production, 162, S11-S25. doi:10.1016/j.jclepro.2016.05.021

[64] Kim, J., Oh, J., & Lee, H. (2019a). Review on battery thermal management system for electric vehicles. Applied Thermal Engineering, 149, 192–212. doi:10.1016/j.applthermaleng.2018.12.020

[65] Kim, W.-Y., Lee, P.-Y., Kim, J., & Kim, K.-S. (2019b). A nonlinear-model-based observer for a state-of-charge estimation of a lithium-ion battery in electric vehicles. Energies, 12(17), 3383. doi:10.3390/en12173383

[66] Kumar, P., Chaudhary, D., Varshney, P., Varshney, U., Yahya, S. M., & Rafat, Y. (2020). Critical review on battery thermal management and role of nanomaterial in heat transfer enhancement for electrical vehicle application. Journal of Energy Storage, 32, 102003. doi:10.1016/j.est.2020.102003

[67] Lévay, P. Z., Drossinos, Y., & Thiel, C. (2017). The effect of fiscal incentives on market penetration of electric vehicles: A pairwise comparison of total cost of ownership. Energy Policy, 105, 524–533. doi:10.1016/j.enpol.2017.02.054

[68] Li, H., Alsolami, M., Yang, S., Alsmadi, Y. M., & Wang, J. (2017a). Lifetime test design for second-use electric vehicle batteries in residential applications. IEEE Transactions on Sustainable Energy, 8(4), 1736–1746. doi:10.1109/tste.2017.2707565

[69] Li, K., Zhou, P., Lu, Y., Han, X., Li, X., & Zheng, Y. (2020). Battery life estimation based on cloud data for electric vehicles. Journal of Power Sources, 468, 228192. doi:10.1016/j.jpowsour.2020.228192

[70] Li, W., Yang, M., Long, R., Mamaril, K., & Chi, Y. (2021). Treatment of electric vehicle battery waste in China: A review of existing policies. Journal of Environmental Engineering and Landscape Management, 29(2), 111–122. doi:10.3846/jeelm.2021.14220

[71] Li, X., Shu, X., Shen, J., Xiao, R., Yan, W., & Chen, Z. (2017b). An on-board remaining useful life estimation algorithm for lithium-ion batteries of electric vehicles. Energies, 10(5), 691. doi:10.3390/en10050691

[72] Li, Z., Duan, L. B., Cheng, A. G., Yao, Z. P., Chen, T., & Yao, W. (2019b). Lightweight and crashworthiness design of an electric vehicle using a six-sigma robust design optimization method. Engineering Optimization, 51(8), 1393–1411. doi:10.1080/0305215x.2018.1521396

[73] Li, Z., Khajepour, A., & Song, J. (2019a). A comprehensive review of the key technologies for pure electric vehicles. Energy, 182, 824–839. doi:10.1016/j.energy.2019.06.077

[74] Lian, Y., Wang, X., Tian, Y., & Liu, K. (2018). Lateral collision avoidance robust control of electric vehicles combining a lane-changing model based on vehicle edge turning trajectory and a vehicle semi-uncertainty dynamic model. International Journal of Automotive Technology, 19(2), 331–343. doi:10.1007/s12239-018-0032-1

[75] Lipu, M. S. H., Hannan, M. A., Hussain, A., Hoque, M. M., Ker, P. J., Saad, M. H. M., & Ayob, A. (2018). A review of state of health and remaining useful life estimation methods for lithium-ion battery in electric vehicles: Challenges and recommendations. Journal of Cleaner Production, 205, 115–133. doi:10.1016/j.jclepro.2018.09.065

[76] Liu, M., Gu, F., & Zhang, Y. (2017). Ride comfort optimization of in-wheel-motor electric vehicles with in-wheel vibration absorbers. Energies, 10(10), 1647. doi:10.3390/en10101647

[77] Machura, P., & Li, Q. (2019). A critical review on wireless charging for electric vehicles. Renewable and Sustainable Energy Reviews, 104, 209–234. doi:10.1016/j.rser.2019.01.027

[78] Mahala, K. M., Gadkari, P., & Deb, A. (2009). Mathematical models for designing vehicles for ride comfort. In ICORD 09: Proceedings of the 2nd International Conference on Research into Design, Bangalore, India 07.-09.01.2009.

[79] MathWorks Help Centre, Root-mean-square value, https://www.mathworks.com/help/matlab/ref/rms.html. Last accessed: 19 April 2022.

[80] Mazumder, H., Al Emran Hassan, M. M., Ektesabi, M., & Kapoor, A. (2012). Performance analysis of EV for different mass distributions to ensure safe handling. Energy Procedia, 14, 949–954. doi:10.1016/j.egypro.2011.12.1038

[81] Meskell, C. (2006). A decrement method for quantifying nonlinear and linear damping parameters. Journal of Sound and Vibration, 296(3), 643–649. doi:10.1016/j.jsv.2006.02.005

[82] Mishra, S., Verma, S., Chowdhury, S., Gaur, A., Mohapatra, S., Dwivedi, G., & Verma, P. (2021). A comprehensive review on developments in electric vehicle charging station infrastructure and present scenario of India. Sustainability, 13(4), 2396. doi:10.3390/su13042396

[83] Mohammed, S. A. Q., & Jung, J.-W. (2021). A comprehensive state-of-the-art review of wired/wireless charging technologies for battery electric vehicles: Classification/common topologies/future research issues. IEEE Access, 9, 19572–19585. doi:10.1109/access.2021.3055027

[84] Münzel, C., Plötz, P., Sprei, F., & Gnann, T. (2019). How large is the effect of financial incentives on electric vehicle sales? – A global review and European analysis. Energy Economics, 84, 104493. doi:10.1016/j.eneco.2019.104493

[85] Narayanan, S., & Senthil, S. (1998). Stochastic optimal active control of a 2-DOF quarter car model with non-linear passive suspension elements. Journal of Sound and Vibration, 211(3), 495–506. doi:10.1006/jsvi.1997.1396

[86] Navale, A. B., Chippa, S. P., Chougule, D. A., & Raut, P. M. (2021). Crashworthiness aspects of electric vehicle design. International Journal of Crashworthiness, 26(4), 368–387. doi:10.1080/13588265.2020.1718462

[87] Nguyen, H. P., Hoang, A. T., Le, A. T., Pham, V. V., & Tran, V. N. (2020). Learned experiences from the policy and roadmap of advanced countries for the strategic orientation to electric vehicles: A case study in Vietnam. Energy Sources, Part A: Recovery, Utilization, and Environmental Effects (in press). doi:10.1080/15567036.2020.1811432

[88] Nimesh, V., Kumari, R., Soni, N., Goswami, A. K., & Mahendra Reddy, V. (2021). Implication viability assessment of electric vehicles for different regions: An approach of life cycle assessment considering exergy analysis and battery degradation. Energy Conversion and Management, 237, 114104. doi:10.1016/j.enconman.2021.114104

[89] Ou, S., Lin, Z., He, X., Przesmitzki, S., & Bouchard, J. (2020). Modeling charging infrastructure impact on the electric vehicle market in China. Transportation Research Part D: Transport and Environment, 81, 102248. doi:10.1016/j.trd.2020.102248

[90] Pandey, A., Manocha, S., & Saini, P. (2020). A study on an automobile revolution and future of electric cars in India. International Journal of Management, 11(3), 107-113.

[91] Parajuly, K., Ternald, D., Kuehr, R. (2020). The Future of Electric Vehicles and Material Resources: A Foresight Brief. United Nations University (UNU)/United Nations Institute for Training and Research (UNITAR) - Sustainable Cycles (SCYCLE) Programme, Bonn, Germany & United Nations Environment Programme (UNEP)-International Environmental Technology Centre (IETC), Osaka, Japan.

[92] Pardo-Ferreira, M. del C., Rubio-Romero, J. C., Galindo-Reyes, F. C., & Lopez-Arquillos, A. (2020). Work-related road safety: The impact of the low noise levels produced by electric vehicles according to experienced drivers. Safety Science, 121, 580–588. doi:10.1016/j.ssci.2019.02.021

[93] Patole, S. S., & Sawant, S. H. (2015). Theoretical and numerical analysis of half car vehicle dynamic model subjected to different road profiles with wheel base delay and nonlinear parameters. International Journal of Multidisciplinary and Current Research, 3, 542-546.

[94] Pelletier, S., Jabali, O., Laporte, G., & Veneroni, M. (2017). Battery degradation and behaviour for electric vehicles: Review and numerical analyses of several models. Transportation Research Part B: Methodological, 103, 158–187. doi:10.1016/j.trb.2017.01.020

[95] Peng, Z. K., Meng, G., Lang, Z. Q., Zhang, W. M., & Chu, F. L. (2012). Study of the effects of cubic nonlinear damping on vibration isolations using Harmonic Balance Method. International Journal of Non-Linear Mechanics, 47(10), 1073–1080. doi:10.1016/j.ijnonlinmec.2011.09.013

[96] Praticò, F. G., Briante, P. G., & Speranza, G. (2020). Acoustic impact of electric vehicles. 2020 IEEE 20th Mediterranean Electrotechnical Conference (MELECON), pp. 7-12. doi:10.1109/melecon48756.2020.9140669

[97] Preeti, M., & Sayali, A. (2021). Scientometric analysis of research on end-of-life electronic waste and electric vehicle battery waste. Journal of Scientometric Research, 10(2), 37–46. doi:10.5530/jscires.10.1.5

[98] Qin, Y., He, C., Ding, P., Dong, M., & Huang, Y. (2018). Suspension hybrid control for in-wheel motor driven electric vehicle with dynamic vibration absorbing structures. IFAC-PapersOnLine, 51(31), 973–978. doi:10.1016/j.ifacol.2018.10.054

[99] Qin, Y., Zhao, Z., Wang, Z., & Li, G. (2021). Study of longitudinal–vertical dynamics for in-wheel motor-driven electric vehicles. Automotive Innovation, 4(2), 227–237. doi:10.1007/s42154-021-00141-5

[100] Quynh, L. V., Cuong, B. V., Liem, N. V., Long, L. X., & Dung, P. T. T. (2019). Effect of in-wheel motor suspension system on electric vehicle ride comfort. Vibroengineering PROCEDIA, 29, 148–152. doi:10.21595/vp.2019.21175

[101] Rajamani, R. (2012). Vehicle Dynamics and Control, 2nd Edition, Springer, New York, USA.

[102] Rajkumar, B., Lakshmi, P., & Rajendiran, S. (2015). Vibration control of quarter car integrated seat suspension with driver model for different road profiles using fuzzy based sliding mode controller. 2015 Seventh International Conference on Advanced Computing (ICoAC), 2015, pp. 1-6. doi:10.1109/ICoAC.2015.7562787.

[103] Redondo-Iglesias, E., Venet, P., & Pelissier, S. (2019). Efficiency degradation model of lithium-ion batteries for electric vehicles. IEEE Transactions on Industry Applications, 55(2), 1932–1940. doi:10.1109/tia.2018.2877166

[104] Reinhardt, R., Christodoulou, I., Gassó-Domingo, S., & Amante García, B. (2019). Towards sustainable business models for electric vehicle battery second use: A critical review. Journal of Environmental Management, 245, 432–446. doi:10.1016/j.jenvman.2019.05.095

[105] Rezvani, Z., Jansson, J., & Bodin, J. (2015). Advances in consumer electric vehicle adoption research: A review and research agenda. Transportation Research Part D: Transport and Environment, 34, 122–136. doi:10.1016/j.trd.2014.10.010

[106] Sazak, S. (2019) İstanbul İçin Öneri: Deniz Ulaşımında Elektrikli Taşıt Kullanımı ile Enerji Verimliliği Sağlanması. Yüksek Lisans Tezi, Altınbaş Üniversitesi Sosyal Bilimler Enstitüsü, İstanbul, Türkiye.

[107] Schmitz, T. L., & Smith, K. S. (2012). Mechanical Vibrations: Modeling and Measurement, Springer, New York, USA.

[108] Sever, M., & Yazici, H. (2017). Active control of vehicle suspension system having driver model via L2 gain state derivative feedback controller. 2017 4th International Conference on Electrical and Electronic Engineering (ICEEE), 2017, pp. 215-222. doi:10.1109/ICEEE2.2017.7935822.

[109] Sever, M., Şendur, H. S., Yazıcı, H., & Arslan, M. S. (2019). Active vibration control of a vehicle suspension system having biodynamic driver model with state derivative feedback LQR. Journal of the Faculty of Engineering and Architecture of Gazi University, 34(3), 1573–1583. doi:10.17341/gazimmfd.570732

[110] Shafiei, B. (2021). Investigating the impact of the velocity of a vehicle with a nonlinear suspension system on the dynamic behavior of a Bernoulli–Euler bridge. SN Applied Sciences, 3(3), 293. doi:10.1007/s42452-021-04280-6

[111] Shafique, M., Azam, A., Rafiq, M., & Luo, X. (2022). Life cycle assessment of electric vehicles and internal combustion engine vehicles: A case study of Hong Kong. Research in Transportation Economics, 91, 101112. doi:10.1016/j.retrec.2021.101112

[112] Shao, X., Naghdy, F., & Du, H. (2017). Reliable fuzzy H∞ control for active suspension of in-wheel motor driven electric vehicles with dynamic damping. Mechanical Systems and Signal Processing, 87, Part A, 365–383. doi:10.1016/j.ymssp.2016.10.032

[113] Shelke, G. D., & Mitra, A. C. (2018). Analysis and validation of linear half car passive suspension system with different road profiles. IOSR Journal of Engineering,

7th National conference on Recent Developments in Mechanical Engineering RDME-2018, pp. 14-19.

[114] Shetty, D. K., Shetty, S., Rodrigues, L. R., Naik, N., Maddodi, C. B., Malarout, N., & Sooriyaperakasam, N. (2020). Barriers to widespread adoption of plug-in electric vehicles in emerging Asian markets: An analysis of consumer behavioral attitudes and perceptions. Cogent Engineering, 7(1), 1796198. doi:10.1080/23311916.2020.1796198

[115] Skeete, J.-P., Wells, P., Dong, X., Heidrich, O., & Harper, G. (2020). Beyond the EVent horizon: Battery waste, recycling, and sustainability in the United Kingdom electric vehicle transition. Energy Research & Social Science, 69, 101581. doi:10.1016/j.erss.2020.101581

[116] Sofia, D., Gioiella, F., Lotrecchiano, N., & Giuliano, A. (2020). Mitigation strategies for reducing air pollution. Environmental Science and Pollution Research, 27(16), 19226–19235. doi:10.1007/s11356-020-08647-x

[117] Sun, L., Ma, D., & Tang, H. (2018). A review of recent trends in wireless power transfer technology and its applications in electric vehicle wireless charging. Renewable and Sustainable Energy Reviews, 91, 490–503. doi:10.1016/j.rser.2018.04.016

[118] Tan, D., & Wang, Q. (2016). Modeling and simulation of the vibration characteristics of the in-wheel motor driving vehicle based on bond graph. Shock and Vibration, 2016, 1982390. doi:10.1155/2016/1982390

[119] Tan, D., Wang, Q., & Wu, Y. (2017). Modal analysis of in-wheel motor-driven electric vehicle based on bond graph theory. Shock and Vibration, 2017, 6459154. doi:10.1155/2017/6459154

[120] Tanyeri, M. N. (2019) An Electrification Solution for Istanbul Metrobus Line. Yüksek Lisans Tezi, Hacettepe Üniversitesi Fen Bilimleri Enstitüsü, Ankara, Türkiye.

[121] Tete, P. R., Gupta, M. M., & Joshi, S. S. (2021). Developments in battery thermal management systems for electric vehicles: A technical review. Journal of Energy Storage, 35, 102255. doi:10.1016/j.est.2021.102255

[122] Toksoy, M. T. (2020) Tekerlek İçi Motora Sahip Elektrikli Bir Aracın Aktif Süspansiyon Sisteminin PID ve Bulanık Mantık Yöntemleri Kullanarak Karşılaştırmalı Kontrolü. Yüksek Lisans Tezi, Bursa Uludağ Üniversitesi Fen Bilimleri Enstitüsü, Bursa, Türkiye.

[123] Tong, W., & Hou, Z. (2013). Vertical vibration analysis on electric vehicle with suspended in-wheel motor drives. EVS27 International Battery, Hybrid and Fuel Cell Electric Vehicle Symposium, Barcelona, Spain, November 17-20, 2013. doi:10.1109/evs.2013.6914998

[124] Triviño, A., González-González, J. M., & Aguado, J. A. (2021). Wireless power transfer technologies applied to electric vehicles: A review. Energies, 14(6), 1547. doi:10.3390/en14061547

[125] Tuncel, E. (2019) Elektrikli Bisikletler İçin Sabit Mıknatıslı Doğru Akım Motoru Tasarımı ve Optimizasyonu. Yüksek Lisans Tezi, Düzce Üniversitesi Fen Bilimleri Enstitüsü, Düzce, Türkiye.

[126] United States Environmental Protection Agency (EPA), https://www.epa.gov/ghgemissions/sources-greenhouse-gas-emissions. Last accessed: 10 September 2021.

[127] Uyar, O. (2019) Elektrikli Bisikletler İçin Akıllı Güç Destek Ünitesi Tasarımı ve Gerçekleştirilmesi. Doktora Tezi, Selçuk Üniversitesi Fen Bilimleri Enstitüsü, Konya, Türkiye.

[128] Varma, M., Mal, H., Pahurkar, R., & Swain, R. (2020). Comparative analysis of green house gases emission in conventional vehicles and electric vehicles. International Journal of Advanced Science and Technology, 29(5s), 689-695.

[129] Vatsa, M., Dharwal, M., Sharma, P., & Kumar Srivastava, A. (2021). Green vehicles more a necessity than an option. Materials Today: Proceedings, 46, 5396–5399. doi:10.1016/j.matpr.2020.09.054

[130] Verma, S., Dwivedi, G., & Verma, P. (2022). Life cycle assessment of electric vehicles in comparison to combustion engine vehicles: A review. Materials Today: Proceedings, 49, Part 2, 217–222. doi:10.1016/j.matpr.2021.01.666

[131] Wachter, A., & Hoeber, H. (2006). Compendium of Theoretical Physics, Springer, New York, USA.

[132] Wang, M., Jiang, F., Zhang, Q., & Song, S. (2014). Matching up the suspension of electric vehicle with the supporting system of battery pack. Mechanika, 20(4), 382-389. doi:10.5755/j01.mech.20.4.6300

[133] Wang, P. (2020). Effect of electric battery mass distribution on electric vehicle movement safety. Vibroengineering PROCEDIA, 33, 78–83. doi:10.21595/vp.2020.21569

[134] Wang, W., & Mu, J. (2019). State of charge estimation for lithium-ion battery in electric vehicle based on Kalman filter considering model error. IEEE Access, 7, 29223–29235. doi:10.1109/access.2019.2895377

[135] Weber P. A. (1998). Towards a Canadian standard for the geometric design of speed humps, Master of Engineering Thesis, Carleton University, Faculty of Graduate Studies and Research, Ottawa, Ontario, Canada.

[136] Wu, H., Kuang, S., & Hou, H. (2019). Research on application of electric vehicle collision based on reliability optimization design method. International Journal of Computational Methods, 16(7), 1950034. doi:10.1142/s0219876219500348

[137] Wu, W., Lin, B., Xie, C., Elliott, R. J. R., & Radcliffe, J. (2020). Does energy storage provide a profitable second life for electric vehicle batteries? Energy Economics, 92, 105010. doi:10.1016/j.eneco.2020.105010

[138] Xia, G., Cao, L., & Bi, G. (2017). A review on battery thermal management in electric vehicle application. Journal of Power Sources, 367, 90–105. doi:10.1016/j.jpowsour.2017.09.046

[139] Xu, C., Zhang, W., He, W., Li, G., Huang, J., & Zhu, H. (2017). Generation and management of waste electric vehicle batteries in China. Environmental Science and Pollution Research, 24(26), 20825–20830. doi:10.1007/s11356-017-9890-8

[140] Xu, J., Ma, J., Zhao, X., Chen, H., Xu, B., & Wu, X. (2020). Detection technology for battery safety in electric vehicles: A review. Energies, 13(18), 4636. doi:10.3390/en13184636

[141] Yang, J., Gu, F., & Guo, J. (2020). Environmental feasibility of secondary use of electric vehicle lithium-ion batteries in communication base stations. Resources, Conservation & Recycling, 156, 104713. doi:10.1016/j.resconrec.2020.104713

[142] Yang, X.-G., Liu, T., & Wang, C.-Y. (2021). Thermally modulated lithium iron phosphate batteries for mass-market electric vehicles. Nature Energy, 6(2), 176–185. doi:10.1038/s41560-020-00757-7

[143] Yildirim, E., & Esen, I. (2020). Dynamic behavior and force analysis of the full vehicle model using Newmark average acceleration method. Engineering, technology & applied science research, 10(1), 5330–5339. doi:10.48084/etasr.3335

[144] Yu, Y., Zhao, L., & Zhou, C. (2019). Influence of rotor-bearing coupling vibration on dynamic behavior of electric vehicle driven by in-wheel motor. IEEE Access, 7, 63540–63549. doi:10.1109/access.2019.2916554

[145] Zhang, Z., Jiang, L., Zhang, L., & Huang, C. (2021). State-of-charge estimation of lithium-ion battery pack by using an adaptive extended Kalman filter for electric vehicles. Journal of Energy Storage, 37, 102457. doi:10.1016/j.est.2021.102457

[146] Zhao, H., Wang, L., Chen, Z., & He, X. (2019). Challenges of fast charging for electric vehicles and the role of red phosphorous as anode material: Review. Energies, 12(20), 3897. doi:10.3390/en12203897

[147] Zhao, Y., Zhao, L., & Gao, H. (2010). Vibration control of seat suspension using H∞ reliable control. Journal of Vibration and Control, 16(12), 1859–1879. doi:10.1177/1077546309349852

[148] Zhou, Z., Duan, B., Kang, Y., Cui, N., Shang, Y., & Zhang, C. (2019). A low-complexity state of charge estimation method for series-connected lithium-ion battery pack used in electric vehicles. Journal of Power Sources, 441, 226972. doi:10.1016/j.jpowsour.2019.226972

[149] Zhu, Q., & Ishitobi, M. (2006). Chaotic vibration of a nonlinear full-vehicle model. International Journal of Solids and Structures, 43(3–4), 747–759. doi:10.1016/j.ijsolstr.2005.06.070

[150] Zilletti, M., Elliott, S. J., & Ghandchi Tehrani, M. (2017). Adaptive control of tonal disturbance in mechanical systems with nonlinear damping. Journal of Vibration and Control, 23(7), 1166–1182. doi:10.1177/1077546315590038

[151] Živčák, J., Kádárová, J., Kočišová, M., Lachvajderová, L., & Puškár, M. (2021). Economic analysis of potential secondary use of batteries from electric vehicles. Applied Sciences, 11(9), 3834. doi:10.3390/app11093834

[152] Zou, J., Guo, X., Xu, L., Abdelkareem, M. A. A., Gong, B., Zhang, J., & Tan, G. (2018). Simulation research of a hydraulic interconnected suspension based on a hydraulic energy regenerative shock absorber. SAE Technical Paper 2018-01-0582. doi:10.4271/2018-01-0582

# CURRICULUM VITAE

**Surname, Name:** Erdoğan, Eralp Osman

## EDUCATION

| Degree | Institution |
|---|---|
| Bachelor of Science | Karadeniz Technical University, Department of Mechanical Engineering, Trabzon |

## PUBLICATIONS FROM THE THESIS

1. **Özdemir, M., Erdoğan, E.O.** (2022). Formulation of a 7-DOF Half-Car Model with Nonlinear Springs and Dampers for Ride Comfort Analysis of In-Wheel-Motor Electric Vehicles. Paper presented at: 6th *International Conference on Computational Mathematics and Engineering Sciences (CMES-2022), 20-22 May 2022, Ordu,* Türkiye.